Light-Matter Interactions in Arbitrary Photonic Environments

Dissertation submitted in partial satisfaction of the requirements for the degree of Doctor of Philosophy.

Mónica Sánchez Barquilla

Supervised by

Johannes Feist

Departamento de Física Teórica de la Materia Condensada
Condensed Matter Physics Center (IFIMAC)
Universidad Autónoma de Madrid
Madrid, España

Marzo 2022

A José, mi compañero.

A mi hermana, mi guía y mi ejemplo.

A mis padres, mi apoyo incondicional.

Agradecimientos

En el proceso de escribir una tesis y condensar en poco más de 100 páginas varios años de una vida, es inevitable acordarse de toda la gente que ha hecho por que esta salga adelante. En primer lugar, a Johannes, mi director de tesis, por todo lo enseñado, por su enorme paciencia y disposición a ser constantemente interrumpido con mis dudas, también por hacer todo el proceso un poco más fácil. Espero haber cumplido con las expectativas. Gracias también a Antonio y FJ, con los que he colaborado en los últimos meses. Gracias por las discusiones y vuestra constante buena actitud. Muchas gracias a todas las personas que han pasado por el grupo, gracias a Javi (del Pino) y a Javi (Galego), especialmente por sus consejos al comienzo de mi tesis. Gracias a Rui, que siempre ha estado dispuesto a echarme una (o mil) manos. Gracias también a las personas que han pasado brevemente o han llegado después, Paloma, Simone, Jacopo, Petros, Diego, Maksim y Daniela. Gracias también a Pablo, por todas las horas dedicadas a enseñarme en qué consiste la investigación y por su incansable esfuerzo durante mi TFG y TFM. I would like also to aknowledge the members of the jury for their availability and wilingness to read this thesis and to attend to my defense.

Dentro del departamento, quiero dar las gracias al grupo de comidas. Gracias Jaime, Nerea, Berta, Guille, José, Samuel, Antonio, Pablo, ... por hacer estos años mucho más amenos. Quiero agradecer especialmente a Clàudia y Rocío por su buen humor y ser la chispa constante del departamento. Gracias también a Carmina, Elena, Francesca y Linda, por su iniciativa y tesón. También a Laura Ramos, por resolver todos mis fallos administrativos con la

mayor paciencia.

Cómo no agradecer especialmente a esas personas que me han prestado su oído y apoyo siempre que lo he necesitado. Gracias Álvaro, por compartirme tus opiniones y consejos más allá de lo científico y por tener siempre tiempo para escuchar mis pensamientos. Gracias Diego, por mostrar siempre interés en lo tenía que decir. Espero haberos podido devolver una milésima parte de todo lo que me habéis aportado.

Gracias a todas las personas que me he encontrado fuera de la ciencia, de las que he aprendido lo indecible. Gracias César, Ricardo, Fabián, Juan y Paz, hacéis de la universidad un lugar mejor. A Desi, con quien he compartido infinitas horas en el tren y cuyo apoyo y amistad empezó mucho antes de la tesis. A Alberto, por tu inmejorable actitud.

Por último, quiero agradecer a las personas sin las que este momento no sería posible. A Carlos, por ser un apoyo constante y la voz de la cordura, incluso en los peores momentos. A Raquel, por ser mi gran ejemplo a seguir. Gracias por escucharme durante horas, días y años, por estar siempre de forma incondicional, incluso en la distancia, y por sacar mi mejor versión. A mis padres, a quienes les debo todo. Gracias por el esfuerzo invertido, por hacerlo todo infinitamente más sencillo, por vuestros consejos y enseñanzas, por ser la razón de que estas líneas sean escritas. A José, por tu cariño y paciencia, por ayudarme a avanzar incluso cuando daba un poco de vértigo. Por ser absolutamente fundamental. Gracias.

Índice general

Abstract

English

Understanding and controlling light-matter interactions are long-standing goals in the field of quantum electrodynamics. One of the main challenges in doing so is the wide variety of photonic setups and quantum emitters that can be used, so that many different effects can take place, both due to the spectral complexity and the lossy character of the photonic environment, and due to internal complexity of the emitters, respectively. Due to the huge number of degrees of freedom, theoretical descriptions of these setups are often focused on the inclusion of the complexity for one of the components, via the inclusion of many different levels and number of emitters while the electromagnetic field is considered a single mode, or via the inclusion of many (lossy) photonic modes while considering a single two-level system as the emitter. In this thesis, the latter situation has been treated.

When describing (cavity-supported) light-matter interactions, the spectral density is a fundamental physical quantity that completely defines the action of the electromagnetic environment on the emitters. Therefore, a successful description of the spectral density ensures a good theoretical representation of these interactions. In the single-emitter case, the spectral density is a frequency-dependent scalar function, while in the multiemitter case (which can also represent, for example, different orientations of the dipoles of the emitter) a generalized spectral density can be defined that fully de-

scribes the interaction between the electromagnetic field and the emitter, including their photon-mediated interactions. This generalized spectral density is a matrix-valued function. One of the most powerful approaches to describe light-matter interactions is macroscopic QED, which provides a way to quantize the medium-assisted electromagnetic fields in arbitrary photonic structures, and can be used to show that the spectral density is fully determined by the Green's function of classical electromagnetism. In this thesis, we develop different approaches for which macroscopic QED is a "starting point", so that all degrees of freedom of the photonic environments are included, and also incoherent effects are described without further assumptions.

Chapter 1 gives an introduction to the topic, while **chapter 2** provides an overview of the theoretical concepts and approaches forming the basis of the description of light-matter interactions in this thesis.

Chapter 3 presents the cumulant expansion method. This method is based on solving the Heisenberg equations of motion for cumulants (or correlations) of the system operators. The expansion is truncated at some order, so that the dynamics of a quantum emitter is obtained without high computational cost and avoiding the inclusion of ad-hoc parameters. This approach is compared to a quasi-exact method.

Chapter 4 uses the chain-mapping model, which consists in transforming the Hamiltonian describing the photonic environment modes into an infinite chain in which the emitter is only coupled to one (collective) mode, while each mode of the environment interacts only with its nearest neighbors. Different strategies to truncate the chain while reproducing long-time dynamics are explored and compared again with quasi-exact methods. We then show that a chain of N lossy modes with next-nearest neighbor interactions can be used to obtain a minimal model for an arbitrary environment, in the sense that the number of effective independent degrees of freedom is equal to that of a system

with the same number of modes but coupling between all of them.

Chapter 5 extends a recently introduced few-mode model for EM field quantization to the case of multiple emitters. The model can represent arbitrary spectral densities using a few discrete interacting and lossy modes, and thus allows a direct mapping to the typical models of quantum optics and cavity QED. This fit allows a great liberty in the election of the emitter parameters so that it is possible to describe the emitter dynamics and their population transfer even beyond the single-excitation subspace. As an example, we find that by placing a "control" emitter in its ground or excited state in the system, the transfer between other two emitters can be suppressed or enhanced.

Castellano

Entender y controlar las interacciones entre la luz y la materia son objetivos históricos en el campo de la electrodinámica cuántica. De cara a lograrlos, uno de los mayores retos consiste en la gran variedad de configuraciones fotónicas y emisores cuánticos que pueden usarse, de forma que muchos efectos diferentes pueden tener lugar debido tanto a la complejidad espectral y las pérdidas del entorno fotónico como a la complejidad interna de los emisores. El gran número de grados de libertad hace por tanto que las descripciones teóricas de estos sistemas estén mayormente enfocadas a incluir la complejidad de uno de los componentes, considerando bien muchos niveles y emisores mientras el campo electromagnético se describe como un único modo, bien incluyendo muchos modos fotónicos (y sus pérdidas) mientras el emisor se describe como un emisor cuántico. En esta tesis se considera la segunda de estas situaciones.

Cuando se describen interacciones entre luz y materia (en cavidades), la densidad espectral define completamente la acción de un entorno electromagnético en los emisores. Por tanto, una descripción precisa de la misma asegura una buena representación de estas interacciones. En el caso de un único emisor, la densidad espectral es una función escalar dependiente de la frecuencia, mientras que en el caso de múltiples emisores (lo que puede representar también otras configuraciones como, por ejemplo, diferentes orientaciones de los dipolos de un emisor) se puede definir la densidad espectral generalizada, que consiste en una matriz de funciones, de forma que describe completamente la interacción entre el campo y los emisores, así como su interacción mediada por fotones. Esta densidad espectral generalizada es una matriz de funcoines. Uno de los modelos más poderosos que permite describir las interacciones entre luz y materia es la electrodinámica cuántica macroscópica, que proporciona una

forma de cuantizar el campo electromagnético soportado por un material en una configuración fotónica arbitraria, y que puede usarse para mostrar que la densidad espectral está completamente determinada por la función de Green del electromagnetismo clásico. En esta tesis, desarrollamos diferentes modelos para los cuales la electrodinámica cuántica macroscópica es el punto de partida, de forma que todos los grados de libertad de los entornos fotónicos se incluyen en la descripción, así como los efectos de incoherencia, que se introducen sin asunciones adicionales.

El **capítulo 1** da una introducción del tema, mientras que el **capítulo 2** ofrece un resumen de los conceptios y los modelos que forman la base de la descripción entre luz y materia en esta tesis.

El **capítulo 3** presenta el método de la expansión de correlaciones. Este método se basa en resolver las ecuaciones de Heisenberg del movimiento para las correlaciones (o cumulantes) de los operadores del sistema. Esta expansión se trunca a algún orden, de forma que la dinámica de un emisor cuántico se obtiene sin requerir un gran coste computacional y evitando la inclusión de parámetros "ad hoc". Este modelo se compara con un método cuasi-exacto.

El **capítulo 4** usa el modelo de transformación de la cadena, que consiste en reemplazar el Hamiltoniano original por uno en forma de cadena infinita donde el emisor está acoplado únicamente a un modo (colectivo) mientras que el resto de modos del entorno interaccionan con su vecino más cercano. Para truncar la cadena reproduciendo la dinámica a tiempos largos, se exploran diferentes estrategias y se comparan con métodos cuasi-exactos. Después se muestra que una cadena con N modos con pérdidas e interacción con sus primeros y segundos vecinos puede usarse para obtener un modelo mínimo para un entorno fotónico arbitrario, en el sentido de que el número efectivo de grados de libertad independientes es igual al de un sistema con el mismo número de modos pero permitiendo acoplamiento entre todos ellos.

El **capítulo 5** extiende un modelo recientemente presentado en el que se cuantiza el campo electromagnético utilizando pocos modos para el caso de múltiples emisores. Este modelo puede representar densidades espectrales arbitrarias usando un pequeño número de modos con pérdidas que interactúan entre sí, y por tanto permite hacer un mapeo directo a los modelos típicos de óptica cuántica y electrodinámica cuántica en cavidades. Este mapeo, además, permite una gran libertad en la elección de los parámetros de los emisores de forma que es posible describir su dinámica y su transferencia de población incluso más allá del subespacio de una única excitación. Como ejemplo, encontramos que colocando en el sistema un emisor "de control" en su estado fundamental o en su estado excitado, la transferencia entre otros dos emisores puede suprimirse o favorecerse.

Chapter 1 | Introduction

1.1 Quantum Electrodynamics

QUANTUM light-matter interactions have been a matter of interest for a long time. When characterizing them, a complete theory is quantum electrodynamics (QED) [1], which describes not only the interactions between light and matter, but also the interaction of particles with each other, in a quantum-mechanical way. In the 1920s, Paul Dirac laid its foundations, and in the 1940s, Richard Feynman, Julian Schwinger, and Tomonaga Shin'ichirō developed this theory.

Many physical effects have been explained within the QED framework, such as the Lamb shift [2] or the Casimir effect [3]. Moreover, its understanding allows the control and manipulation of physical and chemical systems. In particular, when light is confined within a cavity, one can modify the properties of a quantum emitter (QE) [4, 5], which constitute the matter part of the interaction at the microscopic level. The framework that studies the modification of the properties of a QE due to its interaction with a confined EM field is cavity quantum electrodynamics (cQED)[6, 7].

Embedding an emitter (with frequency ω_e) inside a cavity (in which exists

a resonant mode with frequency ω_c) can lead to a modification of its properties due to a change in the optical density of states. One interesting consequence is the Purcell effect [8], which consists of an enhancement of the emission of an atom when it is in resonance with the electromagnetic modes of the cavity, or suppression of the decay rate of its spontaneous emission when the emitter and the modes are off-resonance. The Purcell factor controls this behavior and it is given by the decay rate of the emitter enclosed in the cavity with respect the free-space, $F_P = \gamma/\gamma_0$. This effect is a characteristic feature of the weak coupling (WC) regime, in which the nature of the material constituent and the EM field remains well separated and the energy exchange between light and matter is slower than the individual decay and dephasing of each constituent. Moreover, this process is irreversible and the description of the interaction can be done using perturbative approximations [9]. In this regime the resonant Purcell factor takes the form

$$F_P = \frac{3\lambda_c^3}{4\pi^2 n^3}\frac{Q}{V_{\text{eff}}}, \tag{1.1}$$

where λ_c is the light mode wavelength, n is the dielectric cavity constant, Q is the so-called quality factor, which measures the light confinement, and V_{eff} is the effective cavity mode volume [10–12]. The ratio Q/V_{eff} therefore defines the enhancement or suppression of the emitter decay.

If the emitter and a cavity mode are (nearly) resonant and the coupling strength between light and matter is strong enough so that it overcomes the losses of both constituents, the physical system can reach the strong coupling (SC) regime. In this regime, the light and matter components become profoundly mixed and exchange energy coherently [13]. Then, both elements become indistinguishable from one another and hybrid states, the so-called polaritons, arise [14–16]. The formation of polaritons allows new phenomena to emerge, including but not limited to Bose-Einstein condensation [17], superfluidity [18], polariton lasing [19], quantum information processing [20, 21],

long-range excitation transport [22] or photochemical reactions [23, 24].

There are many different parameters, belonging to both matter and light components, that can be tailored in order to explore different interaction regimes. One example is to increase sufficiently the ratio Q/V_{eff} of the cavity. Another is to choose emitters with sizeable dipole moment $\boldsymbol{\mu}$ and orient them in the same direction as the EM field, or embed a collection of emitters so that the coupling increases due to collective effects [25–27]. This thesis focuses on describing the "cavity" component in detail, while the QEs will be approximated as 2-level systems. Before presenting the principal characteristics of cavities and various examples in the next section, a brief description of some of the main features that characterize quantum emitters is presented.

1.1.1 Quantum emitters

Quantum emitters refer to material systems for which the quantum mechanical nature of the matter becomes apparent, so that they show a discrete set of states that gives rise to resonant light-matter interactions when some conditions are fulfilled. The emitter parameters that characterize the interaction between light and matter are:

- The energy separation between levels. Resonant light-matter interactions thus occur when the photon energy matches the energy difference between two levels of the QE. Moreover, if the emitters are approximated as two-level systems, only the ground state $|g\rangle$ and one excited state $|e\rangle$ are included in the matter description. Therefore, the energy gap between both levels is given by $E_e - E_g = \hbar\omega_e$. This is a suitable approximation for emitters whose higher excited states E_f are far enough in energy from the first excited state E_e, i.e., $E_f - E_e > \hbar\omega_e$ and

the interacting photons are in resonance with the two-level system, i.e., $\hbar\omega_c \approx \hbar\omega_e$.

- The transition dipole moment $\boldsymbol{\mu}_e$. This quantity is a vector, so the orientation of the emitter with respect to the EM field inside the cavity matters when tailoring the light-matter interaction. The small dipole moment of a single atom requires very high finesse cavities or small volumes, which is technically demanding. However, when many emitters are placed in a cavity, many dipoles can contribute to the coupling and the effective dipole moment becomes larger.

- The lifetime of the emitter, i.e., the inverse of the decay rate, which also affects the regime of the interaction. This decay rate has two contributions, the radiative and non-radiative rates, γ_r and γ_{nr}, respectively[1]. Moreover, emitters can also suffer dephasing, a loss of coherence in the system.

There are many different types of emitters, each of them with different properties, that can be used as the matter component in cavity QED implementations. Atoms are well-understood and can often be approximated as two-level systems, as their levels are well separated. They also present significant dipole moments and lifetimes [11, 28]. Quantum dots (QD) [11, 29], which are semiconductor particles, can also be approximated as two-level systems and their dipole moments can be tailored by changing their size [30, 31]. Figure **1.1**(a) shows a schematic representation of a two-level system. Molecules however present a significant internal structure that prevents them from being a good fit for the two-level approximation, as they have some separated electronic states and each of them present vibrational states, which are also excited when the molecule and a photon interact and once they are excited, their relaxation process involves different times scales. Figure **1.1**(b)

[1]The total decay rate is given by $\gamma = \gamma_r + \gamma_{nr}$.

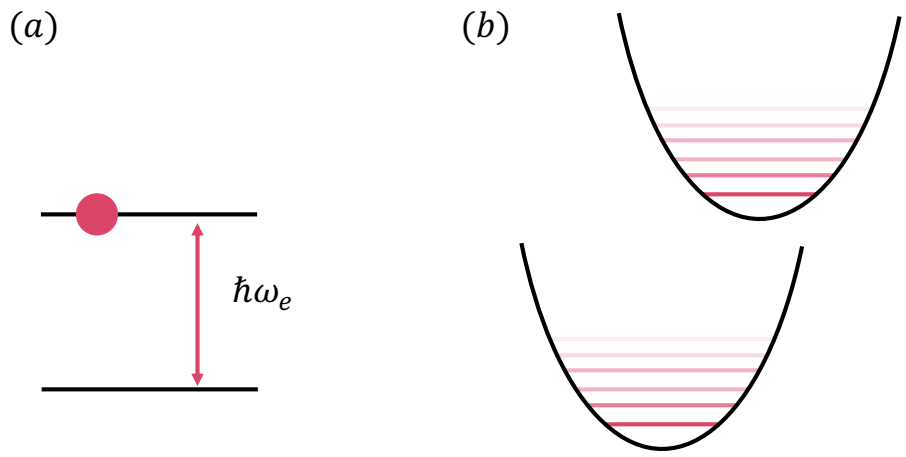

Fig. 1.1.: (a) Two-level system with an energy gap $\hbar\omega_e$. (b) Molecule approximated as two harmonic oscillators with vibrational levels.

shows a schematic representation of a molecule described as two harmonic oscillators. In particular, organic molecules and molecular aggregates present sizeable dipole moments, up to several tens of Debye. In the latter systems, light is absorbed collectively and the dynamics present coherent properties [32].

1.1.2 Cavities

A cavity is a material structure that confines the EM field in a specific arrangement. Over the last decades, it has been shown that a large variety of physical implementations can be used as the "cavity" that provides the electromagnetic field confinement, and different parameters are used to characterize them:

- Quality factor Q, which is defined as

$$Q = \frac{\omega_c}{\kappa}, \tag{1.2}$$

where ω_c is the frequency of the cavity mode and κ is the full width half maximum (cavity field decay rate). For a given cavity frequency ω_c, higher Q indicates a lower energy loss and, therefore, an increase of the cavity lifetime $\tau = 1/\kappa$. Experimentally, the Q factor can be calculated using the measured transmission spectrum of the cavity.

- In cavities where many equally spaced EM modes are allowed, for example in optical Fabry-Pérot cavities, the finesse F is a useful value. It is defined as

$$F = \frac{\Delta\omega_c}{\kappa}, \tag{1.3}$$

where $\Delta\omega_c$ is the separation between the resonances allowed in the cavity. This separation is inversely proportional to the cavity length.

- The mode volume V_{eff}, which gives the volume of space in which the electric field $\boldsymbol{E}$ is concentrated. For lossless, dielectric ($\epsilon > 0$) materials the mode volume is given by

$$V_{\text{eff}} = \frac{\int \epsilon(\boldsymbol{r}) \left|\boldsymbol{E}(\boldsymbol{r})\right|^2 \mathrm{d}^3\boldsymbol{r}}{\max\left(\epsilon(\boldsymbol{r}) \left|\boldsymbol{E}(\boldsymbol{r})\right|^2\right)}, \tag{1.4}$$

where $\epsilon(\boldsymbol{r})$ is the permittivity of the material. Therefore, small V_{eff} increases the field localization and the light-matter coupling strength, related to the mode volume as $g \propto \frac{1}{\sqrt{V_{\text{eff}}}}$. The definition of the mode volume in nanophotonic devices has been the object of intense theoretical activity [33–35].

Cavities with a high Q factor and a small mode volume are preferable to study strong light-matter interactions (microcavities confine the EM field in a volume close to or below the wavelength of light, and therefore they have fewer optical modes than in bigger cavities), although the critical parameter in the achievement of strong coupling is the density of molecules [36], as will be discussed in section **1.2**. Therefore, in particular in the strong coupling

regime when a collection of molecules are embedded inside one cavity, i.e., in the collective regime, different types of cavities may be used, while few- or single-emitter strong coupling at room temperature necessarily requires deep subwavelength confinement of light, so the number of structures that can be used as cavities decrease. Reference [12] reviews many different types of cavities. In the following, some of them are summarized.

Optical cavities

Optical cavities are formed by reflective mirrors in which standing light waves can arise [37]. In this case, the energy is mostly stored in the electric and magnetic fields, and the dielectric functions of the materials can often be treated as approximately constant within the relevant range of frequencies. The size of these cavities is relatively large, and the wavelength of the EM field is similar to the free-space wavelength.

Fabry-Pérot microcavities consist of two parallel reflective mirrors. The distance between them defines the wavelength of the allowed modes within the cavity so that the spectrum inside is discretized. In this case, mode volumes are above the diffraction limit $V \sim \lambda^3$ and depend on the cavity length. Fabry-Pérot cavities can be realized using just one reflective metallic layer for each mirror, but the Q factors in these cavities are limited at optical frequencies because a high Q requires the penetration of light in the barrier material to be small compared to the wavelength.

The Q factor can be improved by using a periodic pattern of dielectric materials called Bragg mirrors. These mirrors can be made from inorganic semiconductors [38, 39] and they can reach extremely high quality factors, $Q \sim 10^8$ [40]. Figure **1.2**(a) shows one example of a sketch of a Fabry-Perot cavity. Planar mirrors confine the light in only one direction, so to control

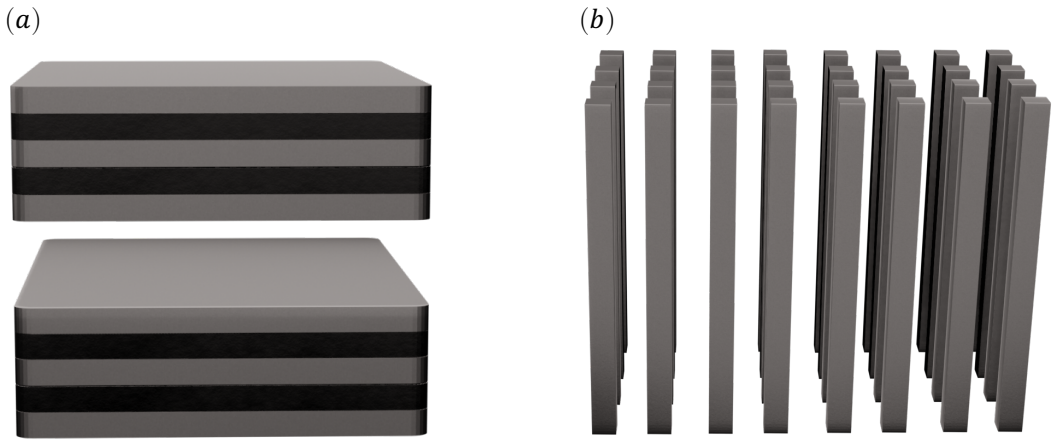

Fig. 1.2.: Examples of cavities: (a) Fabry-Perot resonator, (b) 2 dimensional photonic crystal.

the photonic modes, confinement in the other two dimensions can be achieved using spherical mirrors or pillar microcavities [41].

Another configurations when still using dielectric materials as microcavities are those that support whispering-gallery modes via total internal reflection, such as microdisks [42], microspheres [43] and toroids [44]. Ultrahigh Q-factors of $Q \sim 10^9 - 10^{11}$ have been measured in these structures [45–47].

Photonic crystals are formed by periodic dielectric arrays, intercalating high and low refractive indexes [48]. In a photonic crystal the refractive index contrast gives rise to Bragg scattering of photons, creating a bandgap for particular wavelengths[2], so photons with energies corresponding to these wavelengths can not propagate through the crystal. A defect placed in this structure creates some modes inside the gap. Thus, the EM modes are confined

[2]In 3D photonic crystals, the bandgap is produced in all directions, while in 2D photonic crystals it is created in a plane. In these systems, the confinement in the third direction is due to total internal reflection at the interface of the membrane [49, 50].

within the defect, and it acts as a cavity. These microcavities support small mode volumes $V \approx \lambda^3$ and Q factors above 10^5 [51]. Figure **1.2**(b) shows a sketch of a 2D photonic crystal.

Plasmonic cavities

Plasmons are collective oscillations of the free electron gas in a metallic structure due to their resonant interaction with light. They can occur in the bulk of a metal or be confined in the interface between a conductor and a dielectric medium, forming surface plasmon polaritons (SPPs). By geometrical restriction of the free electron motion in metals, plasmonic structures can concentrate light in subwavelength volumes, leading to an enhancement of the EM field. Therefore, they can be tailored to manipulate light-matter interactions, i.e., they can act as a cavity, allowing strongly subwavelength field confinement [52–55]. In plasmonic resonances, the energy is stored in the electric field and the kinetic energy of the electrons [56]. Despite their relatively high losses, the SC regime can be achieved with one (or a few) molecules due to their small mode volumes [57].

Plasmonic configurations can operate at room temperature, but they are lossy ($Q \sim 10 - 100$), so the mode volume needs to be decreased to achieve strong coupling. Still, it can be observed in metallic planar surfaces [58]. If the surface is modulated with holes of sub-wavelength sizes, a bandgap can be created. SP modes can be excited at the edges of the bandgap, and a strong enhancement of the EM field takes place [59].

Nanoparticles allow the creation of localized surface plasmons (LSP). They alone have low quality factors, but their low volume ($V \sim 10^{-4} \cdot \lambda^3$) also permits to achieve strong coupling when the emitter couples to the near-field of the nanoparticle [60]. Moreover, nanoparticle arrays allow the hy-

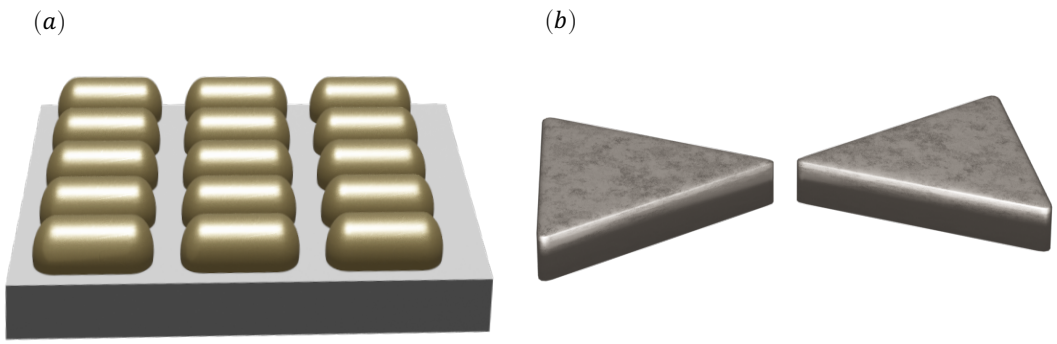

Fig. 1.3.: Examples of cavities: (a) Nanoparticle array embedded in a dielectric material, (b) Bowtie antenna.

bridization of the LSPs in the nanoparticles and the diffracted light of the array [61]. Nanoparticle-on-mirror (NPoM) geometries [57, 62] and bowtie antennas [63, 64] create large field enhancement and extremely low mode volumes ($V \sim 10^{-7} \cdot \lambda^3$) , making it possible to achieve strong coupling even for one or few emitters. Figure **1.3**(a),(b) shows different examples of plasmonic cavities.

Hybrid cavities that combine plasmonic nanoparticles and planar microcavities have been demonstrated to achieve strong coupling in regimes where neither of the structures by themselves can, as they present higher Q factors than the plasmonic particles and smaller mode volumes than dielectric cavities [65–67].

1.2 Theoretical descriptions of complex EM fields

When describing light-matter interactions, in particular in the strong coupling regime, including all the degrees of freedom in both constituents is an arduous task. Then, many models concentrate on taking into account the complexity of one of them, i.e., the theoretical effort is focused on describing the complexity of the photonic structures or including more degrees of freedom in the description of the emitters. As this thesis focuses on the description of the EM structure, a review of some of the theoretical tools available to characterize the EM complexity is presented.

In general, any setup that confines the EM field is determined by "macroscopic" structures consisting of large numbers of atoms, such as Fabry-Pérot cavities, photonic crystals, and metallic nanoparticles or surfaces described in section **1.1.2**. Within these setups, one or several microscopic quantum emitters are placed. It is then customary to treat the macroscopic structure through Maxwell's equations and formally treat the modes arising from these equations as the EM modes of the system.

However, what should be called a "light mode" in a specific arrangement is actually somewhat subtle, and to some degree arbitrary. The only "pure" light modes are free-space modes in vacuum. As cavities are material structures that confine the EM field, the "cavity photon modes" are always partially material excitations [68, 69]. As an operational definition, the confined cavity modes are usually understood as the modes supported by those parts of the full system for which the relevant dynamics can be well-approximated through macroscopic electromagnetism under linear response. This distinc-

tion naturally leads to macroscopic QED framework [68, 70–76], presented in section **2.1**. The resulting EM modes then include those of the different setups presented in the previous section, including both optical cavities and plasmonic resonances. However, it is important to note that the nature of the EM modes that arise in both kinds of cavities is physically distinct. In particular, the dominantly electrostatic character of the fields in deep-subwavelength cavities also has fundamental consequences on the light-matter interaction, as the electric fields are then to a good approximation purely longitudinal and not represented by the vector potential in the standard Coulomb gauge [68, 69, 77].

In order to describe light-matter interactions on a quantum level, these EM modes have to be quantized, which is significantly more challenging than the quantization of free EM modes in conventional quantum electrodynamics (QED) (see Appendix **A**). For one, the presence of material structures complicates the solution of the eigenmodes, which often is only possible numerically. This shortcoming can be solved by the use of numerical packages that solve Maxwell's equations. Nowadays, many commercial and open source packages can be used to this purpose. Furthermore, the material losses and the leakage to the far field cause the modes that arise to be lossy, and only in some approximations do lossless states exist, e.g., when assuming the existence of perfectly conducting mirrors or infinitely long lossless and defect-free waveguides, etc. None of these are typically good approximations for many experimental realizations in nanophotonics. Therefore, taking into account these losses appropriately is necessary. When losses are small enough, one reasonable strategy is to quantize fully bound modes in a fictitious lossless system, and then treat the losses as small perturbations on top of that. However this is not valid in more general descriptions.

When dealing with small enough nanoparticles with localized resonances

(such as plasmonic nanoparticles) and sub-wavelength confinement, for which radiative losses are small due to inefficient emission, the so-called quasistatic approximation is often applicable. In this approximation, retardation effects, and therefore EM propagation into free-space (or bulk dielectric media) is neglected, resulting in purely longitudinal fields. Therefore, light-matter interactions are due to the electrostatic interactions, which simplifies the treatment of beyond-dipole interactions [78–80]. Semi-analytical solutions are then often possible, e.g., using transformation optics [62, 81, 82], with the resulting modes being fully bound while still describing the material losses. Since subwavelength confinement is a prerequisite for the quasistatic approximation, these material losses will always be significant [56]. Moreover, for metals described by a dielectric function of Drude form, the resulting eigenmodes in the quasistatic approximation will always correspond to uncoupled Lorentzians in the spectral density (discussed in more detail below), which allows for a straightforward quantization procedure of the resulting modes [78, 80, 83]. Radiative losses can also be included a posteriori, e.g., by calculating the effective dipole moment of the localized resonances [78, 84].

When the quasistatic approximation is not appropriate and retardation effects have to be taken into account, one of the most general and powerful approaches to nonetheless obtain a quantized description of the EM field is macroscopic QED. This is a formal approach that quantizes the EM field in arbitrary structures, including dispersive and absorbing materials and it is the initial point for the different models presented along this thesis. In this framework the quantized modes are fully described by the dyadic Green's function $\mathbf{G}(\mathbf{r}, \mathbf{r}', \omega)$ of the classical Maxwell equations, which can be obtained from any numerical solver. This description will be presented in detail in section **2.1**. While this approach has proven hugely successful for treating problems where the EM modes are treated perturbatively or integrated out in some other way, it is not directly useful for applying cavity-QED-like approaches in which the

modes are treated as explicit degrees of freedom of the system. For the summary presented in this section, it is important to note that, although the classical description of the EM environment is valid for a wide variety of physical situations, it breaks down when the material and the emitters are physically close enough so that electronic wave functions overlap [85], which happens at subnanometer separations.

For the many situations where the classical Green's function can be used, the EM environment is then a continuum that can be treated as a bath, and therefore the tool of open quantum systems, as will be shown in section **2.5**, can be used. In the weak-coupling regime, the so-called Markov approximation allows the bath to be treated perturbatively [86]. Within this approximation, the effects of the environment on the emitters are a frequency shift, which is often considered included in the emitters frequencies and thus neglected, and a radiative decay with a rate given by the value of the spectral density at the frequency of the emitter.

When the Markovian approximation is not applicable, there are several available methods to treat a bath of harmonic oscillators (the EM modes) exactly using advanced computational tools. One of them is the cumulant expansion method, based on solving the Heisenberg equations of motion for the correlations between the operators. In practice, this expansion must be truncated at some point. In **chapter 3**, different strategies to truncate the cumulant expansion are studied, so that many degrees of freedom can be taken into account at a relatively low computational cost. This treatment is in some sense an extension of mean-field approaches up to an arbitrary order and corresponds to Ref. [87].

Several other commonly used approaches rely on the so-called chain mapping, an orthogonal transformation that maps the Hamiltonian of one emitter coupled to a continuum of modes to a chain-like Hamiltonian where the

emitter is only coupled to the first site in an infinite string of modes coupled through nearest-neighbor interactions. This first site consists of a reaction mode, i.e., a collective environmental mode. In the chain form, tensor network approaches that represent a high-dimensional wave function as a product of many lower-dimensional matrices (a so-called matrix product state) become highly efficient as the entanglement in an effective 1D system such as a chain is limited. Tensor network approaches depend exactly on a truncation of the possible entanglement between different parts of the system. The chain transformation can therefore be employed to describe a photonic environment of the degrees of freedom of molecules. In the context of molecular polaritonics, tensor networks have been shown to allow the description of several molecules coupled to complex environments [88, 89, 92]. When the vibrational modes of a molecule are modeled as a series of displaced harmonic oscillators, they can also be naturally represented in chain form and treated through the same approach. A fully converged tensor network calculation gives exact results, but becomes computationally challenging when long propagation times are desired as the entanglement grows over time.

Furthermore, although formally in the chain representation the system has an infinite length, when performing the calculations it has to be truncated, but to prevent the formation of unphysical reflections due to the finite length of the chain, it has to be linearly increased with time propagation. In order to decrease the length of the chain one approach is to employ transfer tensors, which can be used to propagate to arbitrary times with linear computational cost [93]. Another approach is presented in **chapter 4** and consists on introducing fictitious losses along the chain that lead to damping of the propagating excitations. The addition of damping terms allows shortening the model chain considerably for arbitrary photonic structures even before optimizing the parameters. Moreover, the fit to the chain-like spectral density can improve the description of the dynamics for a given chain. If the chain representation is

extended to allow next-nearest neighbor coupling, the number of parameters used to describe the spectral density is the same as if it is written in its diagonal form. Therefore, the spectral density can be fitted and the dynamics of the emitter can be described up to an arbitrary time, as demonstrated in Ref. [94].

While the description of the EM modes as a structured continuum described by the spectral density is formally exact, it is often advantageous and desired to obtain a description of the environment in terms of a few discrete modes, corresponding to the physical image of isolated cavity modes. When losses are included, these are not true eigenmodes of the system, but resonances with a given bandwidth embedded in the continuum. Several methods have been developed to achieve such a few-mode quantized description in the past few years. One relies on the quasinormal mode theory for Maxwell's equations [95–97], based on forming superpositions of the modes of macroscopic QED that correspond to the quasinormal modes of the material structure, and then performing appropriate approximations to obtain the energies, decay rates, and coherent and incoherent interactions of these modes [66, 98, 99]. In particular, quasinormal modes (QNM) are eigenmodes of the Maxwell equations including losses [97] at complex frequencies. Their quantization allows to expand the EM modes in terms of discrete bosonic modes [100].

An alternative that does not require calculation and explicit quantization of quasinormal modes is based on the fact that two systems with the same spectral density are indistinguishable from the point of view of an emitter. This allows the construction of a model system consisting of a few coupled discrete modes that are themselves coupled to a bath of background modes and reproduces the full spectral density [101]. The parameters that are obtained through the fit of the spectral density are the coupling between the emitter and the discrete modes g_i, the frequencies of these modes and their couplings

ω_{ij} and their dissipation κ_i. This approach, developed for a single emitter in Ref. [101], is extended for several emitters in **chapter 5** and corresponds to Ref. [102].

Chapter 2 | Light-matter interactions

2.1 Macroscopic QED

As has been discussed in the previous chapter, the study of light-matter interactions does not usually happen in free space, but the EM modes arise in "macroscopic" material structures, i.e., assemblies formed by materials with a large number of particles. Macroscopic QED is a formal approach that quantizes the EM field in arbitrary structures, including dispersive and absorbing materials. The quantization scheme in this framework is based on the expansion of the EM field operators in terms of the dyadic Green's function $\mathbf{G}(\mathbf{r}, \mathbf{r}', \omega)$, which is the solution of the Helmholtz equation, and therefore can be obtained classically, as will be mentioned in section **2.1.1**. This can be conceptually understood from the fact that Maxwell's equations are the wave equations describing the dynamics of EM fields, which remains true after quantization.

The macroscopic QED approach has been widely used to describe dispersion forces, which are the ones responsible for the Casimir effect and Casimir-

Polder forces [75, 76]. As this framework is the starting point of the different models presented in this thesis, this section outlines its derivation.

2.1.1 Macroscopic EM in dielectric materials

In a dielectric material, Maxwell's equations can be written, after doing the Fourier transform $\mathbf{E}(\mathbf{r},\omega) = \int_{-\infty}^{\infty} \mathbf{E}(\mathbf{r},t)e^{i\omega t}\mathrm{d}t$, as

$$\nabla \cdot \mathbf{D}(\mathbf{r},\omega) = \tilde{\rho}(\mathbf{r},\omega), \tag{2.1}$$

$$\nabla \times \mathbf{E}(\mathbf{r},\omega) = i\omega\mathbf{B}(\mathbf{r},\omega), \tag{2.2}$$

$$\nabla \cdot \mathbf{B}(\mathbf{r},\omega) = 0, \tag{2.3}$$

$$\nabla \times \mathbf{H}(\mathbf{r},\omega) = \tilde{\mathbf{J}}(\mathbf{r},\omega) - i\omega\mathbf{D}(\mathbf{r},\omega), \tag{2.4}$$

where the time derivatives that appear in free space (see eqs. (A.1) to (A.4)) are simplified, as only the factor $i\omega$ appears with the variables. In the above expressions, $\mathbf{D}(\mathbf{r},\omega) = \epsilon_0\mathbf{E}(\mathbf{r},\omega) + \mathbf{P}(\mathbf{r},\omega)$ is the displacement operator and $\mathbf{H}(\mathbf{r},\omega) = \mu_0\mathbf{B}(\mathbf{r},\omega)+\mathbf{M}(\mathbf{r},\omega)$, where $\mathbf{P}(\mathbf{r},\omega)$ is the polarization of the material and $\mathbf{M}(\mathbf{r},\omega)$ its magnetization. Moreover, within a medium, the charge and current sources do not only describe the "external" sources, which are the only ones existing in free space, but also include the induced ones that are generated due to the material response. Therefore, $\tilde{\rho}(\mathbf{r},\omega) = \rho(\mathbf{r},\omega) + \rho_{ind}(\mathbf{r},\omega)$ and $\tilde{\mathbf{J}}(\mathbf{r},\omega) = \mathbf{J}(\mathbf{r},\omega) + \mathbf{J}_{ind}(\mathbf{r},\omega)$.

In the case of an isotropic, linear, dispersive medium, the displacement operator and the electric field are related by

$$\mathbf{D}(\mathbf{r},\omega) = \epsilon(\mathbf{r},\omega)\mathbf{E}(\mathbf{r},\omega). \tag{2.5}$$

If furthermore the medium is non-magnetic, the wave equation of the electric field can be written as

$$\nabla \times \nabla \times \mathbf{E}(\mathbf{r},\omega) - \omega^2\mu_0\epsilon(\mathbf{r},\omega)\mathbf{E}(\mathbf{r},\omega) = i\mu_0\omega\mathbf{J}(\mathbf{r},\omega). \tag{2.6}$$

At this point, in order to give a general solution, the dyadic Green's function $\mathbf{G}(\mathbf{r}, \mathbf{r}', \omega)$ can be introduced. In particular, this function is a solution of the wave equation for a point source current. Therefore, the wave equation can be written as

$$\nabla \times \nabla \times \mathbf{G}(\mathbf{r}, \mathbf{r}', \omega) - \omega^2 \mu_0 \epsilon(\mathbf{r}, \omega) \mathbf{G}(\mathbf{r}, \mathbf{r}', \omega) = \mu_0 \omega^2 \delta^3(\mathbf{r} - \mathbf{r}'), \tag{2.7}$$

so that, as it is linear, the electric field can be written as an integral of an arbitrary source and the Green's function

$$\mathbf{E}(\mathbf{r}, \omega) = \frac{i}{\omega} \int \mathrm{d}^3 \mathbf{r}' \mathbf{G}(\mathbf{r}, \mathbf{r}', \omega) \cdot \mathbf{J}(\mathbf{r}', \omega). \tag{2.8}$$

2.1.2 Macroscopic QED derivation

The huge number of particles in macroscopic structures is too big to describe the whole system as a collection of microscopic particles interacting with the quantum free-space EM field. Therefore, one can assume that in these structures macroscopic electromagnetism may be capable of reproducing the fields that are formed and propagate along the material (as was pointed out in section **1.2** this assertion is not true when the material and the emitters are close enough for their electronic wave functions to overlap). Then, one strategy is to generalize the free-space description.

When the EM field propagates through a dielectric material, there is a coupling between the matter and the field, whose effect is encoded in the dielectric function $\epsilon(\omega) = \epsilon^R(\omega) + i\epsilon^I(\omega)$. The imaginary part of the dielectric function implies that an expansion in a plane wave representation (as in free space) cannot be made, as the imaginary term leads to damped waves. They are not solutions of the EM fields in free space, but of the combined field-matter system. Then, a naive extension of the free-space derivation cannot be

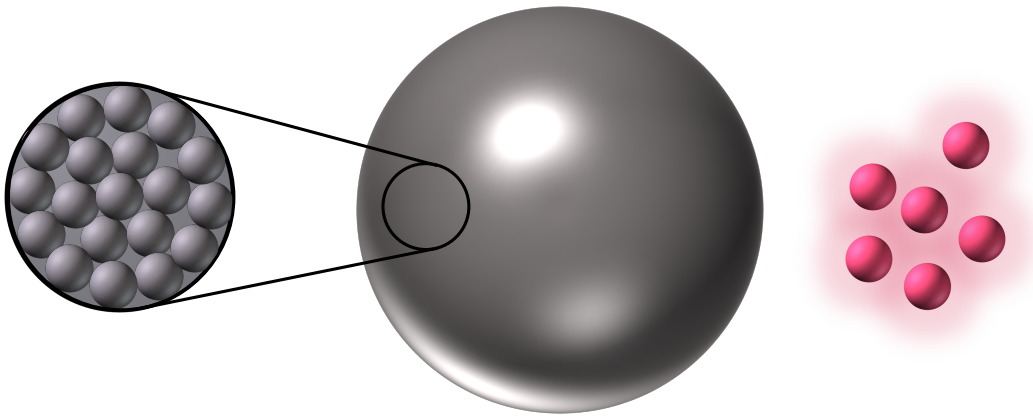

Fig. 2.1.: Collection of quantum emitters (pink) interacting with a material (grey). The material is composed of a collection of microscopic particles. The macroscopic QED framework describes the constitutive relations within the material, while the quantum emitters are included in the Hamiltonian maintaining their microscopic description.

done, and one must consider the EM field coupled to some reservoir that is responsible for dispersion or absorption.

In their model, Huttner and Barnett considered a Hopfield model of a homogenous dielectric material in which a harmonic oscillator field represents the polarization in the material. This field is coupled to a continuum of harmonic oscillators representing the reservoir (which models the absorption) [71, 103]. They assumed that the medium is an absorbing single-resonance dielectric, so this is also presumed in the following. Nevertheless, this model has been generalized to inhomogeneous dielectric bodies [104–106] and bodies with non-local properties [107]. More extensive and alternative derivations can be found in [10, 75, 108]. In this section, the quantization is done without including microscopic particles. They are added in the following section similarly as in free space (see Appendix **A**).

Quantization in absorbing materials

The Lagrangian that describes the previous medium is given by $\mathcal{L} = \mathcal{L}_{\text{EM}} + \mathcal{L}_{\text{mat}} + \mathcal{L}_{\text{int}}$, where

$$\mathcal{L}_{\text{EM}} = \frac{\epsilon_0}{2}\left[\left(\dot{\mathbf{A}}\cdot\nabla\phi\right)^2 - c^2\left(\nabla\times\mathbf{A}\right)^2\right] \tag{2.9}$$

$$\mathcal{L}_{\text{mat}} = \frac{\mu}{2}\left(\dot{\mathbf{X}}^2 - \omega_i^2\mathbf{X}^2\right) + \frac{\mu}{2}\int_0^\infty \mathrm{d}\omega\left(\dot{\mathbf{Y}}_\omega - \omega^2\mathbf{Y}_\omega^2\right), \tag{2.10}$$

$$\mathcal{L}_{\text{int}} = -\alpha\left(\mathbf{A}\cdot\dot{\mathbf{X}} + \phi\nabla\cdot\mathbf{X}\right) - \int_0^\infty \mathrm{d}\omega\nu(\omega)\mathbf{X}\cdot\dot{\mathbf{Y}}_\omega. \tag{2.11}$$

In the previous set of equations $\mathcal{L}_{\text{EM}}$ is the free Hamiltonian of the EM field when external sources are included, $\mathcal{L}_{\text{mat}}$ is the free Hamiltonian of the matter, including the medium and the reservoir, and $\mathcal{L}_{\text{int}}$ gives the interaction between the field, matter and reservoir. The polarization is modelled by $\mathbf{X}$, which is a harmonic oscillator field with frequency ω_i, while $\mathbf{Y}_\omega$ accounts for the continuum of harmonic oscillators that model the losses (both of them with density μ), α is the polarizability (that gives the coupling between the polarization and the field) and $\nu(\omega)$ is the coupling constant between the polarization and the reservoir.

The canonical momenta of the relevant variables in the previous Lagrangian are $\mathbf{\Pi} = -\epsilon_0\dot{\mathbf{A}}$, $\mathbf{P} = \mu\dot{\mathbf{X}} - \alpha\mathbf{A}$ and $\mathbf{Q}_\omega = \mu\dot{\mathbf{Y}}_\omega - \nu(\omega)\mathbf{X}$ respectively. Going to the Fourier space $(\mathbf{k}, t)$, dividing the longitudinal and transverse components and doing a mode decomposition similar to the one made in free space, the mode amplitudes that correspond to each variable can be found. In

particular,

$$\boldsymbol{a}_\lambda(\mathbf{k}) = \sqrt{\frac{\epsilon_0}{2\hbar\tilde{k}c}}\left[\tilde{\mathbf{k}}c\mathbf{A}_\lambda(\tilde{\mathbf{k}}) + \frac{i}{\epsilon_0}\Pi_\lambda(\mathbf{k})\right], \tag{2.12}$$

$$\boldsymbol{b}_\lambda(\mathbf{k}) = \sqrt{\frac{\mu}{2\hbar\tilde{\omega}}}\left[\tilde{\omega}\mathbf{X}_\lambda(\mathbf{k}) + \frac{i}{\mu}P_\lambda(\mathbf{k})\right], \tag{2.13}$$

$$\boldsymbol{b}_\lambda(\mathbf{k},\omega) = \sqrt{\frac{\mu}{2\hbar\omega}}\left[-i\omega\mathbf{Y}_\lambda(\mathbf{k},\omega) + \frac{1}{\mu}Q_\lambda(\mathbf{k},\omega)\right], \tag{2.14}$$

where $\tilde{k}^2 = k^2 + \alpha^2/(\mu\epsilon_0 c)$ and $\tilde{\omega}^2 = \omega^2 + \int_0^\infty \mathrm{d}\omega\nu^2(\omega)/\mu^2$ reflect the level shift due to the interaction between fields. Quantization can be performed by replacing the complex amplitudes $\boldsymbol{a}_\lambda(\mathbf{k})$, $\boldsymbol{b}_\lambda(\mathbf{k})$, $\boldsymbol{b}_\lambda(\mathbf{k},\omega)$ by operators $\hat{\boldsymbol{a}}_\lambda(\mathbf{k})$, $\hat{\boldsymbol{b}}_\lambda(\mathbf{k})$, $\hat{\boldsymbol{b}}_\lambda(\mathbf{k},\omega)$, which fulfil the usual bosonic commutation relations

$$\left[\boldsymbol{a}_\lambda(\mathbf{k}), \boldsymbol{a}^\dagger_{\lambda'}(\mathbf{k}')\right] = \delta_{\lambda,\lambda'}\delta(\mathbf{k}-\mathbf{k}'), \tag{2.15}$$

$$\left[\boldsymbol{b}_\lambda(\mathbf{k}), \boldsymbol{b}^\dagger_{\lambda'}(\mathbf{k}')\right] = \delta_{\lambda,\lambda'}\delta(\mathbf{k}-\mathbf{k}'), \tag{2.16}$$

$$\left[\boldsymbol{b}_\lambda(\mathbf{k},\omega), \boldsymbol{b}^\dagger_{\lambda'}(\mathbf{k}',\omega')\right] = \delta_{\lambda,\lambda'}\delta(\mathbf{k}-\mathbf{k}')\delta(\omega-\omega'). \tag{2.17}$$

Furthermore, the resulting Hamiltonian can be diagonalized by a Bogoliubov transformation. For the transverse components of the material and the reservoir, this leads to

$$\hat{H}_{\mathrm{mat}} = \sum_\lambda \int \mathrm{d}^3k \int \mathrm{d}\omega\hbar\omega\hat{\mathbf{B}}^\dagger_\lambda(k,\omega)\hat{\mathbf{B}}_\lambda(k,\omega), \tag{2.18}$$

where $\hat{\mathbf{B}}_\lambda(k,\omega)$ and $\hat{\mathbf{B}}^\dagger_\lambda(k,\omega)$ are dressed matter operators. Combining them with the field operators, adding the longitudinal components and undoing the Fourier transform leads to the final diagonal Hamiltonian

$$\hat{H}_{\mathrm{F}} = \sum_\lambda \int \mathrm{d}^3\mathbf{r} \int \mathrm{d}\omega\ \hbar\omega\ \hat{\mathbf{f}}^\dagger_\lambda(\mathbf{r},\omega)\hat{\mathbf{f}}_\lambda(\mathbf{r},\omega), \tag{2.19}$$

where the modes $\hat{\mathbf{f}}^\dagger_\lambda(\mathbf{r},\omega)$, $\hat{\mathbf{f}}_\lambda(\mathbf{r},\omega)$ represent the medium-assisted EM fields. As they represent mixed light-matter interactions, they are called "polaritonic" modes.

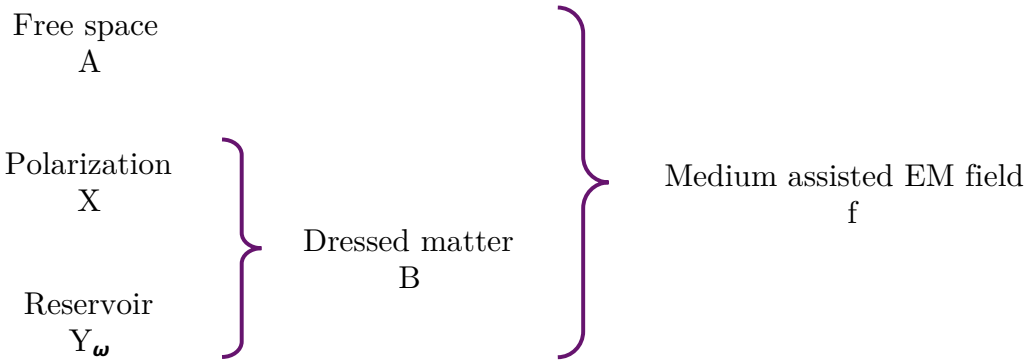

Fig. 2.2.: Scheme of the quantization in macroscopic material structures.

If the vector potential is written in terms of the previous operators, one finds that

$$\hat{\mathbf{A}}(\mathbf{r}) = \sum_{\lambda} \int \frac{\mathrm{d}\omega}{i\omega} \int \mathrm{d}^3\mathbf{r}' \; \mathbf{G}_{\lambda}(\mathbf{r}, \mathbf{r}', \omega) \cdot \hat{\mathbf{f}}_{\lambda}(\mathbf{r}, \omega) + h.c., \tag{2.20}$$

where functions $\mathbf{G}_{\lambda}(\mathbf{r}, \mathbf{r}', \omega)$ are related to the dyadic Green's function $\mathbf{G}(\mathbf{r}, \mathbf{r}', \omega)$ through

$$\mathbf{G}_e(\mathbf{r}, \mathbf{r}', \omega) = i\frac{\omega^2}{c^2}\sqrt{\frac{\hbar}{\pi\epsilon_0}\mathrm{Im}\epsilon(\mathbf{r}', \omega)}\mathbf{G}(\mathbf{r}, \mathbf{r}', \omega), \tag{2.21}$$

$$\mathbf{G}_m(\mathbf{r}, \mathbf{r}', \omega) = i\frac{\omega}{c}\sqrt{-\frac{\hbar}{\pi\epsilon_0}\mathrm{Im}\mu^{-1}(\mathbf{r}', \omega)}\left[\nabla' \times \mathbf{G}(\mathbf{r}', \mathbf{r}, \omega)\right]^T, \tag{2.22}$$

and electric and magnetic fields have similar expressions:

$$\hat{\mathbf{E}}(\mathbf{r}) = \sum_{\lambda} \int \mathrm{d}\omega \int \mathrm{d}^3\mathbf{r}' \; \mathbf{G}_{\lambda}(\mathbf{r}, \mathbf{r}', \omega) \cdot \hat{\mathbf{f}}_{\lambda}(\mathbf{r}, \omega) + h.c., \tag{2.23}$$

$$\hat{\mathbf{B}}(\mathbf{r}) = \sum_{\lambda} \int \frac{\mathrm{d}\omega}{i\omega} \int \mathrm{d}^3\mathbf{r}' \; \nabla \times \mathbf{G}_{\lambda}(\mathbf{r}, \mathbf{r}', \omega) \cdot \hat{\mathbf{f}}_{\lambda}(\mathbf{r}, \omega) + h.c.. \tag{2.24}$$

Interaction with particles

As pointed out before, EM fields can interact with microscopic particles that must be described using a microscopic approach. They can be added in an analogous way as in free-space (the derivation of the interaction between the vacuum EM field and microscopic particles is shown in Appendix **A**), so both the minimal coupling Hamiltonian and the multipolar Hamiltonian can be written within the macroscopic QED framework.

The minimal coupling Hamiltonian for the medium-assisted fields in the presence of microscopic particles is

$$\hat{H} = \hat{H}_{\mathrm{F}} + \sum_i \frac{1}{2m_i} \left[\hat{\mathbf{p}}_i - q_i \hat{\mathbf{A}}(\hat{\mathbf{r}}_i)\right]^2 + \sum_{i,j>i} \frac{q_i q_j}{4\pi\epsilon_0 \left|\hat{\mathbf{r}}_i - \hat{\mathbf{r}}_j\right|} + \sum_i q_i \hat{\phi}_i(\hat{\mathbf{r}}_i), \quad (2.25)$$

where $\hat{H}_{\mathrm{F}}$ is the medium-assisted field Hamiltonian, given by Eq. (2.19) and the last term in the previous equation accounts for the Coulomb interaction between the particles and the material. This term is generally non-zero in the Coulomb gauge[1].

The long-wavelength approximation can be made in the minimal coupling Hamiltonian (2.25). This approximation assumes that the particles are close enough so that the spatial variations of the electric field are small in the volume occupied by the particles. Then, an expansion with respect to the position of the center of mass can be done in the variables. If the lowest term in the expansion is the only one considered relevant, the minimal coupling Hamiltonian

[1]Now, the total electric field is the sum of the previous one derived in Eq. (2.23) and the one generated by the particles, i.e., $\hat{\mathcal{E}} = \hat{\mathbf{E}} - \nabla\hat{\phi}_A(\hat{\mathbf{r}}_A)$, where $\hat{\phi}_A$ is the scalar potential for the charged particles, while the magnetic field remains unchanged, as in Eq. (2.24).

is then reduced to

$$\hat{H} \approx \sum_{\lambda} \int \mathrm{d}^3\mathbf{r} \int \mathrm{d}\omega \hbar\omega \hat{\mathbf{f}}_{\lambda}^{\dagger}(\mathbf{r},\omega)\hat{\mathbf{f}}_{\lambda}(\mathbf{r},\omega) + \sum_i \frac{\hat{\mathbf{p}}_i^2}{2m_i} + \sum_{i,j>i} \frac{q_i q_j}{4\pi\epsilon_0 \left|\hat{\mathbf{r}}_i - \hat{\mathbf{r}}_j\right|} - \sum_i \frac{q_i}{m_i}\hat{\bar{p}}_i \cdot \hat{\mathbf{A}}(\hat{\mathbf{r}}_i) + \sum_i \left[\frac{q_i^2}{2m_i}\hat{\mathbf{A}}^2(\hat{\mathbf{r}}_i) - \hat{\boldsymbol{\mu}}_i \cdot \hat{\mathbf{E}}^{\parallel}(\hat{\mathbf{r}}_i)\right], \tag{2.26}$$

where $\hat{\boldsymbol{\mu}}_i = \sum_j q_j \hat{\bar{r}}_j$ is the dipole moment operator and $\hat{\bar{p}}_i$ and $\hat{\bar{r}}_i$ refer to the momentum and position of the center of mass. Therefore, it has become explicit that the emitter-field interaction in material structures has two components, one longitudinal given by the Coulomb interaction between the particles and the macroscopic structure and one transverse described by the vector potential.

The multipolar Hamiltonian can be obtained by applying the Power-Zienau-Woolley transformation so that the transformed Hamiltonian uses the global variables $\mathbf{E}$ and $\mathbf{B}$ instead of their longitudinal and perpendicular components. When the charges are bounded in different emitters, this transformation also removes the explicit interaction between charges of different emitters, as they are already taken into account in the fields. The multipolar Hamiltonian allows a systematic expansion of the field-emitter interactions in terms of the so-called multipolar components, allowing to discard non-relevant interactions in a simple way. The Power-Zienau-Woolley transformation is $\hat{O}' = \hat{U}\hat{O}\hat{U}^{\dagger}$, where

$$\hat{U} = \exp\left[\frac{i}{\hbar}\int \mathrm{d}^3 r \sum_i \hat{\mathbf{P}}_i(\mathbf{r}) \cdot \hat{\mathbf{A}}(\mathbf{r})\right], \tag{2.27}$$

is a unitary transformation, $\hat{\mathbf{P}}_i(\mathbf{r}) = \sum_{j\in i} q_j \hat{\bar{r}}_j \int_0^1 d\sigma \delta\left(\mathbf{r} - \mathbf{r}_i - \sigma\hat{\bar{r}}_j\right)$ is the polarization operator for the emitter i and $\hat{\bar{\mathbf{r}}}_j = \hat{\mathbf{r}}_j - \hat{\mathbf{r}}_i$ is the relative position of the charge j belonging to emitter i.

Applying Eq. (2.27), to the minimal coupling Hamiltonian given by Eq. (2.25), the transformed bosonic operators are

$$\hat{\mathbf{f}}'_\lambda(\mathbf{r},\omega) = \hat{\mathbf{f}}_\lambda(\mathbf{r},\omega) + \frac{1}{\hbar\omega}\int \mathrm{d}^3\mathbf{r}'\hat{\mathbf{P}}^\perp_{\vec{A}}(\mathbf{r}')\cdot\mathbf{G}^*_\lambda(\mathbf{r}',\mathbf{r},\omega), \tag{2.28}$$

so that the electric field $\hat{\mathbf{E}}$ is changed, while the magnetic field $\hat{\mathbf{B}}$ remains the same (and therefore the vector potential $\hat{\mathbf{A}}$). The scalar potential ϕ also remains unchanged. Furthermore, as the Power-Zienau-Woolley transformation is unitary, the commutation relation between the transformed operators remains the same as before. The transformed Hamiltonian is

$$\begin{aligned}\hat{H}' = &\sum_\lambda \int \mathrm{d}^3\mathbf{r}\int \mathrm{d}\omega\ \hbar\omega\hat{\mathbf{f}}'^\dagger_\lambda(\mathbf{r},\omega)\hat{\mathbf{f}}'_\lambda(\mathbf{r},\omega) - \sum_i\int \mathrm{d}^3\mathbf{r}\ \hat{\mathbf{P}}_i\cdot\hat{\mathbf{E}}'(\mathbf{r})\\ &+\sum_i\left[\sum_{j\in i}\frac{\hat{\mathbf{p}}'^2_j}{2m_j} + \frac{1}{2\epsilon_0}\int \mathrm{d}^3\mathbf{r}\ \hat{\mathbf{P}}^2_i(\mathbf{r}) + \int \mathrm{d}^3\mathbf{r}\ \hat{\boldsymbol{\Xi}}_j(\mathbf{r})\times\hat{\mathbf{B}}(\mathbf{r})\right],\end{aligned} \tag{2.29}$$

where $\hat{\boldsymbol{\Xi}}_j(\mathbf{r}) = q_j\hat{\boldsymbol{\Theta}}_j(\mathbf{r}) - \frac{m_j}{m_i}\sum_{k\in i}q_k\hat{\boldsymbol{\Theta}}_k(\mathbf{r}) + \frac{m_j}{m_i}\hat{\mathbf{P}}_i(\mathbf{r})$ and $\hat{\boldsymbol{\Theta}}_j = \hat{\mathbf{r}}\int_0^1 \mathrm{d}\sigma\sigma\delta(\mathbf{r} - \mathbf{r}_i - \sigma\hat{\mathbf{r}}_j)$. If all the interactions with the magnetic field are neglected and the long-wavelength limit is done, the Hamiltonian simplifies to

$$\begin{aligned}\hat{H}' \approx &\sum_\lambda \int \mathrm{d}^3\mathbf{r}\int \mathrm{d}\omega\ \hbar\omega\hat{\mathbf{f}}'^\dagger_\lambda(\mathbf{r},\omega)\hat{\mathbf{f}}'_\lambda(\mathbf{r},\omega) - \sum_i \hat{\boldsymbol{\mu}}_i\cdot\hat{\mathbf{E}}'(\mathbf{r}_i)\\ &+\sum_i\left[\sum_{j\in i}\frac{\hat{\mathbf{p}}'^2_j}{2m_j} + \frac{1}{2\epsilon_0}\int \mathrm{d}^3\mathbf{r}\ \hat{\mathbf{P}}^2_i(\mathbf{r})\right],\end{aligned} \tag{2.30}$$

where the transformed electric field operator $\hat{\mathbf{E}}'(\mathbf{r})$ can be expressed in terms of the ladder operators through its relation with the vector potential.

Addition of classical fields

The macroscopic QED framework also allows the inclusion of external fields that can be described classically, like laser pulses. This can be done by

applying a time-dependent displacement operator [109]

$$T(t) = e^{\sum_n \alpha_n^*(t) f_n - \alpha_n(t) f_n^\dagger}, \tag{2.31}$$

which makes a displacement of a mode n (which runs over $\{\lambda, \mathbf{r}, \omega\}$) in the phase space by an amount $\alpha_n(t) = \alpha_n(0)e^{-i\omega_n t}$, where $\alpha_n(0)$ correspond to the classical amplitudes obtained when the laser is expressed in the basis of these modes. In particular, when this operator is applied to the vacuum, the resulting state is a coherent state (or in this case, a product of coherent states). Then, when a classical field is applied to the empty EM environment, the initial wave function can be taken as a product of coherent states,

$$|\psi(0)\rangle = \prod_n |\alpha_n(0)\rangle = \prod_n e^{\alpha_n(0) f_n^\dagger - \alpha_n(0)^* f_n} |0\rangle. \tag{2.32}$$

Applying the inverse of the displacement operator given by Eq. (2.31), the classical and quantum fields can be split in the Hamiltonian, in order to avoid the necessity for explicitly propagating this classical field within the quantum calculation. This transformation adds a time-dependent energy shift that does not affect the dynamics but allows to write the electric field as a sum of two different components $\hat{\tilde{\mathbf{E}}}(\mathbf{r}) = \hat{\mathbf{E}}(\mathbf{r}) + \mathbf{E}_{cl}(\mathbf{r})$. Then, the classical component can describe the action of an external field into the full system without any additional terms. It is worth noting that $\mathbf{E}_{cl}(\mathbf{r})$ refers to the medium-assisted classical pulse at the position of the emitters, so any deformation due to the material structure must be included in this term. Moreover, as the medium-assisted field operators $\hat{\mathbf{E}}(\mathbf{r})$ and $\hat{\mathbf{B}}(\mathbf{r})$, expressed in terms of $\hat{\mathbf{f}}_\lambda(\mathbf{r}, \omega)$, solve Maxwell's equations, the classical pulse can be obtained by classical solutions of Maxwell's equations.

Therefore, the wave function transforms as $|\psi'\rangle = T(t)|\psi\rangle$, which corresponds to transforming the Hamiltonian as

$$\hat{\mathcal{H}} = T(t)\hat{H}'T^\dagger(t) - iT(t)\partial_t T^\dagger(t) = \hat{H}' - \sum_i \hat{\boldsymbol{\mu}}_i \cdot \mathcal{E}(t, \mathbf{r}_i), \tag{2.33}$$

where $\mathcal{E}(t, \mathbf{r}_i) = \sum_n g_n (\alpha_n(t) + \alpha_n^*(t))$ is the classical field at each emitter position. From the previous transformation, also a term $\sum_n \omega_n \alpha_n(t)\alpha_n^*(t) = \sum_n \omega_n |\alpha_n(0)|^2$ arises, but this can be neglected because it just corresponds to a constant energy shift. Eq. (2.33) is the effective Hamiltonian that takes the initial state as the vacuum state with the emitter in its ground state.

When the above transformation is applied to the Hamiltonian, the observables are also transformed according to

$$\langle \psi | A | \psi \rangle = \langle \psi' | T(t) A T^\dagger(t) | \psi' \rangle, \tag{2.34}$$

such that, e.g., $\langle \psi | a_n | \psi \rangle = \langle \psi' | a_n + \alpha_n(t) | \psi' \rangle$. This takes into account that the "quantum" field generated by the laser-emitter interaction interferes with the classical pulse propagating through the structure, and ensures a correct description of absorption of the pulse, coherent scattering, and similar effects. The above properties imply that within this framework, the action of any incoming laser pulse on the full emitter-cavity system can be described purely by the medium-enhanced classical electric field driving the emitter, with no additional explicit driving of any EM modes.

2.2 Two-level system interacting with the EM field

Macroscopic QED describes general medium-assisted light-matter interactions. However, as in the following the quantum emitters will be always approximated as two-level systems, the general Hamiltonian can be specialized to this case. Then, the QE consists of an excited state $|e\rangle$ and a ground state $|g\rangle$ separated an energy $\hbar\omega_e$. The state of the two-level system can be

thus written as

$$|\psi(t)\rangle = c_g(t)|g\rangle + c_e(t)|e\rangle, \tag{2.35}$$

where $c_g(t)$ and $c_e(t)$ are (normal) time-dependent complex scalars that define the probability amplitude of the system to be in the ground or the excited states, respectively. Applying the atomic Hamiltonian to the previous (eigen)states gives

$$\hat{H}_e|g\rangle = 0|g\rangle, \qquad \hat{H}_e|e\rangle = \omega_e|e\rangle, \tag{2.36}$$

where it is considered that the origin in energy is the ground state of the two-level system. Imposing the closure theorem, $|g\rangle\langle g| + |e\rangle\langle e| = 1$ and the orthogonality between states, one finds that the atomic Hamiltonian is

$$H_e = \hbar\omega_e|e\rangle\langle e|. \tag{2.37}$$

Moreover, $|g\rangle$ and $|e\rangle$ form a basis in the Hilbert space and they can be written in the canonical basis as

$$|g\rangle = \begin{pmatrix} 1 \\ 0 \end{pmatrix}, \qquad |e\rangle = \begin{pmatrix} 0 \\ 1 \end{pmatrix}. \tag{2.38}$$

This representation allows to define raising and lowering operators, $\hat{\sigma}^+$ and $\hat{\sigma}^-$ respectively, which can also be written in matrix form

$$\hat{\sigma}^- = |g\rangle\langle e| = \begin{pmatrix} 0 & 1 \\ 0 & 0 \end{pmatrix}, \qquad \hat{\sigma}^+ = |e\rangle\langle g| = \begin{pmatrix} 0 & 0 \\ 1 & 0 \end{pmatrix}. \tag{2.39}$$

Both operators describe a transition between the ground and the excited state and follow the anticommutation relation[2]

$$\left\{\hat{\sigma}^+, \hat{\sigma}^-\right\} = \mathbb{I}. \tag{2.40}$$

[2]In general, $\left[\sigma_i^-, \sigma_j^+\right] = \left(1 - 2\sigma_i^+\sigma_i^-\right)\delta_{ij}$, i.e., each emitter fulfil the anticommutation relation with itself ($i = j$) but the system is not fermionic, in the sense that the wavefunction is symmetric under an exchange of two emitters positions.

Moreover, these operators can be related with the Pauli matrices, so that the interaction between one emitter and a photon can be expressed through them. The Pauli matrices are

$$\hat{\sigma}^x = \begin{pmatrix} 0 & 1 \\ 1 & 0 \end{pmatrix}, \qquad \hat{\sigma}^y = \begin{pmatrix} 0 & -i \\ i & 0 \end{pmatrix}, \qquad \hat{\sigma}^z = \begin{pmatrix} 1 & 0 \\ 0 & -1 \end{pmatrix}, \tag{2.41}$$

so that $\hat{\sigma}^x = \left(\hat{\sigma}^+ + \hat{\sigma}^-\right)$, $\hat{\sigma}^y = -i\left(\hat{\sigma}^+ - \hat{\sigma}^-\right)$ and $\hat{\sigma}^z = \hat{\sigma}^+\hat{\sigma}^- + \hat{\sigma}^-\hat{\sigma}^+$.

The interaction between the field and one two-level system can also be derived so that in the long-wavelength limit the dipole moment, shown in Eq. (2.30), becomes (for $i = 1$) $\hat{\boldsymbol{\mu}} = \boldsymbol{\mu}^{eg}\left(|e\rangle\langle g| + |g\rangle\langle e|\right)$, where $\boldsymbol{\mu}^{eg} = \langle g|\hat{\boldsymbol{\mu}}|e\rangle = \langle e|\hat{\boldsymbol{\mu}}|g\rangle$ is the transition dipole moment between the states of the emitter and can be assumed real. Finally, the Hamiltonian (2.30) can be written as

$$\hat{H}' \approx \sum_{\lambda} \int \mathrm{d}^3\mathbf{r} \int \mathrm{d}\omega\ \hbar\omega\ \hat{\mathbf{f}}'^{\dagger}_{\lambda}(\mathbf{r},\omega)\hat{\mathbf{f}}'_{\lambda}(\mathbf{r},\omega) + \frac{\omega_e}{2}\hat{\sigma}^z - \left(\hat{\sigma}^+ + \hat{\sigma}^-\right)\boldsymbol{\mu}^{eg}\cdot\hat{\mathbf{E}}'(\mathbf{r}_e). \tag{2.42}$$

2.3 Spectral density

To characterize the light-matter interaction, we will consider the spontaneous decay of an excited two-level emitter and the emission of one photon to the vacuum, i.e., the classical Wigner-Weisskopf problem [110]. For simplicity, starting with Eq. (2.42) the rotating wave approximation (RWA) is made. This approximation neglects the terms $e^{\pm(\omega_e+\omega)t}$, which rotate rapidly and can be averaged away, while the terms $e^{\pm(\omega_e-\omega)t}$ survive. Then, the Hamilto-

nian (2.42) is of the form

$$\begin{aligned}\hat{H} = &\sum_{\lambda}\int \mathrm{d}^3\mathbf{r}\int \mathrm{d}\omega\ \hbar\omega\hat{\mathbf{f}}^{\dagger}_{\lambda}(\mathbf{r},\omega)\hat{\mathbf{f}}_{\lambda}(\mathbf{r},\omega) + \frac{\omega_e}{2}\hat{\sigma}^z \\ &-\sum_{\lambda}\int \mathrm{d}^3\mathbf{r}\int \mathrm{d}\omega\left(\boldsymbol{\mu}_e\cdot\mathbf{G}_{\lambda}(\mathbf{r}_e,\mathbf{r},\omega)\hat{\mathbf{f}}_{\lambda}(\mathbf{r},\omega)\sigma^{+} + \mathrm{H.c.}\right),\end{aligned} \tag{2.43}$$

where the electric field has been substituted by its expansion in terms of the field operators given by Eq. (2.23). In the interaction picture, the total system obeys the Schrödinger equation

$$\frac{\mathrm{d}}{\mathrm{d}t}\psi(t) = -iH_I(t)\psi(t), \tag{2.44}$$

where $H_I(t)$ is given by the second line of Eq. (2.43) and $\psi(t)$ is the wave-function, which in it most general form within the single-excitation subspace is

$$|\psi(t)\rangle = \alpha(t)|e,0\rangle + \int \mathrm{d}\mathbf{r}\int \mathrm{d}\omega\beta_{\lambda}(\mathbf{r},\omega,t)|g,1_{\mathbf{r},\omega}\rangle. \tag{2.45}$$

Here $|g,1_{\mathbf{r},\lambda,\omega}\rangle = \hat{\mathbf{f}}^{\dagger}_{\lambda}(\mathbf{r},\omega)|g,0\rangle$ and $\alpha(t)$ and $\beta_{\lambda}(\mathbf{r},\omega,t)$ are time-dependent scalars that give the amplitude probability of the wave-function to be in one of the states. Using the Schrödinger equation the decay of the quantum emitter in the environment can be derived, so that the amplitudes of the emitter $\alpha(t)$ and the mode $\beta_{\lambda}(\mathbf{r},\omega,t)$ are given by

$$\frac{\mathrm{d}}{\mathrm{d}t}\tilde{\alpha}(t) = -\frac{i}{\hbar}\sum_{\lambda}\int \mathrm{d}^3\mathbf{r}\int \mathrm{d}\omega e^{-i(\omega-\omega_e)t}\mu_e\cdot\mathbf{G}_{\lambda}(\mathbf{r}_e,\mathbf{r},\omega)\tilde{\beta}_{\lambda}(\mathbf{r},\omega,t), \tag{2.46}$$

$$\frac{\mathrm{d}}{\mathrm{d}t}\tilde{\beta}_{\lambda}(\mathbf{r},\omega,t) = -\frac{i}{\hbar}e^{i(\omega-\omega_e)t}\mu_e\cdot\mathbf{G}^{*}_{\lambda}(\mathbf{r}_e,\mathbf{r},\omega)\tilde{\beta}_{\lambda}(\mathbf{r},\omega,t), \tag{2.47}$$

where the tilde variables are $\tilde{\alpha}(t) = \alpha(t)e^{i\omega_e t}$ and $\tilde{\beta}_{\lambda}(\mathbf{r},\omega,t) = \beta_{\lambda}(\mathbf{r},\omega,t)e^{i\omega t}$. Assuming that there are no excitations in the reservoir at the initial state, i.e., $\beta_{\lambda}(t=0) = 0$, the closed equation for the quantum emitter is

$$\frac{\partial}{\partial t}\tilde{\alpha}(t) = -\int_0^t \mathrm{d}t' K(t-t')\tilde{\alpha}(t'), \tag{2.48}$$

where $K(t-t')$ is the kernel, which is given by

$$K(t-t') = \int_0^\infty \mathrm{d}\omega e^{i(\omega-\omega_e)(t-t')} \frac{\hbar\omega^2}{\pi\epsilon_0 c^2} \boldsymbol{\mu}_e \cdot \mathrm{Im}\mathbf{G}(\mathbf{r}_e, \mathbf{r}_e, \omega) \cdot \boldsymbol{\mu}_e. \tag{2.49}$$

The previous expression is obtained by using the Green's function identity,

$$\sum_\lambda \int \mathrm{d}^3\mathbf{s}\ \mathbf{G}_\lambda(\mathbf{r}, \mathbf{s}, \omega) \cdot \mathbf{G}_\lambda^{*T}(\mathbf{r}', \mathbf{s}, \omega) = \frac{\hbar\omega^2}{\pi\epsilon_0 c^2} \mathrm{Im}\mathbf{G}(\mathbf{r}, \mathbf{r}', \omega), \tag{2.50}$$

where $\mathbf{r} = \mathbf{r}' = \mathbf{r}_e$. The kernel can be written in terms of the spectral density, $J(\omega)$, which is is related to the Green's function by [68, 74, 75, 111]

$$J(\omega) = \frac{\hbar\omega^2}{\pi\epsilon_0 c^2} \boldsymbol{\mu}_e \cdot \mathrm{Im}\mathbf{G}(\mathbf{r}_e, \mathbf{r}_e, \omega) \cdot \boldsymbol{\mu}_e, \tag{2.51}$$

Therefore, the kernel (2.54) can be rewritten as

$$K(t-t') = \int \mathrm{d}\omega J(\omega) e^{i(\omega_e-\omega)(t-t')}, \tag{2.52}$$

so that the interaction between the quantum emitter and EM modes is completely determined by $J(\omega)$. In general, the solution to the time evolution of $\tilde{\alpha}(t)$ is very complicated, as the dynamics at time t depend on all previous times $0 < t' < t$. Therefore, in general it must be solved numerically.

Although the previous derivation has been done in the context of EM modes, the same can be done for a general Hamiltonian describing the interaction between a quantum emitter and a collection of bosonic modes, which reads

$$H = H_e + A^\dagger \cdot \mathbf{H} \cdot \vec{A} + \vec{g} \cdot \left(\vec{A} + \vec{A}^\dagger\right), \tag{2.53}$$

where $\vec{A}^T = (a_1, a_2, \ldots, a_n, \ldots)^T$ describes the collection of bosonic modes and $\vec{g}^T = (g_1, g_2, \ldots, g_\alpha, \ldots)^T$ describes the interaction operators between the matter component and the environment. Analogous equations to Eqs. (2.46), (2.47) can be derived by simply substituting the interaction terms by g_n (note here that in the previous derivation the frequency was treated as a continuum and

now the collection of modes are discrete in frequency, so the integral must also be replaced by a sum). In this notation, it is easier to see that the kernel (2.49) is given by the correlation function

$$K(t-t') = \mathrm{Tr}_R \left\{ \mathcal{G}(t)\mathcal{G}^\dagger(t')\rho_R \right\} e^{i\omega_e(t-t')}, \tag{2.54}$$

where $\mathcal{G} = \vec{g} \cdot \vec{A}$ and ρ_R is the state of the collection of modes. The spectral density, defined as the product of the interaction strength between the emitter and the reservoir mode n, weighted by the density of states of the environment, is for $T = 0$ (where $\rho_R = |0\rangle\langle 0|$ is the vacuum state of the reservoir)

$$J(\omega) = \sum_n |g_n|^2 \, \delta(\omega - \omega_n), \tag{2.55}$$

and it is a physical quantity general for any quantum system (it is not limited to the interaction between matter and EM fields).

When the temperature is non-zero, the density of the reservoir can be assumed to be in a thermal state so that

$$\rho_{R,\omega} = \frac{e^{-\omega \mathbf{f}^\dagger(\omega)\mathbf{f}(\omega)/T}}{\mathrm{Tr}_R e^{-\omega \mathbf{f}^\dagger(\omega)\mathbf{f}(\omega)/T}}, \tag{2.56}$$

and the interaction between the emitter and the collection of modes is described by both the spectral density and the temperature of the bath[112].

Using the Sokhotski-Plemelj formula, $\lim_{\epsilon\to 0} \frac{1}{\omega'-\omega-i\epsilon} = \mathcal{P}\frac{1}{\omega'-\omega} + i\pi\delta(\omega'-\omega)$, the spectral density in Eq. (2.55) can be written in the form

$$J(\omega) = \lim_{\epsilon\to 0} \frac{1}{\pi} \vec{g}\, \mathrm{Im}\left[\frac{1}{\mathbf{H} - \omega - i\epsilon}\right] \vec{g}^\dagger. \tag{2.57}$$

This expression (and its generalization to multiple emitters and multiple dipole moment operators) will be especially useful in **chapter 5**.

2.4 Coupling regimes

When a QE interacts with a collection of EM modes, there are different regimes of interaction that can be distinguished depending on the parameters of the system. To discuss them, we consider a cavity or resonator in which the spectral density can be approximated as a Lorentzian, so that

$$J(\omega) = \frac{g^2}{\pi} \frac{\kappa/2}{(\omega - \omega_c)^2 + \kappa^2/4}, \tag{2.58}$$

where κ describes the Lorentzian width, and therefore the cavity losses.

Weak coupling regime

The weak coupling regime occurs when the coupling strength is much lower than the losses ($g \ll \kappa, \gamma$), so that the width of the spectral density is large compared to its amplitude, and therefore $J(\omega)$ is sufficiently smooth so that in equation (2.52) the integral oscillates rapidly except for $\omega \approx \omega_e$. Equation (2.48) can be written as

$$\frac{\partial}{\partial t}\tilde{\alpha}(t) = -J(\omega_e) \int_0^t \mathrm{d}t' \int_0^\infty e^{i(\omega_e - \omega)(t-t')} \tilde{\alpha}(t'). \tag{2.59}$$

The same argument of rapidly rotating terms allows to replace the lower limit in the integral by $-\infty$, such that the frequency integral becomes a representation of the Dirac delta function $\int_{-\infty}^{\infty} e^{-i\omega t} \mathrm{d}\omega = 2\pi\delta(t)$, leading to

$$\frac{\partial}{\partial t}\tilde{\alpha}(t) \approx -2\pi J(\omega_e) \int_0^t \mathrm{d}t' \approx -\pi J(\omega_e)\tilde{\alpha}(t), \tag{2.60}$$

where the δ-function has been split since the upper limit of the last integral is centered at the function. Therefore, the decay of the QE is given by

$$\tilde{\alpha}(t) = e^{-\frac{1}{2}\gamma t}, \tag{2.61}$$

where $\gamma = 2\pi J(\omega_e)$ is the radiative decay rate. Therefore, the probability of the quantum emitter to be in its excited state, which is given by $|\tilde{\alpha}(t)|^2$, decays exponentially with rate γ. The previous assumption is known as the Markov approximation. In particular, when the cavity mode and the QE are on resonance, the decay is $\gamma = 4g^2/\kappa$.

In free-space the spectral density in is given by

$$J_0(\omega) = \frac{\omega^3 |\mu_e|^2}{6\pi^2 \hbar \epsilon_0 c^3}, \tag{2.62}$$

where c is the speed of light an ϵ_0 the free-space dielectric permittivity. To achieve the previous expression Eq. (2.55) can be used, knowing that for free space $\mathrm{Im}\mathbf{G}_0(\mathbf{r}, \mathbf{r}, \omega) = \omega/6\pi c$, so that the decay rate is given by $\gamma_0 = \frac{\omega^3 |\mu_e|^2}{3\pi\hbar\epsilon_0 c^3}$. This decay rate is the same as the one given by Fermi's Golden rule [10].

The difference in the decay rates for an emitter enclosed in a cavity and in free space is because the vacuum density of states at the position of the emitter changes when the EM field is confined. Therefore, if one of the resonant cavity modes and the emitter are in resonance, the emission is enhanced via the Purcell effect [8]. The Purcell factor is defined as

$$F_P = \frac{\gamma}{\gamma_0} = \frac{J(\omega)}{J_0(\omega)} = \frac{6\pi c}{\omega} \vec{n} \cdot \mathbf{G}(\mathbf{r}_e, \mathbf{r}_e, \omega) \cdot \vec{n}, \tag{2.63}$$

where $\vec{n}$ is the unit vector defining the orientation of the emitter. Figure **2.3** shows a sketch of a two-level system inside a cavity in the weak coupling regime (left). The spontaneous decay from the excited state of a resonant emitter to its ground state is enhanced inside the cavity with respect to free space (right).

Purcell predicted the enhancement of the spontaneous transition rate of a nuclear magnetic moment coupled to a resonant electronic device compared to the free-space rate in 1946. However, the experimental observation of this effect requires the dimensions of the device to be similar to the emission wavelength, which was technically demanding. In 1966, the effect of planar interfaces on

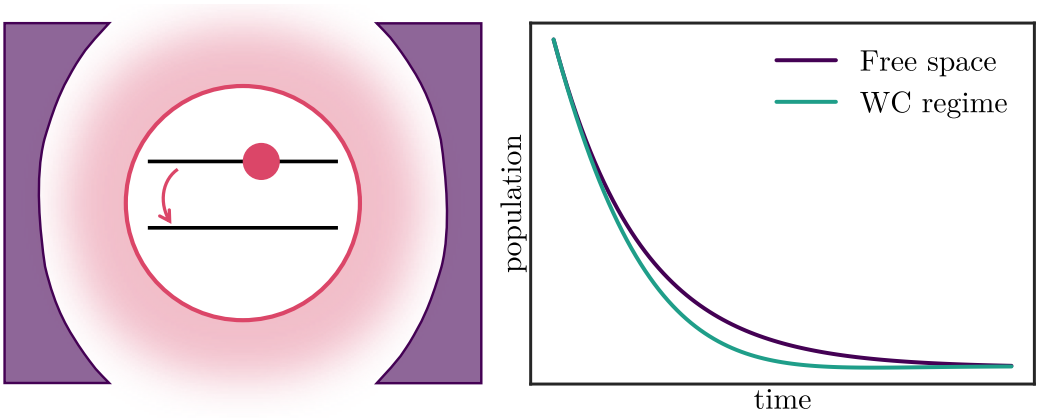

Fig. 2.3.: Sketch of one QE, represented as a 2-level emitter, inside a cavity in the weak coupling regime (left). The coupling between the QE and the EM field inside the cavity is smaller than the losses, so an excitation of the emitter decays exponentially (right). The EM field inside the cavity changes with respect to the free space, enhancing the QEs emission.

the decay rate of molecules was observed [113] and the effect of a cavity on atomic decay rates was studied in 1983 using Rydberg atoms [114]. Moreover, the emitter's emission can also be suppressed if the QE and the cavity modes are off-resonance [115, 116]. Before Purcell's prediction, it was believed that the emission of an emitter was an intrinsic property that depended only on it. However, these two effects demonstrated that it is not the case, but the emission depends on the EM environment surrounding it.

Strong coupling regime

Considering a more general scenario in which the spectral density is not necessarily dominated by the losses, but instead assuming that $\kappa \ll \omega_c$, so that the frequency integral can be extended to the whole real axis, a new expression

for the interaction kernel can be written,

$$K(t-t') \approx \int_{-\infty}^{\infty} \frac{g^2}{\pi} \frac{e^{i(\omega_e-\omega)(t-t')}\kappa/2}{(\omega-\omega_c)^2+\kappa^2/4} = g^2 e^{-i\left(\omega_c - i\frac{\kappa}{2}\right)(t-t')}, \tag{2.64}$$

so that Eq. (2.48) transforms to

$$\frac{\partial}{\partial t}\tilde{\alpha}(t) = -g^2 \int_0^t \mathrm{d}t' e^{-i\left(\omega_c - i\frac{\kappa}{2} - \omega_e\right)(t-t')}\tilde{\alpha}(t'). \tag{2.65}$$

The previous dynamics are equivalent to those of one QE interacting with a single cavity mode with frequency $\Omega_C = \omega_c - i\frac{\kappa}{2}$. The Hamiltonian in this case is, in the RWA[3], the so-called Jaynes-Cummings (JC) model [118]

$$H_{JC} = \hbar\omega_e|e\rangle\langle e| + \hbar\Omega_C\left(a^\dagger a + \frac{1}{2}\right) - g(\sigma^- a^\dagger + \sigma^+ a), \tag{2.66}$$

where the coupling strength g is given by

$$g = \boldsymbol{\mu}\cdot\boldsymbol{E}_{1ph} = \boldsymbol{\mu}\cdot\boldsymbol{n}_{\boldsymbol{E}}\sqrt{\frac{\hbar\omega_e}{2\epsilon_0 V_{\text{eff}}}}. \tag{2.67}$$

Here $\boldsymbol{\mu}$ is the dipole transition moment of the emitter and $\left|\mathbf{E}_{1ph}\right|$ is the quantized electric field strength of the mode, associated with one photon, at the emitter position.

Writing the JC Hamiltonian in matrix form and diagonalizing, one finds that the eigenvalues are

$$E_\pm = \frac{\omega_e + \Omega_C}{2} \pm \frac{1}{2}\sqrt{(\omega_e - \Omega_C)^2 + 4|g|^2}. \tag{2.68}$$

In the previous equation the decay of the emitter can also be included by simply substituting $\omega_e \to \omega_e - i\frac{\gamma}{2}$. Therefore, when $g = 0$ the dynamics are

[3]The Hamiltonian that describes the interaction between one QE and a single EM mode including the counter-rotating terms is known as the Rabi model [117], $H_R = \hbar\omega_e|e\rangle\langle e| + \hbar\Omega_C\left(a^\dagger a + \frac{1}{2}\right) - g(\sigma^+ + \sigma^-)(a^\dagger + a)$. This Hamiltonian, in contrast to the JC mode, does not conserve the number of excitations $N_{\text{exc}} = a^\dagger a + \sigma^+\sigma^-$.

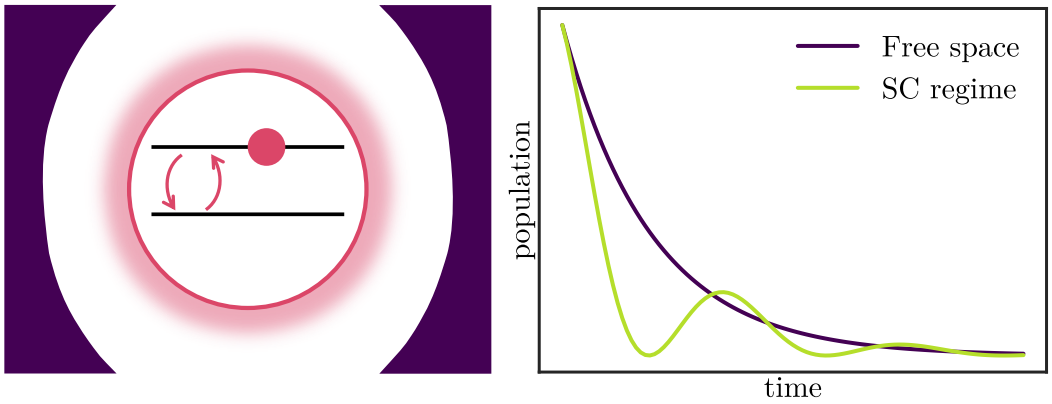

Fig. 2.4.: Sketch of one QE, represented as a 2-level emitter, inside a cavity in the strong coupling regime (left). The coupling between the QE and the EM field inside the cavity overcomes the losses, so Rabi oscillations are seen in the QE population. As the system still presents losses, the population is damped exponentially.

governed by the losses, which results in the exponential decay characteristic of the weak-coupling regime. When the coupling increases and overcomes the decay rates of both the cavity and the emitter, i.e., $g \gg \kappa, \gamma$, the system enters in the strong coupling regime. Then, the dynamics change and show the so-called Rabi oscillations, which indicate a coherent energy exchange between the EM mode and the QE. On resonance, this exchange happens at the Rabi frequency[4] $\Omega_R = 2g$. The left panel in figure **2.4** shows a sketch of a QE inside a cavity in the strong coupling regime, and the right panel shows the decay in free space (purple line) and the Rabi oscillations of an initially excited QE (green line), which emits and reabsorbs a photon several times before it leaves the cavity. The amplitude of the oscillations decreases exponentially[5] due to the emitter and cavity decay rates.

[4]The coupling strength determines the Rabi frequency so that as it increases, Rabi oscillations are quicker.

[5]The decay rate that gives the exponential damping of the population amplitude is determined by the QE and cavity losses.

This oscillatory behavior indicates that the QE and the field are not the eigenstates of the system anymore, but both subsystems hybridize, forming polaritons, whose eigenfrequencies are given by Eq. (2.68). The one with a lower frequency is known as Lower Polariton (LP), while the one with a higher frequency is called Upper Polariton (UP). Figure **2.5**(a) shows a sketch of the hybridization of the eigenstates and the formation of polaritons. The difference between the polariton frequencies is the Rabi frequency Ω_R. Panel (b) shows the real part of the eigenfrequencies with respect to the energy difference between the cavity mode and the emitter for a fixed coupling $g = 0.07\omega_e$, while the detuning between the cavity and the emitter changes. Black dashed lines correspond to the "bare" emitter and cavity frequencies, i.e., $g = 0$. For the SC case, when the emitter and the cavity are off-resonance, the eigenfrequencies are very similar to the "bare" ones. When they are resonant, there is an anticrossing behavior. Here again, the distance between both eigenfrequencies at 0 detuning gives the Rabi splitting.

Moreover, the real (panel (c)) and imaginary (panel (d)) parts of the eigenfrequencies with respect to the coupling strength (normalized by the real part of the emitter frequency) are shown in figure **2.5**. Now, $\omega_e = \omega_c$, while $\kappa = 0.1\omega_e$ and $\gamma = 0.04\omega_e$. When the coupling is small compared to the losses, the real value of the eigenfrequencies is degenerate and it is not affected by changes in the coupling, while the imaginary part starts in $-\kappa/2$ and $-\gamma/2$ for $g = 0$ and changes as the coupling increases (WC regime). When the coupling exceeds the losses, the real part of the eigenfrequencies split, and their distance increases linearly with the coupling, while the imaginary part is degenerated and does not change with g (SC regime). The distance between the real part of both eigenfrequencies at one fixed coupling strength corresponds to the Rabi splitting.

Finally, it is noted here that although the diagonalization has been done

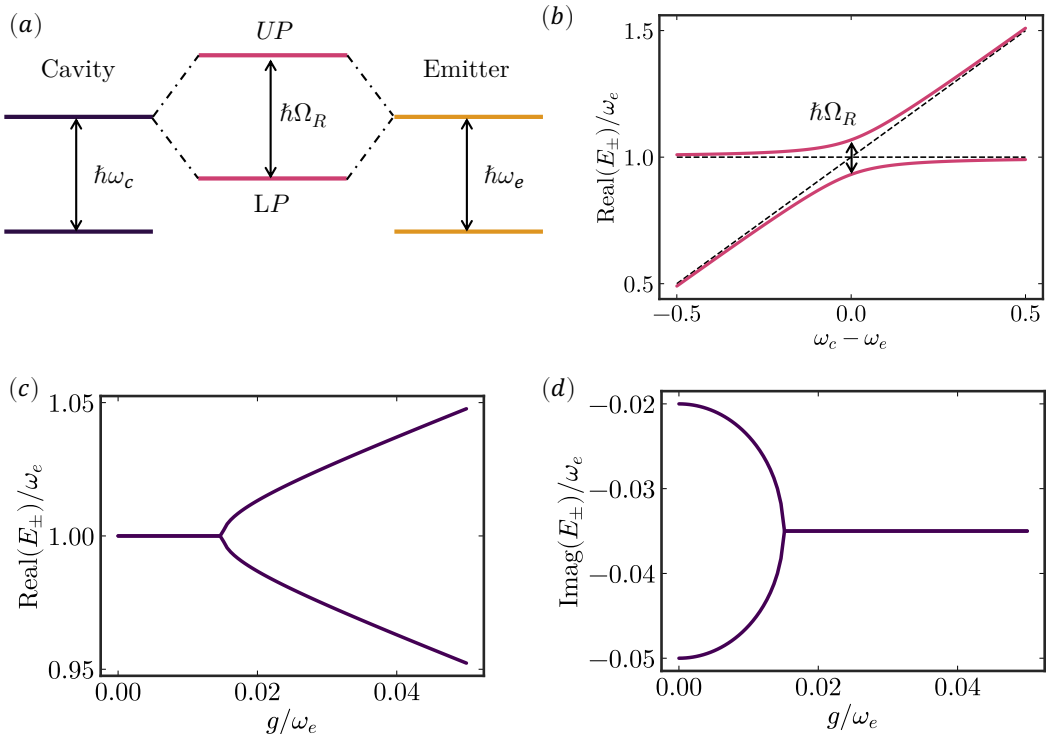

Fig. 2.5.: (a) Scheme of the hybridization of one EM mode (purple) with frequency $\hbar\omega_c$ and a quantum emitter (yellow) with energy $\hbar\omega_e$. The upper (UP) and lower (LP) polaritons are formed, separated by the Rabi splitting $\hbar\Omega_R$. (b) Real part of the eigenenergies for a coupling $g = 0.07\omega_e$. The straight dashed lines show the "bare" frequencies of both constituents. (c) Real and (d) imaginary part of $E_\pm$ with respect to the coupling strength.

for the RWA, the same conclusions can be made for the Rabi model in the scope of this thesis, where the couplings achieved will always be small enough for the counter-rotating terms to be negligible[6]. Moreover, the SC is not necessarily a

[6]The inclusion of counter-rotating terms also changes the lowest-energy state so that while in the JC model it consists of an empty cavity and the emitter in its ground state, in the Rabi model there can be some atomic and photonic excitations. As the coupling increases, the system is more favorable to present these excitations and the counter rotating terms become significant. Therefore, the RWA approximation is justified in the weak and strong coupling regimes, but

quantum effect and can often be modeled through classical electromagnetism (EM) [14, 119]. In that case, the material excitations are represented through the dielectric function of the medium (e.g., through a resonance of Drude-Lorentz form) or through a polarizable dipole for single emitters [120, 121].

The first experimental observation of strong coupling was in 1965 [122] between light and the bulk modes of a crystal, while surface exciton-polaritons where observed approximately a decade later [123]. Strong coupling within a high-Q microwave cavity was realized in 1983 using a collection of Rydberg atoms [124]. When an ensemble of N QEs interact with a single photonic mode within a cavity, the coupling strength increases as $g_N = g\sqrt{N}$ [125]. This phenomenon is known as collective strong coupling and is a common approach when measuring strong coupling in optical cavities because the Rabi splitting is increased at the same rate as the coupling strength, thus making it more feasible to measure. It occurs because an excitation in this case can be coherently distributed over the N emitters, forming a so-called bright state with increased light-matter coupling. At the same time, all $N-1$ orthogonal ways of distributing an excitation over the emitters show negligible coupling to the cavity mode due to destructive interference between the dipole transitions in the different emitters. These superpositions are the so-called dark states (DS), which play a major role in molecular polariton dynamics [126, 127]. Collective SC is theoretically described by the Tavis-Cummings model [128] when the RWA approximation is made and the Dicke model [129] otherwise.

When realizing collective SC, the maximally reachable Rabi splitting for a given material is determined by the density of dipoles but independent of the specifics of the photon mode [130, 132, 133]. This can be shown explicitly by introducing Eq. (2.67) into the expression of the collective coupling strength

fails in the ultra strong coupling regime, where coupling strengths are comparable to the transition frequencies.

and using that the effective mode volume is related to the physical volume occupied by the mode. Therefore,

$$g_N \propto \mu\sqrt{N/V} \propto \mu\sqrt{\rho}, \tag{2.69}$$

where ρ is the density of the material. The number of emitters interacting with the mode is thus proportional to the their density times the volume. A more careful calculation shows that the Rabi splitting depends on the dipole density multiplied by a "filling factor" between 0 and 1 that determines what fraction of the mode volume is filled with the material (weighted with the position-dependent quantized field strength) [35, 130].

For single emitters, achieving the strong coupling regime is noticeably more challenging than in the collective regime. In this situation, the single-emitter coupling strength g has to become comparable to the emitter and cavity decoherence rates, which can only be achieved by either increasing the coupling strength or decreasing the decoherence rate sufficiently. Nevertheless, single atom SC interacting with a microwave cavity was measured in 1985 [134]. Rabi oscillations were measured two years later [135], and strong coupling within an optical cavity was observed in 1992 [136]. Along this decade, Rabi splittings of $1 - 20$ meV were measured for Quantum Wells (QW) in semiconductor microcavities [38, 137, 138]. In 2004, the SC regime for a single quantum dot in a semiconductor micropillar cavity was achieved, with a Rabi splitting of ~ 100 μeV [139]. These setups, where the absolute coupling strength is a small fraction of the excitation energy, necessarily require very long-lived emitters and cavity modes, which in turn implies cryogenic temperatures. Rabi splittings from 100 meV to more than 1 eV have been measured using organic molecules even at room temperature [39, 140–142] and the SC regime has also been achieved for single organic molecules at room temperature by using extremely localized surface plasmons in narrow gaps [57]. Very recently, strong coupling and quantum nonlinearity have been observed for a single molecule

at cryogenic temperatures [143]. The dependence of the Rabi splitting on the density and the filling factor explains why similar Rabi splittings have been observed in the literature for very different photonic systems: when a cavity is completely filled with the material in question, the Rabi splitting is equal to the bulk polariton splitting obtained by Hopfield in 1958 [144].

If the coupling strength increases more and becomes comparable to the QE frequency $g \sim 0.1\omega_e$, higher-order processes, which hybridize states with different number of excitations, become observable. These observations correspond to the Ultrastrong Coupling (USC) regime, and this size of Rabi splittings was measured in 2009 in a microcavity-embedded doped GaAs quantum well [145] and in 2010 in a superconducting circuit with a single two-level system [146]. Several kinds of organic materials can reach the ultrastrong coupling regime [147]. Although the limit between SC and USC is taken at $g \sim 0.1\omega_e$, this is a historical convention and higher-order properties, such as the existence of excitations in the lowest-energy state of the emitter-cavity system, scale continuously with the coupling strength. Apart from the molecule density, the alignment of the dipole moments of the molecules with the electric field inside the cavity also modifies the Rabi splitting. Therefore, if instead of randomly oriented molecules, aligned dipole moments are used, large Rabi splittings up to $\Omega_R = 1.8$ eV have been measured [148]. These large values also mean that cavity modes with very large decay rates κ (or equivalently, short lifetimes $\tau = 1/\kappa$ or low quality factors ω_c/κ) can be used while still reaching the strong coupling regime.

2.5 Open quantum systems

As mentioned in the previous section, the light-matter interaction is completely characterized by the spectral density, and the treatment of a quantum emitter interacting with a collection of EM modes is analogous to a more general description of an emitter (or even more general, a "system") interacting with an "environment" (or "reservoir" or "bath") of bosonic modes. Therefore, the framework of open quantum systems is also valid to study light-matter interactions [86, 149, 150]. In a particular setup, the distinction between the system and the environment is in principle arbitrary, but is often based on a clear difference in their physical properties (for an atom enclosed in a cavity, for example, the system corresponds to the bare emitter and the environment is the medium-assisted ensemble of EM modes). Moreover, the system constitutes the part of the whole arrangement whose dynamics are of interest, while the environment is formed by a large number of modes that additionally are not affected by the system. This framework is also valid for other quantum systems, in which typical environments can be, for example, phonons [151], or ensembles of auxiliary quantum systems [152].

To describe the interaction between some system and its surroundings the master equation formalism is used for both closed and open quantum systems. The time evolution of a quantum system is given, according to the Schrödinger equation, by

$$\frac{\mathrm{d}}{\mathrm{d}t}|\psi(t)\rangle = -\frac{i}{\hbar}\hat{H}(t)|\psi(t)\rangle. \tag{2.70}$$

The solution to this equation can be expressed in terms of the unitary evolution operator $U(t, t_0)$, which transforms one state from time t_0 to time t, i.e., $|\psi(t)\rangle = U(t, t_0)|\psi(t_0)\rangle$. Substituting this expression in Eq. (2.70), one obtains

$$\frac{\mathrm{d}}{\mathrm{d}t}U(t, t_0) = -\frac{i}{\hbar}\hat{H}(t)U(t, t_0). \tag{2.71}$$

If the whole quantum system is closed, i.e., it is isolated from its environment, the Hamiltonian is time-independent and the evolution operator is

$$U(t,t_0) = e^{-\frac{i}{\hbar}\hat{H}(t-t_0)}. \tag{2.72}$$

When the system in consideration is in a mixed state, i.e., consists of a mixture of several states $|\psi_n(t_0)\rangle$, sometimes it is convenient to express it in terms of the density matrix $\hat{\rho}$. This matrix is defined, for an initial time t_0, as

$$\hat{\rho}(t_0) = \sum_n w_n |\psi_n(t_0)\rangle\langle\psi_n(t_0)|, \tag{2.73}$$

where w_n are normalized positive weights. As each of the states $|\psi_n(t_0)\rangle$ evolves following the Schrödinger equation, the density matrix evolves in time as

$$\hat{\rho}(t) = U(t,t_0)\hat{\rho}(t_0)U^\dagger(t,t_0), \tag{2.74}$$

so by differentiating it one can get the Liouville-von Neumann equation

$$\partial_t\hat{\rho}(t) = -\frac{i}{\hbar}\left[\hat{H}(t),\hat{\rho}(t)\right]. \tag{2.75}$$

If the time-dependence is transferred from the density matrix to the operators that act in the system one moves from the Schrödinger picture to the Heisenberg picture. This picture is the one used in the cumulant expansion derivation of **chapter 3**. To do the transformation it is assumed that the density matrix in both formulations coincides[7] at the initial time t_0, i.e., $\hat{\rho}(t_0) = \hat{\rho}_H(t_0)$. Considering an operator $\hat{A}$, both pictures are related by the transformation $\hat{A}_H(t) = U^\dagger(t,t_0)\ \hat{A}\ U(t,t_0)$, so that the expectation value of the operators are the same in both pictures,

$$\langle\hat{A}(t)\rangle = \mathrm{tr}\left\{\hat{A}\hat{\rho}(t)\right\} = \mathrm{tr}\left\{\hat{A}_H(t)\hat{\rho}(t_0)\right\}. \tag{2.76}$$

[7]To distinguish both pictures, all the operators in the Heisenberg picture will have the subscript "H". This subscript will be dropped in next chapters.

Therefore, the differential equation for the operators in the Heisenberg picture, which is called Heisenberg equation of motion, can be derived

$$\frac{\mathrm{d}}{\mathrm{d}t}\hat{A}_H(t) = \frac{i}{\hbar}\left[\hat{H}_H(t), \hat{A}_H(t)\right] + \frac{\partial \hat{A}_H(t)}{\partial t}, \tag{2.77}$$

in which the last term only appears when the operator $\hat{A}_H$ has an explicit dependence on time, and $\hat{H}_H(t)$ is the Hamiltonian in the Heisenberg picture, which is transformed in the same way as the operators.

The Schrödinger and the Heisenberg pictures are limiting cases of an intermediate one, the interaction picture. The Hamiltonian in this picture can be written as $\hat{H}(t) = \hat{H}_0 + \hat{H}_I(t)$, assuming that the "bare" Hamiltonian H_0, which is the sum of the "bare" subsystems, is time-independent and $H_I(t)$ describes the interaction between the system and the reservoir. The time-evolution operator is now $U_I(t, t_0) = e^{i\hat{H}_0(t-t_0)}U(t, t_0)$, so that $\hat{\rho}_I(t) = U_I(t, t_0)\hat{\rho}(t_0)U_I^\dagger(t, t_0)$. Therefore, the Liouville-von Neumann equation can be written just in terms of the interaction Hamiltonian

$$\begin{aligned} &\partial_t \hat{\rho}_I(t) = -\frac{i}{\hbar}\left[\hat{H}_I(t), \hat{\rho}_I(t)\right] \rightarrow \\ &\hat{\rho}_I(t) = \hat{\rho}_I(t_0) - \frac{i}{\hbar}\int_{t_0}^{t} \mathrm{d}s \left[\hat{H}_I(s), \hat{\rho}_I(s)\right]. \end{aligned} \tag{2.78}$$

As we are interested only in the description of the system's dynamics, and it is assumed that it does not affect the reservoir, a reduced state space may be used. The expectation value of a system operator can be written as

$$\langle A_S \rangle = \mathrm{tr}_S\{A\hat{\rho}_S\}, \tag{2.79}$$

where $\hat{\rho}_S = \mathrm{tr}_R\{\hat{\rho}\}$ is the partial trace over the degrees of freedom of the reservoir. Therefore, one only needs to know the density matrix of the system, and an effective master equation can be derived.

Markov approximation

To know the time evolution of the density matrix of the system the starting point is the Liouville-von Neumann equation (2.78). Taking the integrated solution and inserting it in the original equation (with $t_0 = 0$) gives

$$\partial_t \rho_I(t) = -\frac{i}{\hbar}\left[H_I(t), \rho_I(0)\right] - \frac{1}{\hbar}\int_0^t \left[H_I(t), \left[H_I(s), \rho(s)\right]\right] \mathrm{d}s, \tag{2.80}$$

where the density matrix on the right-hand side of the equation depends on all the previous times $0 < s < t$. In order to remove this dependence, the integrated expression of $\rho_I(t)$ given in Eq. (2.78) can be used again, so that in the previous equation the double commutator contains only $\rho(t)$ but a new term with three interaction operators is added. However, this last term is neglected when the interaction between the system and the environment is weak. This is the first Born approximation, i.e., perturbation theory to lowest order. Finally, in order to obtain the evolution of the system density matrix, the reservoir degrees of freedom are traced out and we perform the second Born approximation, which consists in assuming that initially ($t = 0$) the system and the reservoir are not correlated and that the reservoir is not perturbed by the system, i.e., $\rho_I(0) = \rho_S(0) \otimes \rho_R$, where $\rho_R = \rho_R(0)$. Finally, by assuming that the reservoir is a thermal state, i.e., $\rho_R = E^{-H_R/k_BT}/\mathrm{Tr}_R\left(e^{-H_R/k_BT}\right)$, the first term in the right-hand of the previous equation can be dropped [153] and

$$\partial_t \rho_S(t) = -\frac{1}{\hbar^2}\mathrm{Tr}_R \int_0^t \left[H_I(t), \left[H_I(s), \rho_S(t) \otimes \rho_R\right]\right] \mathrm{d}s. \tag{2.81}$$

Next, we assume that perturbations of the environment caused by the system do not act back on it at later times, i.e., the environment essentially has no "memory" about the dynamics that the system underwent at earlier times, so that the interaction is Markovian. This approximation requires to assume that the reservoir correlations disappear quickly enough so that the

integral (2.81) is only determined by times s close to t and the equation of the system density is finally given by

$$\partial_t \rho_S(t) = -\frac{1}{\hbar^2} \mathrm{Tr}_R \int_0^\infty [H_I(t), [H_I(t-s), \rho_S(t) \otimes \rho_R]] \, \mathrm{d}s. \tag{2.82}$$

Lack of memory does not necessarily require or imply that the environment fully equilibrates to its original state – for example, a photon emitted from an atom in free space will never interact with the atom again even if it is not absorbed or otherwise affected by another object after being emitted.

Finally, from Eq. (2.82), the Lindblad master equation can be derived (for example, Refs. [86, 153] show this derivation). The general master equation of a quantum system is therefore

$$\partial_t \rho_S = -\frac{i}{\hbar} [H, \rho_S] + \sum_i \gamma_i L_{A_i}[\rho_S], \tag{2.83}$$

where $L_{A_i}[\rho] = A_i \rho A_i^\dagger - \frac{1}{2} \left\{ A_i^\dagger A_i, \rho \right\}$ are the Lindblad dissipators, γ_i are dissipation rates and A_i are quantum jump operators.

Chapter 3 | Cumulant Expansion Method

3.1 Theory

When describing arbitrary photonic structures, in which there are many degrees of freedom, macroscopic QED is the starting point. However, including all of these degrees in a quantum-mechanical way, i.e., using wave functions or density matrices, is an intractable problem. One practical limitation is the scaling of the size of the matrices that represent the quantum system. For example, for a collection of 2-level systems (that can represent photons and emitters, each of them with a single excited state), the size of the Hilbert space scales as 2^N, where N is the number of particles.

To reduce the size of the system many techniques can be used. One of the most common assumptions is to consider that the quantum emitter interacts only with a single mode of the EM field, as mentioned in section **2.4**. This leads to the Rabi and the Jaynes-Cummings model for one emitter and to the Dicke and Tavis-Cummings models for a collection of emitters, depending

on the approximations performed [125, 149, 154–156], all of which have been successfully used and extended to describe a wide variety of experimental implementations. Nevertheless, the simplification to a single or few quantized light modes in the treatment of the electromagnetic field is not always a good approximation, and for many experimental realizations the EM field modes are not well-described by isolated lossy cavity modes.

In some cases, the quantum character of the electromagnetic field may be neglected and it is possible to rely on Maxwell's equations. In such mean-field approaches, the classical EM field is then coupled to the dipole of the quantum emitters and the coupled Maxwell-Schrödinger or Maxwell-Bloch equations are solved [157, 158]. This approach, in principle, allows for the description of arbitrary photonic structures but misses all effects due to the quantization of the EM field, such as spontaneous emission. To allow the description of some quantum effects, and therefore a more complete description, some extensions to the mean-field approach can be made. Some of them are based on an Ehrenfest+Relaxation approach [159] or cavity quantum electrodynamics with multi-trajectory Ehrenfest dynamics [160].

Another method that allows to give a more complete description than the mean-field approximations is the cumulant expansion method, in which the correlations between the operators that describe the system can be represented as products of the expectation values of operators with less and the same order. Truncating this expansion, just the correlations up to some order are taken into account, while all the correlations above it are neglected. This can be done if the operators are statistically independent from one another. Moreover, instead of working with quantum operators, the magnitudes to compute are complex values, so in the end there is a closed set of numerical differential equations that, although still computationally demanding, allows to take into account many quantum effects with a large number of degrees of freedom in a

systematic way.

The cumulant expansion method has been shown to work in open quantum systems problems such as lasing [161, 162]. It also has been used to describe differences between lasing and condensation in the Dicke model [163, 164] and to describe polariton condensation in organic microstructures [165].

3.1.1 Hamiltonian

Within the framework of macroscopic QED, the Hamiltonian that describes the interaction between one emitter and a medium-assisted electromagnetic field is given, within the dipole approximation [166], by Eq. (2.30), which for a single emitter can be written (assuming $\hbar = 1$) as,

$$H = \sum_{\lambda=e,m} \int d\mathbf{r}^3 \int_0^\infty d\omega\ \omega\ \mathbf{f}_\lambda^\dagger(\mathbf{r},\omega)\mathbf{f}_\lambda(\mathbf{r},\omega) + H_{\rm em} - \hat{\boldsymbol{\mu}} \cdot \mathbf{E}(\mathbf{r}_e), \tag{3.1}$$

where $\mathbf{f}_\lambda(\mathbf{r},\omega)$ and $\mathbf{f}_\lambda^\dagger(\mathbf{r},\omega)$ are the bosonic annihilation and creation operators, $H_{\rm em}$ is the bare-emitter Hamiltonian, $\hat{\boldsymbol{\mu}}$ is its dipole operator, and $\mathbf{E}(\mathbf{r}_e)$ is the electric field operator, which is given by a superposition of the bosonic operators $\hat{\mathbf{f}}_\lambda(\mathbf{r},\omega)$ with weights determined by the classical Green's tensor $\mathbf{G}(\mathbf{r}_e,\mathbf{r},\omega)$. Within this framework, the EM field is created locally at every point in space and frequency. As realized by Buhmann et al. [166] and later independently by other groups [167, 168] a unitary frequency-dependent transformation can be used to transform the general operators $\mathbf{f}_\lambda(\mathbf{r},\omega)$, $\mathbf{f}_\lambda^\dagger(\mathbf{r},\omega)$ to a set of new modes in which the emitter interacts only with a single bosonic operator $a(\omega)$, $a^\dagger(\omega)$ at each frequency (under the assumption that only a single polarization direction interacts with the emitter dipole operator).

Furthermore, the quantum emitter is approximated as a two-level system described by the Pauli matrices σ^i ($i \in \{x, y, z\}$), with transition frequency ω_e

and transition dipole moment $\boldsymbol{\mu}$. The Hamiltonian then becomes

$$H = \int_0^\infty \mathrm{d}\omega\ \omega a^\dagger(\omega)a(\omega) + \frac{\omega_e}{2}\sigma^z + \int_0^\infty \mathrm{d}\omega\ g(\omega)\left(a^\dagger(\omega) + a(\omega)\right)\sigma^x, \quad (3.2)$$

where $g(\omega)$ is the coupling between the emitter and the electromagnetic modes,

$$g(\omega) = \sqrt{\frac{\mu_0}{\pi}\omega^2 \boldsymbol{\mu}\cdot \mathrm{Im}\mathbf{G}(\mathbf{r}_e,\mathbf{r}_e,\omega)\cdot\boldsymbol{\mu}} = \sqrt{J(\mathbf{r}_e,\omega)}, \quad (3.3)$$

where $\mathbf{r}_e$ is the position of the emitter and $J(\mathbf{r}_e,\omega)$ is the spectral density at its position.

For the numerical implementation, the frequency integrals are discretized on a grid with regular spacing $\Delta\omega$. To do so, the definition of the commutation relation for the discrete operators $\left[a_n, a_m^\dagger\right] = \delta_{nm}$ is imposed, so the normalized relation between them and the continuum modes is

$$a_n^{(\dagger)} = \sqrt{\Delta\omega}\int_{\omega_n-\Delta\omega/2}^{\omega_n+\Delta\omega/2} \mathrm{d}\omega\ a^{(\dagger)}(\omega). \quad (3.4)$$

This leads to the discrete Hamiltonian

$$H_d = \sum_n \omega_n a_n^\dagger a_n + \frac{\omega_e}{2}\sigma^z + \sum_n g_n\left(a_n^\dagger + a_n\right)\sigma^x, \quad (3.5)$$

where $g_n = \sqrt{J(\mathbf{r}_A,\omega_n)\Delta\omega}$.

As introduced in section **2.1.2**, the action of an incoming classical EM field can be introduced by applying a displacement operator (2.31), so that the final Hamiltonian is

$$\mathcal{H} = \sum_n \omega_n a_n^\dagger a_n + \frac{\omega_e}{2}\sigma^z + \sum_n g_n\left(a_n^\dagger + a_n\right)\sigma^x - \mu\mathcal{E}(t)\sigma^x. \quad (3.6)$$

3.1.2 Heisenberg equations

The evolution of any expectation value $\langle A\rangle = \langle\psi'|A|\psi'\rangle$ can be described by the Heisenberg equation of motion (derived in section **2.5**)

$$\partial_t\langle O\rangle = i\langle[\mathcal{H}, A]\rangle. \tag{3.7}$$

In general, the time derivative of products of N operators $\langle A_1A_2\dots A_N\rangle$ includes the contribution of $N+1$ operators $\langle A_1A_2\dots A_NA_{N+1}\rangle$, i.e.

$$\partial_t\langle A_1A_2A_3\dots A_N\rangle \propto \langle A_1A_2A_3...A_N\rangle + \langle A_1A_2A_3...A_NA_{N+1}\rangle, \tag{3.8}$$

due to the bilinear matter-field coupling in Eq. (3.6), so one obtains an infinite set of equations that represent the dynamics of the system. For the previous Hamiltonian, the set of equations that arise for the fundamental operators is

$$\partial_t\langle a_n\rangle = -i\omega_n\langle a_n\rangle - ig_n\langle\sigma^x\rangle, \tag{3.9a}$$

$$\partial_t\langle\sigma^x\rangle = -i\omega_e\langle\sigma^y\rangle, \tag{3.9b}$$

$$\partial_t\langle\sigma^y\rangle = \omega_e\langle\sigma^x\rangle - 2\sum_n g_n\langle a_n^\dagger\sigma^z\rangle - 2\sum_n g_n\langle a_n\sigma^z\rangle + 2\mu\mathcal{E}(t)\langle\sigma^z\rangle, \tag{3.9c}$$

$$\partial_t\langle\sigma^z\rangle = 2\sum_n g_n\langle a_n^\dagger\sigma^y\rangle + 2\sum_n g_n\langle a_n\sigma^y\rangle - 2\mu\mathcal{E}(t)\langle\sigma^y\rangle. \tag{3.9d}$$

Cumulant expansion

The cumulant expansion method allows to express the expectation value of a set of operators as sums and products of expectation values of a smaller number of operators and their correlations. The expansion of the average of N operators can be obtained using the general formula [169, 170]:

$$\langle A_1\dots A_N\rangle = \sum_{p\in P(\mathcal{I})\setminus\mathcal{I}} (|p|-1)!\,(-1)^{|p|}\prod_{B\in p}\left\langle\prod_{i\in B}A_i\right\rangle + \langle A_1\dots A_N\rangle_C, \tag{3.10}$$

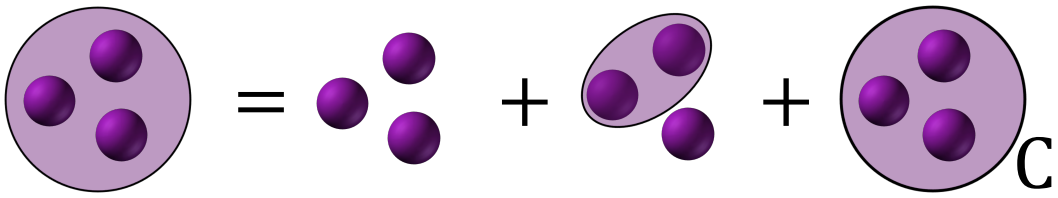

Fig. 3.1.: Conceptual scheme of the cumulant expansion for three emitters, corresponding to Eq. (3.11b).

where $P(\mathcal{I})$ is the set of all partitions (which are all the combinations of expectation values for N operators), $|p|$ is the length of the partition, and B runs over the block of each partition. To illustrate the general equation (3.10), the explicit cumulant expansion for two and three operators are derived:

$$\langle ab\rangle = \langle a\rangle\langle b\rangle + \langle ab\rangle_C, \tag{3.11a}$$

$$\begin{aligned}\langle abc\rangle &= \langle a\rangle\langle b\rangle\langle c\rangle + \langle a\rangle\langle bc\rangle_C + \langle b\rangle\langle ac\rangle_C + \langle c\rangle\langle ab\rangle_C + \langle abc\rangle_C = \\ &= -2\langle a\rangle\langle b\rangle\langle c\rangle + \langle a\rangle\langle bc\rangle + \langle b\rangle\langle ac\rangle + \langle c\rangle\langle ab\rangle + \langle abc\rangle_C.\end{aligned} \tag{3.11b}$$

Each of the equations above express the expectation values of a set of operators in terms of the expectation values of a lower number of operators and the correlations of the original set of operators. Figure **3.1** shows the idea behind the cumulant expansion schematically. The full interaction between three operators (left hand of the equation) can be described by the contribution of the individual operators (first term in the right hand), the contribution by the correlations between two operators (middle term) and the correlations between the three operators (right term). Moreover, by substituting Eq. (3.11a) in Eq. (3.11b), one can express the expectation values using only mean values of singular operators and correlations. The cumulant expansion itself does not imply any approximation. However, this method is useful when some correlations are neglected, so a set of differential equations (for example in Eqs. (3.9)) can be solved. In particular, the cumulant expansion method allows to discard correlations in a systematic way.

Then, the order of approximation indicates the maximum order of correlations taken into account. It is worth noting that the meaning of "order of the approximation" depends on which set of operators is used to represent the system. For example, in Eq. (3.6) σ^x, σ^y, and σ^z are used as the "fundamental" operators, but it would be equally possible to use only σ^x and σ^y (or more conventionally $\sigma^{\pm} = \frac{1}{2}\sigma^x \pm \frac{i}{2}\sigma^y$) as $\sigma^z = \sigma^+\sigma^- - \sigma^-\sigma^+ = 2\sigma^+\sigma^- - 1$. Similarly, for the photonic modes, a_n and $a_n^\dagger$ are used, but it would be equally possible to add the number operator n_N and thus obtain photonic populations at lower orders. This particular convention here is chosen because of the direct connection to Maxwell-Bloch and other mean-field approximations, where the population of the two-level system is considered explicitly within the set of equations, while only the coherent part of the EM fields is treated.

In addition to the different levels of approximation for the dynamics obtained by truncating the systems at various orders, it should be noted that the order of the expansion needed to describe the system also depends on the expectation values of interest. For example, the second-order correlation function $g^{(2)}(0)$ contains expectation values of products of four operators and is exactly equal to unity within the mean-field approximation.

Taking all the previous comments into consideration, the first-order (or mean-field) approximation is made when neglecting all the correlations between fundamental operators, i.e., assuming $\langle ab\rangle = \langle a\rangle\langle b\rangle$, and therefore $\langle ab\rangle_C \approx 0$. When the correlations of two operators are taken into account, the description of the dynamics is beyond the mean-field approximation (and one has the second-order approximation). Now, a new set of equations must

be added to the previous one

$$\partial_t\langle a_n^\dagger\sigma^x\rangle = i\omega_n\langle a_n^\dagger\sigma^x\rangle - \omega_e\langle a_n^\dagger\sigma^y\rangle + ig_n, \tag{3.12a}$$

$$\partial_t\langle a_n^\dagger\sigma^y\rangle = i\omega_n\langle a_n^\dagger\sigma^y\rangle + \omega_e\langle a_n^\dagger\sigma^x\rangle - g_n\langle\sigma^z\rangle - 2E_n^{(z)} + 2\mu\mathcal{E}(t)\langle a_n^\dagger\sigma^z\rangle, \tag{3.12b}$$

$$\partial_t\langle a_n^\dagger\sigma^z\rangle = i\omega_n\langle a_n^\dagger\sigma^z\rangle + g_n\langle\sigma^y\rangle + 2E_n^{(y)} - 2\mu\mathcal{E}(t)\langle a_n^\dagger\sigma^y\rangle, \tag{3.12c}$$

$$\partial_t\langle a_n^\dagger a_m\rangle = i\left(\omega_n - \omega_m\right)\langle a_n^\dagger a_m\rangle + ig_n\langle a_m\sigma^x\rangle - ig_m\langle a_n^\dagger\sigma^x\rangle, \tag{3.12d}$$

$$\partial_t\langle a_n^\dagger a_m^\dagger\rangle = i\left(\omega_n + \omega_m\right)\langle a_n^\dagger a_m^\dagger\rangle + ig_n\langle a_m^\dagger\sigma^x\rangle + ig_m\langle a_n^\dagger\sigma^x\rangle, \tag{3.12e}$$

where $E_n^{(y),(z)} = \sum_m g_m\left(\langle a_n^\dagger a_m^\dagger\sigma^{z,y}\rangle + \langle a_n^\dagger a_m\sigma^{z,y}\rangle\right)$. Since $\langle a_n\sigma^i\rangle = \langle a_n^\dagger\sigma^i\rangle^*$ and $\langle a_n^\dagger a_m^\dagger\rangle = \langle a_m a_n\rangle^*$, Eqs. (3.12) are enough to describe all combinations of two operators. The set of equations written in terms of the correlations is

$$\partial_t\langle a_n^\dagger\sigma^x\rangle_C = i\omega_n\langle a_n^\dagger\sigma^x\rangle_C - \omega_e\langle a_n^\dagger\sigma^y\rangle_C + ig_n\left(1 - \langle\sigma^x\rangle\langle\sigma^x\rangle\right), \tag{3.13a}$$

$$\begin{aligned}\partial_t\langle a_n^\dagger\sigma^y\rangle_C = {}& i\omega_n\langle a_n^\dagger\sigma^y\rangle_C + \omega_e\langle a_n^\dagger\sigma^x\rangle_C - g_n\left(\langle\sigma^z\rangle - i\langle\sigma^x\rangle\langle\sigma^y\rangle\right)\\ & - 2C_n^z + 2\mu\mathcal{E}(t)\langle a_n^\dagger\sigma^z\rangle_C,\end{aligned} \tag{3.13b}$$

$$\begin{aligned}\partial_t\langle a_n^\dagger\sigma^z\rangle_C = {}& i\omega_n\langle a_n^\dagger\sigma^z\rangle_C + g_n\left(\langle\sigma^y\rangle - i\langle\sigma^x\rangle\langle\sigma^z\rangle\right)\\ & + 2C_n^y - 2\mu\mathcal{E}(t)\langle a_n^\dagger\sigma^y\rangle_C,\end{aligned} \tag{3.13c}$$

$$\partial_t\langle a_n^\dagger a_m\rangle_C = i\left(\omega_n - \omega_m\right)\langle a_n^\dagger a_m\rangle_C + ig_n\langle a_m\sigma^x\rangle_C - ig_m\langle a_n^\dagger\sigma^x\rangle_C, \tag{3.13d}$$

$$\partial_t\langle a_n^\dagger a_m^\dagger\rangle_C = i\left(\omega_n + \omega_m\right)\langle a_n^\dagger a_m^\dagger\rangle_C + ig_n\langle a_m^\dagger\sigma^x\rangle_C + ig_m\langle a_n^\dagger\sigma^x\rangle_C, \tag{3.13e}$$

where

$$\begin{aligned}C_n^{y,z} = \sum_m g_m\big(&\langle a_m^\dagger\rangle\langle a_n^\dagger\sigma^{y,z}\rangle_C + \langle a_m\rangle\langle a_n^\dagger\sigma^{y,z}\rangle_C + \langle\sigma^{y,z}\rangle\langle a_n^\dagger a_m^\dagger\rangle_C\\ &+ \langle\sigma^{y,z}\rangle\langle a_n^\dagger a_m\rangle_C + \langle a_n^\dagger a_m^\dagger\sigma^{y,z}\rangle_C + \langle a_n^\dagger a_m\sigma^{y,z}\rangle_C\big).\end{aligned} \tag{3.14}$$

The cumulant expansion thus provides a systematic way to approximate the true solution of the system. However, while Eqs. (3.12) describing the expectation values are linear, the corresponding correlation expansion, Eqs. (3.13) corresponds to a nonlinear system depending on products of the state variables (expectation values and correlations). These nonlinearities make the obtained set of equations numerically more unstable.

In Eqs. (3.13) no approximations have been made yet. To obtain a closed set of equations that may allow the description of the time evolution of the system, some correlations have to be neglected again. The second-order cumulant expansion approximation means to neglect the correlations of products of three or more operators, ($\langle abc\rangle_C \simeq 0$), so that equations (3.9) and (3.13) form a closed set that can be solved.

The same procedure as above can be followed to obtain the equations up to, in principle, an arbitrary order. The main problem going to high orders is the number of equations, that increase fast with the order. In the following, results up to the third-order are obtained, which imply neglecting correlations of four or more operators. The third-order equations needed are:

$$\partial_t\langle a_n^\dagger a_m\sigma^x\rangle = i\delta_{n,m}\langle a_n^\dagger a_m\sigma^x\rangle - \omega_e\langle a_n^\dagger a_m\sigma^y\rangle + ig_n\langle a_m\rangle - ig_m\langle a_n^\dagger\rangle, \tag{3.15a}$$

$$\begin{aligned}\partial_t\langle a_n^\dagger a_m\sigma^y\rangle &= i\delta_{n,m}\langle a_n^\dagger a_m\sigma^y\rangle + \omega_e\langle a_n^\dagger a_m\sigma^x\rangle - D_{nm}^z \\ &\quad + 2\mu\mathcal{E}(t)\langle a_n^\dagger a_m\sigma^z\rangle,\end{aligned} \tag{3.15b}$$

$$\partial_t\langle a_n^\dagger a_m\sigma^z\rangle = i\delta_{nm}\langle a_n^\dagger a_m\sigma^z\rangle + D_{nm}^y - 2\mu\mathcal{E}(t)\langle a_n^\dagger a_m\sigma^y\rangle, \tag{3.15c}$$

$$\partial_t\langle a_n^\dagger a_m^\dagger\sigma^x\rangle = i\Delta_{nm}\langle a_n^\dagger a_m^\dagger\sigma^x\rangle - \omega_e\langle a_n^\dagger a_m^\dagger\sigma^y\rangle + ig_n\langle a_m^\dagger\rangle + ig_m\langle a_n^\dagger\rangle, \tag{3.15d}$$

$$\begin{aligned}\partial_t\langle a_n^\dagger a_m^\dagger\sigma^y\rangle &= i\Delta_{nm}\langle a_n^\dagger a_m^\dagger\sigma^y\rangle + \omega_e\langle a_n^\dagger a_m^\dagger\sigma^x\rangle - D_{nm}^{z^\dagger} \\ &\quad + 2\mu\mathcal{E}(t)\langle a_n^\dagger a_m^\dagger\sigma^z\rangle,\end{aligned} \tag{3.15e}$$

$$\partial_t\langle a_n^\dagger a_m^\dagger\sigma^z\rangle = i\Delta_{nm}\langle a_n^\dagger a_m^\dagger\sigma^z\rangle + D_{n,m}^{y^\dagger} - 2\mu\mathcal{E}(t)\langle a_n^\dagger a_m^\dagger\sigma^y\rangle, \tag{3.15f}$$

$$\begin{aligned}\partial_t\langle a_n^\dagger a_m^\dagger a_l\rangle &= i\delta_{nml}\langle a_n^\dagger a_m^\dagger a_l\rangle + ig_n\langle a_m^\dagger a_l\sigma^x\rangle \\ &\quad + ig_m\langle a_n^\dagger a_l\sigma^x\rangle - ig_l\langle a_n^\dagger a_m^\dagger\sigma^x\rangle,\end{aligned} \tag{3.15g}$$

$$\begin{aligned}\partial_t\langle a_n^\dagger a_m^\dagger a_l^\dagger\rangle &= i\Delta_{nml}\langle a_n^\dagger a_m^\dagger a_l^\dagger\rangle + ig_n\langle a_m^\dagger a_l^\dagger\sigma^x\rangle \\ &\quad + ig_m\langle a_n^\dagger a_l^\dagger\sigma^x\rangle + ig_l\langle a_n^\dagger a_m^\dagger\sigma^x\rangle.\end{aligned} \tag{3.15h}$$

In the precious set of equations $\delta_{nm} = \omega_n - \omega_m$, $\Delta_{nm} = \omega_n + \omega_m$, $\delta_{nml} =$

$\omega_n + \omega_m - \omega_l$, $\Delta_{nml} = \omega_n + \omega_m + \omega_l$ and

$$\begin{aligned} D_{nm}^{y,z^{(\dagger)}} &= g_n \langle a_m^{(\dagger)} \sigma^{y,z} \rangle + g_m \langle a_n^\dagger \sigma^{y,z} \rangle \\ &+ 2 \sum_l g_l \left(\langle a_n^\dagger a_l^\dagger a_m^{(\dagger)} \sigma^{y,z} \rangle + \langle a_n^\dagger a_m^{(\dagger)} a_l \sigma^{y,z} \rangle \right). \end{aligned} \tag{3.16}$$

Many of these equations have been obtained using the QuantumAlgebra.jl package [171], which does quantum operator algebra for symbolic calculation of quantum operator dynamics. The numerical implementation of the equations is performed within the Julia programming language [172]. The code runs on graphical processing units (GPUs), which provides a significant speedup (≈ 20 for our available setup) over the CPU variant of the same code. For the time propagation, the DifferentialEquations.jl package [173] is used.

3.2 Results

3.2.1 Free space

To illustrate this method, first the free space is considered. As shown in section **2.4**, the spectral density of an emitter in free space is

$$J_0(\omega) = \hbar \omega^3 \frac{|\mu|^2}{6\pi^2 \epsilon_0 c^3}. \tag{3.17}$$

Discretizing this spectral density with frequency spacing $\Delta\omega$ is equivalent to describing an emitter in the center of a spherical box of radius $R = \pi c/\Delta\omega$ [10], where c is the speed of light in vacuum. Therefore, the maximum time propagation that can be obtained is $T_{\max} \approx 2R/c = 2\pi/\Delta\omega$, which corresponds to the time that it takes a photon that leaves the emitter to reach the surface of the sphere and return to the emitter. If time propagation is performed over too

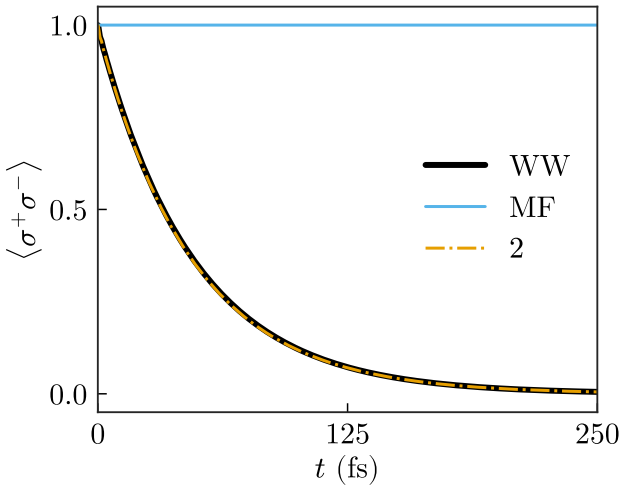

Fig. 3.2.: Excited-state population of the emitter in time in free space. Comparison between Wigner-Weisskopf approximation (black line), mean-field (light blue line), and second-order approximation (orange dash-dotted line).

long times, exceeding $T_{\max}$, artificial reflections of the emitted photons from the boundaries of the sphere are obtained and they interact with the emitter again.

As a first example, the spontaneous emission from an initially excited emitter is treated, i.e., the classical Wigner-Weisskopf problem (introduced in section **2.3**). As the lifetime of typical emitters (atoms, molecules, quantum dots) is on the scale of nanoseconds, an accurate description would require a very small frequency spacing and thus a very large box, and additionally, propagation over very long times. To avoid this, the emitter dipole moment is set to the unrealistically large value of $\mu = 2565$ D, for which the spontaneous emission lifetime at the emitter frequency of $\omega_e = 2.72$ eV is given by $\tau \approx 46$ fs. $N = 400$ photonic modes on a regular grid in frequency from 0 eV to 5.44 eV are taken. For these parameters, spontaneous emission occurs within a time shorter than $2R/c$.

The spontaneous emission dynamics of an initially excited single emitter in free space are shown in Fig. **3.2**, which shows the excited-state population of the emitter as a function of time, calculated using three different numerical methods: Perturbative Wigner-Weisskopf theory (WW), which simply predicts exponential decay with rate $\gamma = 2\pi J(\omega_e)$, mean-field (MF), and second-order cumulant expansion (2).

The mean-field approximation neglects all the expectation values of two or more operators (so in this approximation $\langle a_n^\dagger a_m \rangle \approx \langle a_n^\dagger \rangle \langle a_m \rangle$). Since $\langle a_n \rangle = \langle \sigma^x \rangle = \langle \sigma^x \rangle = 0$ at $t = 0$ and no external electric field affects the system, no dynamics are predicted and hence, it does not predict any spontaneous emission, as is well-known. The spontaneous emission can be explained as the interaction of the emitter with the vacuum fluctuations $\langle a_n^\dagger a_m \rangle$, which are neglected in this approximation and therefore going beyond the mean-field is essential to describe it [174, 175]. On the other hand, the second-order cumulant expansion (and all higher-order approaches, not shown) already perfectly describes the free-space spontaneous decay of $\langle \sigma^+ \sigma^- \rangle$ due to the vacuum fluctuations.

Next, an emitter initially in its ground state is considered, i.e., $\langle \sigma^+ \sigma^- \rangle (t = 0) = 0$. A classical electric field $\mathcal{E}(t)$, which can have an arbitrary shape, pumps the system. For the free space example, the electric field considered is a short Gaussian pulse in resonance with the emitter transition frequency, $\mathcal{E}(t) = \mathcal{E}_0 e^{-(t-t_0)^2/2T^2} \sin(\omega_e t)$. To describe a more realistic system, the dipole moment of the emitter is set to $\mu = 2.56$ D, corresponding to a spontaneous emission lifetime in free space of $\tau \approx 46$ ns. The pulse parameters are $t_0 = 77.76$ fs and $T = 24.20$ fs. Now the comparison of the different cumulant expansion approaches is made with a semiclassical approximation in which no quantized light modes are present at all, and the interaction between the

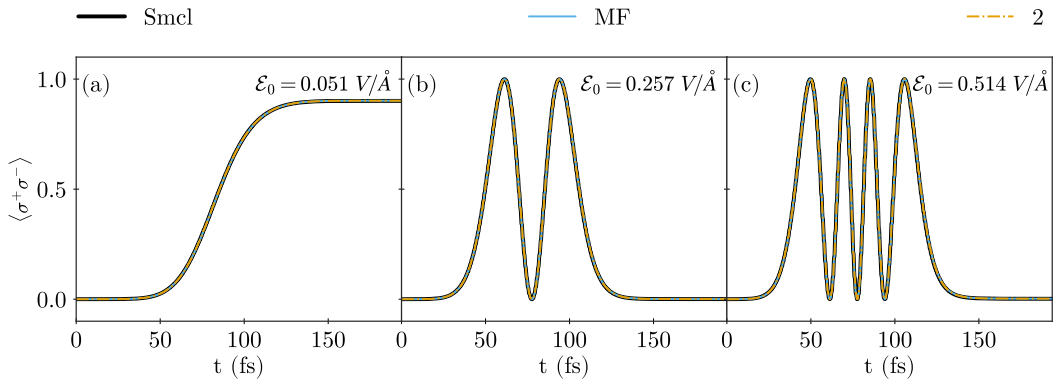

Fig. 3.3.: Excited-state population of a single emitter in free space under driving by a short Gaussian pulse. The peak electric field amplitude increases from (a) to (c) and is shown in each subplot. Comparison between semi-classical approximation (black line), mean-field (blue line) and second-order approximation (dot-dashed orange line). All lines are indistinguishable for this case.

two-level system and the EM field is described via the equations

$$\frac{\partial}{\partial t}\begin{pmatrix} C_g \\ C_e \end{pmatrix} = -i \begin{pmatrix} 0 & -\mu \cdot \mathcal{E}(t) \\ -\mu \cdot \mathcal{E}(t) & \omega_e \end{pmatrix} \cdot \begin{pmatrix} C_g \\ C_e \end{pmatrix}, \tag{3.18}$$

where C_g and C_e are the ground-state and excited-state amplitudes, respectively. Figure **3.3** shows the excited-state population of the emitter for different amplitudes of the electric field. In particular, $\mathcal{E}_0 = 0.051$ V/Å in panel (a), $\mathcal{E}_0 = 0.257$ V/Å in panel (b) and $\mathcal{E}_0 = 0.514$ V/Å in panel (c). For the weakest driving considered, the system is already in the nonlinear regime. Still, the electric field is weak enough so that no Rabi oscillations are seen in the emitter dynamics (subplot (a)), i.e., the emitter population increase just one time. In contrast, the two stronger fields lead to a strongly nonlinear response with driven Rabi oscillations (subplots (b) and (c)), with the number of oscillations increasing as the coupling becomes stronger.

In this case, the coupling to the free-space modes is so weak that they are not expected to have any influence on the dynamics, and this is indeed observed

in Fig. **3.3**. Both approaches (mean-field and second-order cumulant expansion) accurately describe the emitter dynamics and they agree perfectly with the semiclassical approximation. Therefore, while the classical pulse interacts with the emitter, correlations between the photonic modes and the emitter can be neglected. After the end of the pulse, only the second-order approach can describe the slow spontaneous decay of any left excitation of the emitter, while the mean-field approach predicts a steady value for the population after the classical pulse vanishes. However, this difference is not noticeable in the timescales investigated here due to the long lifetime of the emitter ($\tau \approx 46$ ns).

3.2.2 Cavity

The cavity considered is the one whose spectral density represents a single lossy cavity mode. This is achieved using a Lorentzian frequency dependence,

$$J(\omega) = \frac{g^2}{\pi} \frac{\gamma/2}{(\omega - \omega_c)^2 + (\gamma/2)^2}. \tag{3.19}$$

When describing the interaction of a single emitter with a single quantized mode, the dynamics predicted using this spectral density are mathematically equivalent to those of the Lindblad master equation

$$\partial_t \rho = -i\,[H_R, \rho] + \gamma \mathcal{L}_a[\rho] \tag{3.20}$$

where H_R is the Rabi Hamiltonian

$$H_R = \frac{\omega_e}{2}\sigma^z + \omega_c a^\dagger a + g(a + a^\dagger)\sigma^x, \tag{3.21}$$

while $\mathcal{L}_a[\rho] = a\rho a^\dagger - \frac{1}{2}\{a^\dagger a, \rho\}$ is the Lindblad operator that describes the cavity losses. The effective coupling $g = \mu E_{1ph}$ is determined by the amplitude of the Lorentzian spectral density, the effective losses are given by its width γ, and the frequency of the photonic mode is the resonance frequency ω_c of the Lorentzian [155, 176].

The emitter and cavity frequencies are both set to $\omega_e = \omega_c = 2.72$ eV. A bandwidth of $\gamma = 0.027$ eV is chosen, so the quality factor is $Q = \omega_c/\gamma = 100$, while the coupling g will take different values. The number of modes considered is $N = 400$ and the frequencies are taken from $\omega_{\min} = 2.04$ eV to $\omega_{\max} = 3.40$ eV (grid spacing $\Delta\omega = 3.4$ meV) so the range is wide enough and the number of modes large enough to represent the Lorentzian spectral density.

Spontaneous decay

The emitter is initially in its excited state $\langle\sigma^+\sigma^-\rangle(t = 0) = 1$ and evolves freely in the cavity, without any external electric field. In figure **3.4** the evolution of the emitter population is shown for different coupling strengths, so that from top to bottom it increases. In particular, $g = 0.008$ eV in panels (a) and (b), $g = 0.024$ eV in panels (c) and (d) and $g = 0.086$ eV in panels (e) and (f). For the weakest coupling considered here, shown in Fig. **3.4**(a), **3.4**(b), the system is already close to the strong-coupling regime ($4g > \gamma$) [14]. When the coupling strength is increased to $g = 0.024$ eV and $g = 0.086$ eV, the system is squarely in the strong-coupling regime where vacuum Rabi oscillations are expected, as shown in Figs. **3.4**(c), **3.4**(d) for the former coupling and in Figs. **3.4**(e), **3.4**(f) for the latter.

In contrast to the free-space case, even for the weakest coupling the second-order approximation, shown in Fig. **3.4**(a), now starts to show some differences with respect to the exact solution obtained with the Rabi model, with the population even reaching nonphysical values, $\langle\sigma^+\sigma^-\rangle < 0$. As the coupling increases, the non physical values introduced by the second-order approximation become more evident, as shown in panels (c) and (e) of figure **3.4**. However, the frequency of the Rabi oscillation is well described.

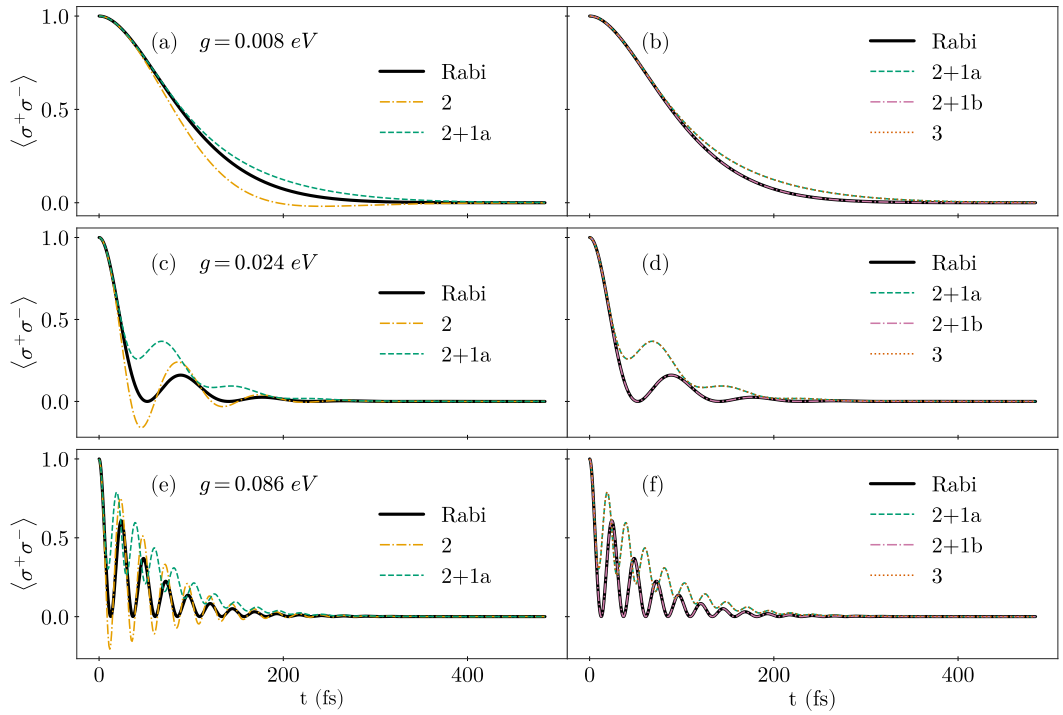

Fig. 3.4.: Excited-state population for an initially excited emitter in a cavity for different couplings. (a), (c) and (e): Comparison between the exact Rabi model solution (black line), 2nd order (orange dashed-dotted line) and 2+1a (dashed green line) approximation. (b), (d) and (f): Comparison between the Rabi solution (black line), 2+1a approximation (dashed green line), 2+1b approximation (dashed-dotted pink line), and 3rd order (dotted red line).

This implies that some third-order terms are required to obtain the correct dynamics, but it is not clear a priori which additional terms have to be included. Then, different extensions of the second-order expansion can be compared by successively adding higher-order terms. In the first one, the second-order set of equations (3.9) and (3.13) is used, but in Eq. (3.13b), the term $\langle a_n^\dagger a_m \sigma^z \rangle_C$ and its dynamics are not neglected. In the following, this extension will be referred to as "2+1a". The importance of including this particular third-order term has been previously pointed out in the literature [177]: it is the third-order correction with the largest value. Taking into account that, to

a good approximation, the state during the dynamics is described by a single excitation, $|\psi\rangle \approx (\alpha\sigma^+ + \sum_n \beta_n a_n^\dagger)|0\rangle$, the relevance of this term can be seen by inspecting the cumulant expansion of the third-order expectation values. For $\langle a_n^\dagger a_m \sigma^z\rangle$, the expansion is

$$\begin{aligned}\langle a_n^\dagger a_m \sigma^z\rangle = \langle a_n^\dagger\rangle\langle a_m\rangle\langle\sigma^z\rangle + \langle a_n^\dagger\rangle\langle a_m\sigma^z\rangle_C + \\ \langle a_m\rangle\langle a_n^\dagger\sigma^z\rangle_C + \langle\sigma^z\rangle\langle a_n^\dagger a_m\rangle_C + \langle a_n^\dagger a_m\sigma^z\rangle_C.\end{aligned} \tag{3.22}$$

The first three terms are negligible since $\langle a_n\rangle \approx 0$, but the product $\langle\sigma^z\rangle\langle a_n^\dagger a_m\rangle_C$ is non-negligible since both the emitter and photonic mode populations are non-zero. At the same time, it does not approximate the value of $\langle a_n^\dagger a_m\sigma^z\rangle$ well, so the correlation $\langle a_n^\dagger a_m\sigma^z\rangle_C$ is necessarily non-zero. In contrast, the expansion of $\langle a_n^\dagger a_m\sigma^y\rangle$ gives

$$\begin{aligned}\langle a_n^\dagger a_m \sigma^y\rangle = \langle a_n^\dagger\rangle\langle a_m\rangle\langle\sigma^y\rangle + \langle a_n^\dagger\rangle\langle a_m\sigma^y\rangle_C + \\ \langle a_m\rangle\langle a_n^\dagger\sigma^y\rangle_C + \langle\sigma^y\rangle\langle a_n^\dagger a_m\rangle_C + \langle a_n^\dagger a_m\sigma^y\rangle_C.\end{aligned} \tag{3.23}$$

Here, all the product terms contain at least one negligible value as $\langle\sigma^y\rangle \approx 0$, while $\langle a_n^\dagger a_m\sigma^y\rangle$ is also zero for the single-excitation state given above. This implies that the correlation $\langle a_n^\dagger a_m\sigma^y\rangle_C$ is in turn also negligible.

In the equation of motion of the new term $\langle a_n^\dagger a_m\sigma^z\rangle$, fourth-order expectation values appear, as shown in Eq. (3.15c). Performing the cumulant expansion on them and neglecting the fourth-order correlation, it is easy to see that only third-order correlations that are neglected in the other equations appear, and by consistency, these terms are approximated up to the second-order as well, leading to

$$\begin{aligned}\partial_t\langle a_n^\dagger a_m\sigma^z\rangle_C = G_{lnm} - ig_n\left(\langle\sigma^x\rangle\langle a_m\sigma^z\rangle_C + \langle\sigma^z\rangle\langle a_m\sigma^x\rangle_C\right) \\ + ig_m\left(\langle\sigma^x\rangle\langle a_n^\dagger\sigma^z\rangle_C + \langle\sigma^z\rangle\langle a_n^\dagger\sigma^x\rangle_C\right) + i\left(\omega_n - \omega_m\right)\langle a_n^\dagger a_m\sigma^z\rangle_C,\end{aligned} \tag{3.24}$$

where

$$\begin{aligned}G_{lnm} = g_n\langle a_m\sigma^y\rangle_C + g_m\langle a_n^\dagger\sigma^y\rangle_C + 2\sum_l g_l\Big(\langle a_l^\dagger a_n^\dagger\rangle_C\langle a_m\sigma^y\rangle_C \\ + \langle a_l^\dagger a_m\rangle_C\langle a_n^\dagger\sigma^y\rangle_C + \langle a_n^\dagger a_l\rangle_C\langle a_m\sigma^y\rangle_C + \langle a_l a_m\rangle_C\langle a_n^\dagger\sigma^y\rangle_C\Big).\end{aligned} \tag{3.25}$$

The expansion for one of the fourth-order expectation value is

$$\begin{aligned}
&\langle a_n^\dagger a_m a_l \sigma^y\rangle = \langle a_n^\dagger a_m a_l \sigma^y\rangle_C + \langle a_n^\dagger\rangle\langle a_m\rangle\langle a_l\rangle\langle\sigma^y\rangle + \\
&\langle a_n^\dagger\rangle\langle a_m\rangle\langle a_l\sigma^y\rangle_C + \langle a_n^\dagger a_m\rangle_C\langle a_l\rangle\langle\sigma^y\rangle + \langle a_n^\dagger a_m\rangle_C\langle a_l\sigma^y\rangle_C + \langle a_n^\dagger\rangle\langle a_m a_l\sigma^y\rangle_C + \\
&\langle a_n^\dagger\rangle\langle a_l\rangle\langle a_m\sigma^y\rangle_C + \langle a_n^\dagger a_l\rangle_C\langle a_m\rangle\langle\sigma^y\rangle + \langle a_n^\dagger a_l\rangle_C\langle a_m\sigma^y\rangle_C + \langle a_m\rangle\langle a_n^\dagger a_l\sigma^y\rangle_C + \\
&\langle a_n^\dagger\rangle\langle\sigma^y\rangle\langle a_m a_l\rangle_C + \langle a_n^\dagger\sigma^y\rangle_C\langle a_m\rangle\langle a_l\rangle + \langle a_n^\dagger\sigma^y\rangle_C\langle a_m a_l\rangle_C + \langle a_l\rangle\langle a_n^\dagger a_m\sigma^y\rangle_C,
\end{aligned} \tag{3.26}$$

and the terms $\langle a_n^\dagger a_m a_l\sigma^y\rangle_C$, $\langle a_m a_l\sigma^y\rangle_C$, $\langle a_n^\dagger a_l\sigma^y\rangle_C$ and $\langle a_n^\dagger a_m\sigma^y\rangle_C$ are neglected. The correlations inside the last bracket in Eq. (3.24) make this term non-negligible, although the expectation values in Eq. (3.15c) are analytically zero.

Going back to the spontaneous decay of a two level system in a cavity, the 2+1a approximation changes the description of the dynamics. This can be seen in subplots (a), (c) and (e) of figure **3.4**. When introducing this extension, the population never reaches negative values. However, it still does not agree with the exact solution provided by the Rabi model and is now overestimated. Moreover, when the coupling increases and Rabi oscillations are formed, it is not reproduced well.

Inspection of the equation of motion for $\langle a_n^\dagger a_m\sigma^z\rangle$, Eq. (3.15c), shows that this contains fourth-order terms that involve two photonic creation or annihilation operators. For the current dynamics, where to a good approximation only one excitation is present in the system, these fourth-order expectation values are thus approximately zero. Within the 2+1a approximation, they are however represented by products of non-negligible second-order correlations that have non-zero values, as can be also seen in Eq. (3.24). Furthermore, the correlations that appear in the equation of motion of $\langle a_n^\dagger a_m\sigma^z\rangle_C$ interact via the coupling, so if the coupling increases, the modifications produced by the spurious correlations are also more noticeable.

It is then possible to improve the approximation by not performing a cumulant expansion on the fourth-order terms in Eq. (3.15c), but by neglecting them directly, i.e., Eq. (3.15c) is again the only one added but instead of doing the cumulant expansion of the higher-order terms that appear in this equation, the condition $\langle a_n^\dagger a_l^\dagger a_m \sigma^y \rangle = \langle a_n^\dagger a_l a_m \sigma^y \rangle = 0$ is imposed directly. This approximation is referred as "2+1b". When using it, as shown in panels (b), (d) and (f) of Fig. **3.4**, the emission dynamics are now correctly obtained even when the coupling is increased, since the system remains in the single-excitation subspace even in strong coupling.

Finally, the full third-order expansion is shown. Now, the cumulant expansion is performed on all expectation values and fourth-order correlations are neglected. The third-order approximation, which is also shown in Fig. **3.4**(b), **3.4**(d) and **3.4**(f), provides identical results as the 2+1a approach, proving that, indeed, all third-order correlations apart from $\langle a_n^\dagger a_m \sigma^z \rangle_C$ can be neglected. However, for good agreement with the exact results, the same correction as in the 2+1b approach would have to be performed, or alternatively the full expansion would have to be done up to at least the fourth order.

Both approximations 2+1a and 2+1b are only slightly more costly numerically than the second-order expansion, since the added term $\langle a_n^\dagger a_m \sigma^z \rangle_C$ only contains two continuum indices n and m. In contrast, the full third-order expansion contains terms of the form $\langle a_n a_m a_l \rangle_C$ with three continuum mode indices (represented by $N \times N \times N$ arrays), and is thus significantly more expensive to implement.

Classical electric field

In this section, the same physical system and the same approximations are examined, but now not for the case of spontaneous emission and vacuum Rabi

oscillations, but for the emitter initially in its ground state, $\langle\sigma^+\sigma^-\rangle(t=0)=0$, and driven by an incoming classical electric field. Two different pulses are also considered.

$$\mathcal{E}(t)=\begin{cases}\mathcal{E}_0 e^{-(t-t_0)^2/2T^2}\sin(\omega_e t)\\ \mathcal{E}_0\sin(\omega_e t)(\theta(t_0-t)e^{-(t-t_0)^2/2T^2}+\theta(t-t_0))\end{cases}. \tag{3.27}$$

The former expression of the electric field corresponds to the same short Gaussian pulse considered in free space (assumed to be the pulse reaching the emitter after enhancement and distortion by propagating through the cavity structure, as discussed in section **2.1.2**). The latter corresponds to an electric field that smoothly turns on and then remains at a stationary intensity indefinitely ($\theta(t)$ is the Heaviside theta function), allowing to study if and how a steady state is reached in the time propagation. In both cases, the pump laser frequency is in resonance with the emitter and cavity resonances.

The dynamics, and in particular the emitter excited-state population, produced by both lasers at different order of approximation is shown for the weakest coupling ($g=0.008$ eV) in figure **3.5** for the Gaussian pulse and in figure **3.6** for the steady-state pulse. Again, all approximations are compared with the exact Rabi model solution. The amplitudes of the electric field interacting with the emitter are the same as in free space, given by $\mu\mathcal{E}_0=0.026$ eV (subplots (a) and (b), upper panel), $\mu\mathcal{E}_0=0.132$ eV (subplots (c) and (d), center panel), and $\mu\mathcal{E}_0=0.263$ eV (subplots (e) and (f), lower panel).

In contrast to the free-space case, the quantum effects due to fluctuations, such as spontaneous emission, are not negligible here, and the mean-field approximation, shown in subplots (a), (c) and (e), fails to capture the dynamics as it can only represent the coherent contribution to the light-matter interaction [175]. In the short-pulse case, Fig. **3.5**, this is mostly seen in the dynamics after the pulse, but is also reflected in Rabi oscillations during the pulses with bigger amplitudes than the ones predicted by the exact solution. Still, the

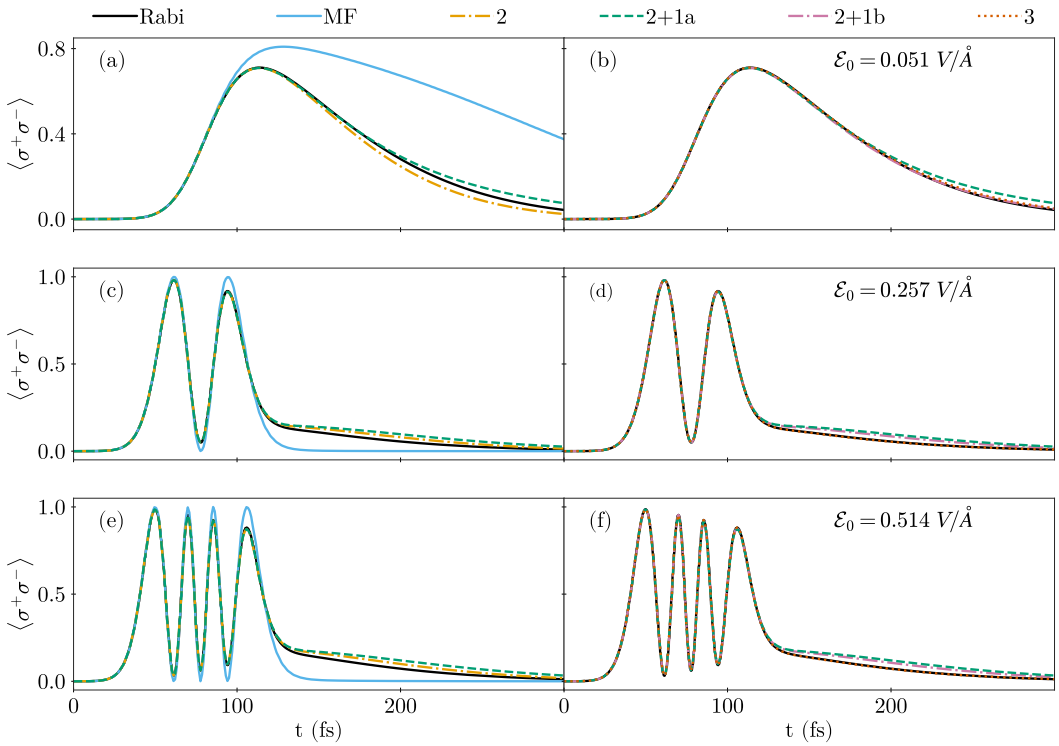

Fig. 3.5.: Excited-state population for an emitter initially in the ground state within a cavity with $g = 0.008$ eV, driven by a short classical electric field pulse (see text for details), for three different peak amplitudes as indicated in the subplots. Comparison between the Rabi solution (black line), 2+1a approximation (green dashed line), (a), (c), (e): mean-field (blue line), 2^{nd} order (orange dash-dotted line) (b), (d), (f): 2+1b approach (dashed-dotted pink line), and 3^{rd} order (dotted red line).

mean-field approximation does give a qualitatively correct prediction of the behavior of the emitter. In the case of the long pulse, Fig **3.6**, the initial driven oscillations are well-described but, as there is no coupling between the fluctuations and the emitter, the population keeps oscillating indefinitely without achieving any steady state. When the decay rate of the emitter is known, the mean-field description can be used and incoherent contributions to the emitter dynamics can be incorporated *ad hoc* using phenomenological decay constants [178]. However, obtaining these constants is not always easy and is

only straightforward in the weak-coupling regime where the light and matter degrees of freedom are not mixed. In those cases, the validity and simplicity of the mean-field approximation make it a common tool in describing a wide range of systems pumped by lasers [155, 179].

The second-order approximation, shown in subplots (a), (c) and (e), is sufficient to describe qualitatively the dynamics for the weakest coupling. When moreover the amplitude of the electric field is not to high ($\mathcal{E}_0 = 0.051$ V/Å) and the pulse is short (Fig. **3.5**(a)), the dynamics predicted by this approximation are much more similar to the Rabi solution, as incoherent contributions are taken into account via the second-order terms. For a long pulse (Fig. **3.6**(a)), the oscillations are not accurately described, neither in shape nor in amplitude, but it also does give a qualitative prediction of the oscillations and the steady state. If the driving electric field is more intense, shown in subplots (c), (d), (e) and (f), the second-order approximation (subplots (c) and (e)) gives a correct description of the shape of the Rabi oscillations, but their amplitude is underestimated.

The extensions 2+1a and 2+1b to the second-order change the dynamics slightly just for the weakest electric field, while when the amplitude of the field increases, the correlations introduced by both extensions are negligible. For the weakest amplitude, the 2+1a correction maintains the qualitative description, but the extra correlations included lead to a decrease of the oscillation amplitude. The 2+1b correction, in which the fourth-order expectation values are enforced to be zero (subplot (b)), i.e, the system is enforced to have only one excitation, hardly changes the prediction of the emitter dynamics. When the driving is stronger ($\mathcal{E}_0 = 0.257$ V/Å and $\mathcal{E}_0 = 0.514$ V/Å) the contribution of the classical driving with respect the coupling is more important. Then approximations 2+1a and 2+1b, shown in subplots (d) and (f), do not show any difference with respect to the "bare" second-order. Thus, due to the interaction

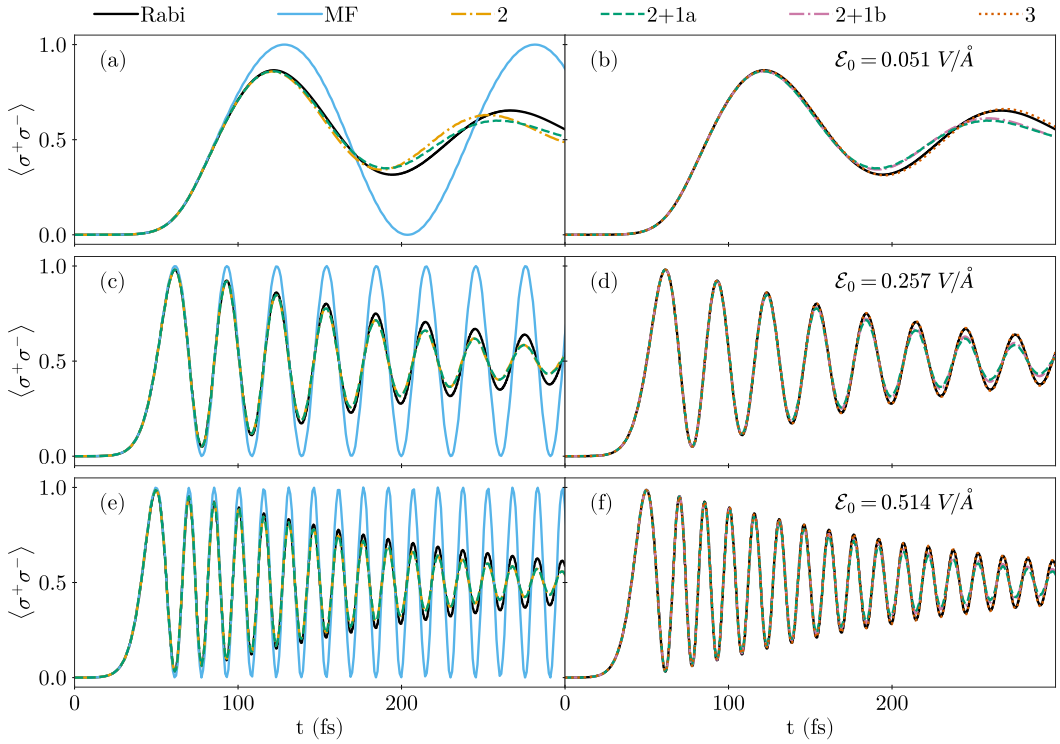

Fig. 3.6.: Like **3.5**, but for a semi-infinite driving pulse with constant amplitude after a smooth turn-on (see text for details).

of a strong laser pulse, the order of correlation needed to give a qualitative description of the dynamics decrease and correlations that change the description of the dynamics completely in the case of spontaneous emission do not matter much in the more classical case of driving by a strong laser pulse.

Finally, the third-order approximation is shown in subplots (b), (d) and (f). Adding all the third-order correlations sufficiently modifies the dynamics to achieve an accurate prediction in good agreement with the Rabi model. Therefore, from the results in figures **3.5** and **3.6**, it can be concluded that when the light-matter coupling is not too strong, the second-order correlations are the most important and in general this order of approximation is enough to describe the main characteristics of the solution. If a more quantitative description is required, the third-order approximation achieves almost perfect

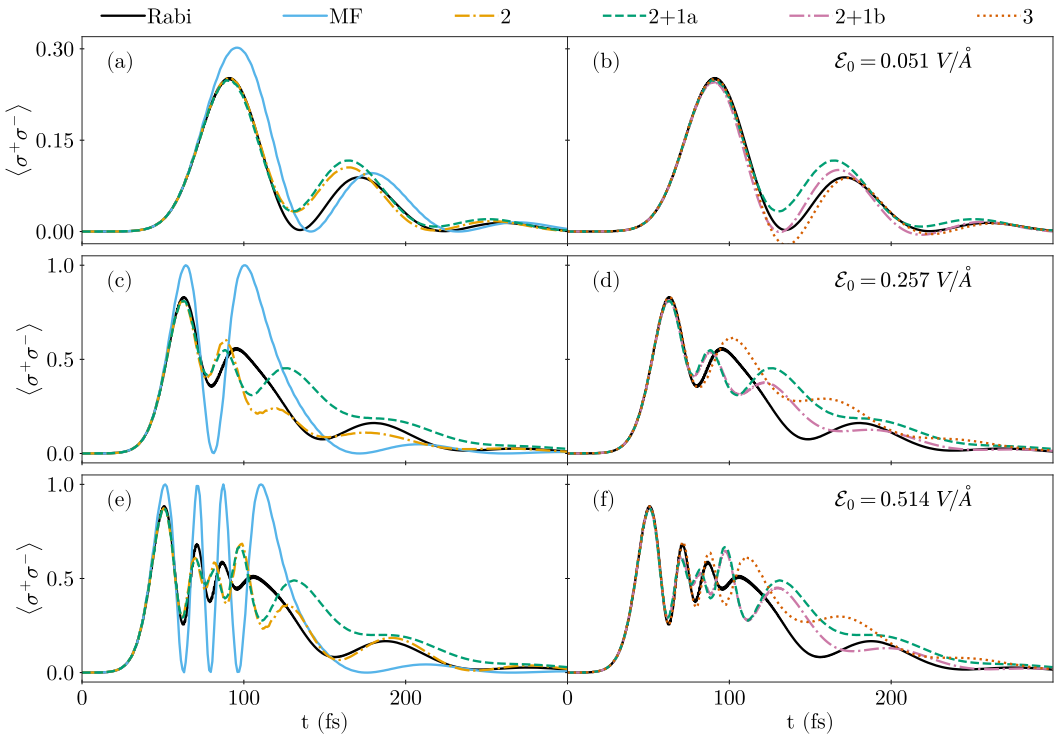

Fig. 3.7.: Like **3.5**, but for emitter-cavity coupling of $g = 0.024$ eV.

agreement with the exact dynamics.

An effect similar to the one observed in the previous figures when the amplitude of the classical field increases is observed when the coupling with the cavity modes becomes stronger. The results obtained when the light-matter coupling strength is $g = 0.024$ eV are shown in Fig. **3.7** for the Gaussian pulse and in Fig. **3.8** for the semi-infinite pulse, with the same driving pulses as in the previous case. When the amplitude of the electric field is $\mathcal{E}_0 = 0.051$ V/Å (subplots (a) and (b)), its magnitude is comparable to the coupling strength. The mean-field approximation, shown in subplot (a), then overestimates the population oscillations for both classical fields. This continues for more intense driving fields (subplots (c) and (e)). As mentioned above, while the mean-field approximation cannot reproduce spontaneous decay by itself, adding phenomenological decay constants to the mean-field equations

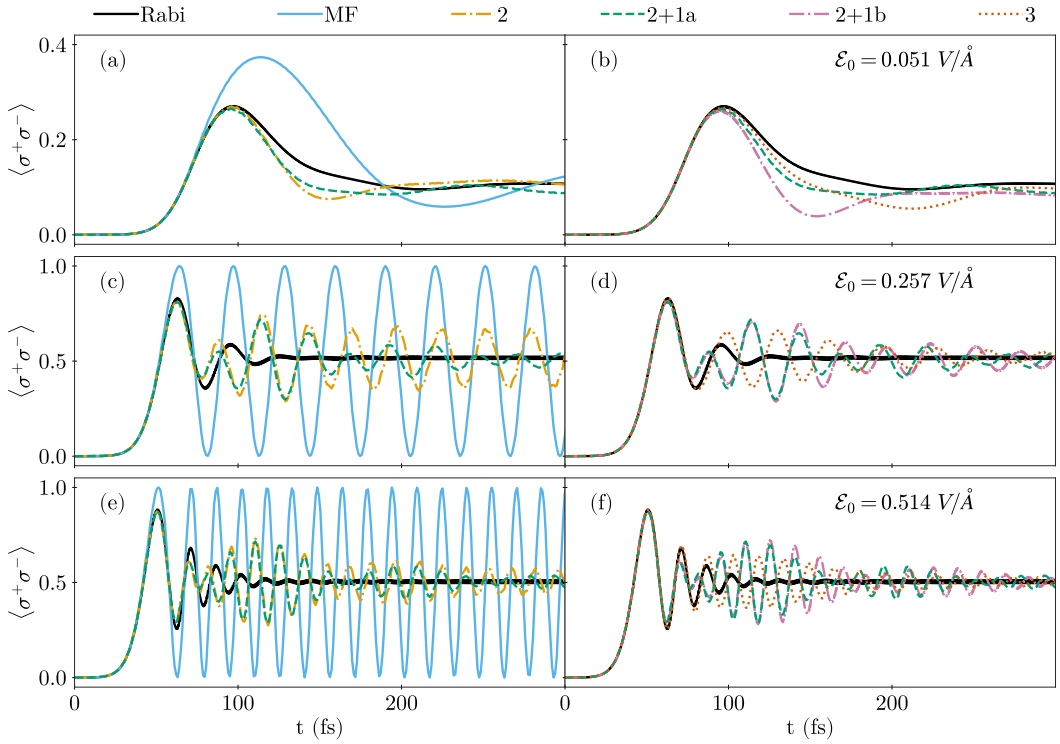

Fig. 3.8.: Like **3.7**, but for a semi-infinite driving pulse with constant amplitude after a smooth turn-on.

can be used to achieve reasonable descriptions of the strong-coupling regime for intense classical fields [180]. However, doing so means that the photons emitted due to field fluctuations are not represented, so that, e.g., the spontaneous emission from polaritonic states [181] could not be monitored in the emitted field.

Compared to the mean-field approach, the second-order approximation better predicts both the short-time dynamics as well as the steady-state limit for the semi-infinite pulse, but slightly overestimates the population at intermediate times, and the steady state in this approximation is achieved at latter times than in the dissipative Rabi model. This overall picture applies for all driving strengths studied. The corrections 2+1a and 2+1b somewhat improve upon the bare second-order calculation, with 2+1a working slightly

better for the semi-infinite pulses, Fig. **3.8**, and 2+1b working slightly better under short-pulse driving, Fig. **3.7**.

Finally, as could be expected, the third-order approximation improves the results for both the short and semi-infinite pulses. In particular, it perfectly reproduces the exact results at short times and, for intermediate and strong driving fields, during the first few Rabi oscillations. Although the description of the dynamics is not accurate after these oscillations, it also converges to the correct steady-state limit under the semi-infinite driving faster than the lower-order expansions. However, even the third-order expansion does not fully reproduce the dynamics at intermediate times, where decoherence starts to set in and induces corrections to the coherent dynamics, which are reflected in higher-order light-matter correlations at intermediate times. At longer times, where the system becomes mostly incoherent, the light-matter correlations are again well-described by lower-order expansions, and the steady state is thus well-represented within both second-order and third-order approximations.

To push the approximations more to their limit, the emitter-cavity coupling is increased to $g = 0.086$ eV. Again, the emitter population dynamics under short-pulse driving are shown in Fig. **3.9**, while for a semi-infinite pulse in Fig. **3.10**. The amplitudes of the classical electric fields and their parameters are the same as in the previous figures. For these parameters, the coupling is approaching the ultrastrong-coupling regime [147], as the Rabi splitting $\Omega_R \approx 2g = 0.172$ eV becomes non-negligible compared to the emitter frequency $\omega_e = 2.72$ eV. As was discussed in section **2.4**, now the counter-rotating terms in the light-matter interaction become important and even the ground state becomes dressed. Therefore, the system is coupled and its ground state does not correspond to the uncoupled ground state, i.e., both the emitter and the cavity modes in their ground states. However, this is the initial state chosen in this situation, which leads to fast "quenching" or "ringdown" oscil-

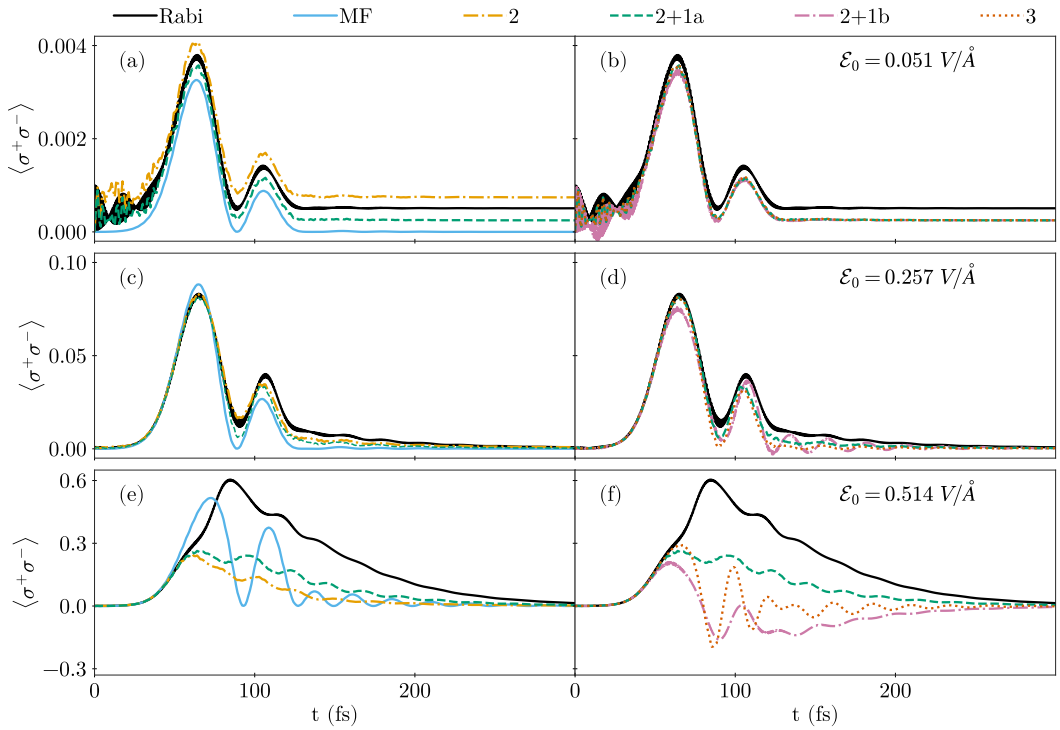

Fig. 3.9.: Like **3.5**, but for emitter-cavity coupling of $g = 0.086$ eV.

lations at short times when starting the dynamics. These are seen for weak driving fields in subplots (a) and (b) of figures **3.9** and **3.10**. Additionally, the very strong coupling implies that the polaritonic states of the coupled cavity-emitter system at $\omega_\pm \approx \omega_e \pm g$ are now quite strongly detuned from the driving pulse, which is tuned to resonance with the bare-emitter (and cavity) resonance frequency. The excitation amplitudes and driven Rabi oscillation frequencies in this case are therefore significantly smaller than for the previously treated systems with smaller light-matter coupling strengths.

Here again, the validity of the various approximations is investigated. The mean-field approximation cannot represent the ultrastrong-coupling induced changes, which only show up in correlations but do not lead to coherent fields. Therefore, neither the ground state nor the steady state of the system can be described correctly. This is especially noticeable under weak driving, as shown

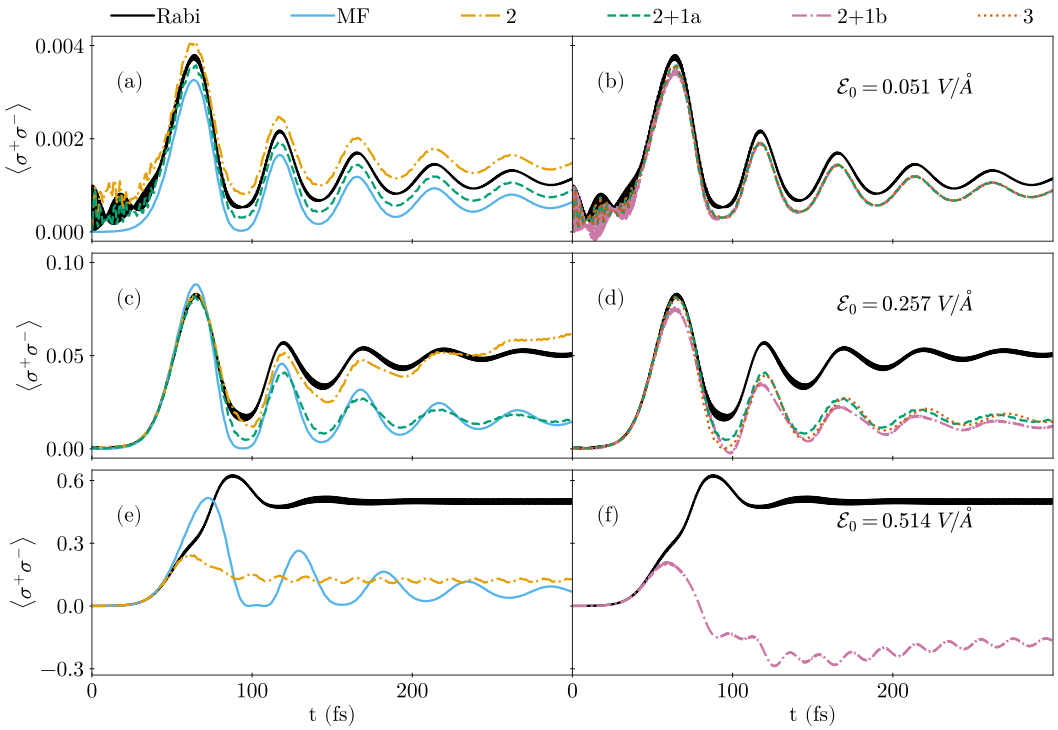

Fig. 3.10.: Like **3.9**, but for a semi-infinite driving pulse with constant amplitude after a smooth turn-on.

in subplots (a) and (b), where the shape of the driven oscillations is predicted reasonably well, but the final populations are underestimated for both types of driving. When the driving field amplitude is increased (subplots (c) and (d) in figures **3.9** and **3.10**), the correction to the population due to the counter-rotating terms becomes less noticeable since the laser-induced populations are larger and for the most intense driving fields (subplots e and f in figures **3.9** and Fig. **3.10**) the mean-field approximation breaks down .

The higher-order expansions improve on the prediction of the mean-fields just for the weakest driving. The 2+1a, 2+1b and third-order approximations all perform almost identically and neither of them manages to fully reproduce the dynamics. For higher driving fields, the predictions of the cumulant expansion methods start to diverge more and more from the exact results obtained

within the dissipative Rabi model.

This failure is most likely due to the fact that the low-order correlation expansions now have to reproduce both the ultrastrong-coupling induced correlations as well as the driving-pulse induced correlations, so that overall, higher-order correlations become more important than in cases with weaker emitter-cavity coupling. Still, under weak driving, all approximations manage to represent the overall dynamics reasonably well up to a global shift.

For strong drivings, the combination of them with the (ultra)strong light-matter coupling induces large correlations between light and matter that fail to be described within low-order cumulant expansions. In particular, in the case of the semi-infinite pulse, the results obtained within the cumulant expansion fail to reproduce the steady-state results even qualitatively and lead to significant shifts. It should be noted that these effects are expected to be less relevant when many emitters are included in the cavity [182].

Finally, for the most intense driving, none of the approximations reproduces the Rabi model even qualitatively for the short pulse, with the 2+1b and third-order results again reaching unphysical values of the emitter population, $\langle \sigma^+ \sigma^- \rangle < 0$. For the case of the semi-infinite pulse, Fig. **3.10**, a similar picture presents itself. For these strong driving pulses, none of the approximations captures the emitter dynamics well. In particular, the simulations using the 2+1a and third-order approximations break down even more dramatically shortly after the start of the pulse, with the emitter population diverging towards infinity. These results are therefore not shown here. These divergences, as far as can be determined in this study, are not due to numerical issues that could be solved by using better integration algorithms, but correspond to the actual behavior of the system description at the chosen level, and thus indicate a complete breakdown of the approximations.

3.3 Conclusions

In this chapter the cumulant expansion method has been explored to calculate the Heisenberg equations of motion for one emitter coupled to an arbitrary number of EM modes with an arbitrary spectral density, as obtained through the formalism of macroscopic QED in nanophotonic and plasmonic systems. In order to benchmark the method, its results have been compared to two well-known cases where quasi-exact solutions are available: An emitter in free-space, where perturbative approaches to light-matter coupling are valid, and a Lorentzian spectral density that can be mapped analytically to a Lindblad master equation describing the dissipative Rabi model, i.e., coupling of the emitter to a single cavity mode with losses. In the case of the cavity, the change in behavior as the coupling strength is increased from the weak up to the ultrastrong coupling regime has also been studied. Both the spontaneous emission dynamics where the emitter is initially excited and the behavior when a classical pulse pumps the system have been calculated and compared to exact solutions with the predictions at different orders of approximation.

For the initially excited emitter, going beyond the mean-field approximation is essential to describe spontaneous emission. However, while in free space the second-order approximation is enough to describe the emitter decay, in the cavity the fact that the photon can be reabsorbed after emission leads to corrections that are only well-described at higher orders of approximation. There is a single third-order term that encloses the main contribution at that order, $\langle a_n^\dagger a_m \sigma^z \rangle_C$, but the expansion of this term (via de 2+1a approach), although is a systematic correction of the second-order that does not imply specific assumptions, introduces non-neglgbible correlations that affect to de description of the dynamic. Then, it is necessary to explicitly disregard a fourth-order

expectation value, instead of performing the cumulant expansion on it (thus using the approximation we call 2+1b). Then, for this situation, assuming that the correlation expansion is a better approximation is not correct, as neglecting expectation values allows a better description of the dynamics without including to high order correlations.

As expected, the mean-field approximation is able to describe the emitter dynamics when a classical field pumps the system if coherent interactions are predominant. In free space the description is accurate, although the slow (nanosecond-scale) spontaneous emission and associated decay after the pulse again cannot be represented. The second-order approximation again can reproduce this decay.

In the strong coupling regime, i.e., when the emitter is coupled to a cavity mode with coupling strengths similar to or larger than the cavity losses, the second-order approximation fails to describe the dynamics in several cases. The combined action of the coherent driving laser pulse and the strong light-matter coupling with the cavity mode lead to an increase of light-matter correlations at intermediate times which is proportional to both the driving field strength and the light-matter coupling strength. In order to describe these correlations well, the order of the expansion has to be increased, with the third-order expansion being sufficient to describe most investigated cases. At later times, either after the pulse in short-pulse driving or when a steady state is approached under continuous driving, the required order of the approximation needed to describe the system well again decreases. However, for large enough emitter-cavity coupling strengths and driving intensities, the cumulant expansions at the orders used here fail to describe the dynamics and become unstable. In general, the order of approximation or even the validity of the cumulant expansion method to describe the emitter dynamics depends strongly on the physical system and the initial conditions and driving. This shortcoming in the cumulant expan-

sion method can be addressed by increasing the number of emitters so that if it is large enough, the second-order in the cumulant expansion converges much earlier [165].

Chapter 4 | Chain mapping models

4.1 Motivation

In the previous chapter, the dynamics of a QE were described without including any terms to explicitly account for the losses. Some quantum behaviors, like spontaneous emission, can be described by considering a huge number of modes. However, even when the coupling strength is weak enough so that a low order expansion can describe its dynamics accurately, this description can only be done up to some maximum time (given by the number of modes), at which the emitter photons interact again with the emitter. Therefore, the system was considered, in practice, isolated. However, any quantum system is coupled to its external environment with a large (essentially infinite) number of degrees of freedom, leading to the notion of open quantum systems (as presented in section **2.5**). Then, this chapter is devoted to the development of an approach so that the light-matter interactions between a QE and its surroundings can be done even for long times.

When perturbations of the environment caused by the system do not act back on it at later times, the Markovian limit is reached, and the dynamics of the system can be approximately described using a Lindblad master equation (discussed in section **2.5**). While the Markovian approximation is extremely useful in many situations, there are many cases in which it does not apply and thus require a more general treatment. Then, there is some memory time-scale for which the energy from the system to the environment feeds back into the system, and the interaction is non-Markovian.

4.2 Reaction coordinate mapping

Within this chapter, it is assumed that the environment is well-approximated as a collection of harmonic oscillators and that all relevant environment modes are of the same nature and thus interact with the system through the same system operator A_S. The Hamiltonian that describes a system S interacting with a harmonic environment, schematically depicted in figure **4.1**(a), can then be written as (with $\hbar = 1$)

$$H_0 = H_S + \sum_k \frac{\omega_k}{2}\left(\frac{p_k^2}{\alpha_k^2} + \alpha_k^2 x_k^2\right) + A_S \sum_k c_k \alpha_k x_k, \tag{4.1}$$

where H_S is the bare system Hamiltonian, A_S is the system part of the system-bath interaction operator, and $x_k = \frac{1}{\alpha_k\sqrt{2}}\left(a_k^\dagger + a_k\right)$ and $p_k = \frac{i\alpha_k}{\sqrt{2}}\left(a_k^\dagger - a_k\right)$ are (generalized) position and momentum operators for the kth harmonic oscillator with frequency ω_k, with an arbitrary scaling factor α_k that preserves the commutation relation $[x_k, p_l] = i\delta_{kl}$. The scaled variables $\alpha_k x_k$ and p_k/α_k are unitless, such that the units of x_k and p_k are determined by α_k. For example, the choice $\alpha_k = \sqrt{m\omega_k}$ gives the normal position and momentum operators for a massive particle with mass m. The real constants c_k characterize the cou-

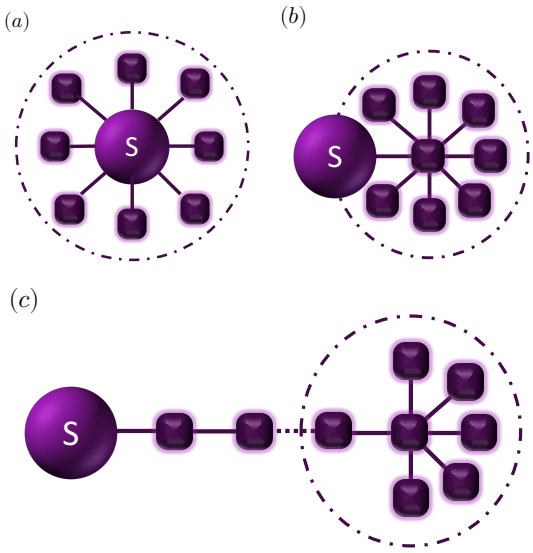

Fig. 4.1.: (a) Quantum system coupled to a discrete set of environment modes. (b) Quantum system coupled to a reaction mode (a collective environment mode), with this mode coupled to a residual bath of modes. (c) Chain mapping for the environment modes after n steps, with a residual bath of $N - n$ modes at the end of the chain.

pling between the bath modes and the system, with units of frequency if A_S is chosen unitless. The general form given in Eq. (4.1) can represent any physical system that can be (approximately) described by a collection of harmonic oscillators.

As has been discussed previously, the information about the interaction between a system and its surrounding environment is fully encoded in the spectral density $J_0(\omega) = \sum_k c_k^2 \delta(\omega - \omega_k)$. In many cases of practical importance, the bath modes are either continuous in frequency or their density is high enough that $J_0(\omega)$ can be treated as a continuous function (for example, the spectral density that describes the interaction between a two-level emitter and the electromagnetic modes of an arbitrary environment described through macroscopic electromagnetism, and is given by Eq. (2.55)). A structured spectral density therefore indicates that the bath has "memory", i.e., its influence on

the system depends on interactions at earlier times, while featureless spectral densities indicate memoryless (Markovian) environments.

Over the last decades, many methods to describe non-Markovian dynamics in arbitrary environments have been developed, among them the hierarchical equations of motion (HEOM) [183–186], stochastic methods [187–189] and time-adaptive density matrix renormalization group treatments [190–192]. In general, these descriptions are computationally costly, especially if the dynamics at long times are of interest.

In this context, a general conceptual approach is to transform structured baths in such a way that they either become amenable to approximate treatments or take a form for which specific numerical treatments become more efficient due to the transformed structure of the problem. In particular, such approaches are often based on taking the terms that contain the "memory" and transforming them so that the final description is more amenable, while this approximate system is also coupled to a residual bath that has little or no memory. The idea to achieve this is to enlarge the system by including one (or several) "reaction modes" of the environment that contain the memory. Among these approaches are the pseudomode method [193–196], effective Lindblad master equation procedure [197] and reaction coordinate mappings [198–201].

In the reaction coordinate mapping, an orthogonal transformation is applied to the bath modes such that the interaction between the system and the full environment is captured by a single mode, which itself interacts with the residual bath, as is shown in figure **4.1**(b). Applying this approach iteratively leads to a chain-like description of the environment, as shown in figure **4.1**(c), in which each mode is only coupled with its nearest neighbors [191, 202–204]. In particular, this representation allows a numerically efficient treatment based on tensor networks/matrix product states [90, 205]. Still, this technique is limited by the scaling of the computational effort with the size of the system, as

the size of the chain limits the maximum time at which the dynamics can be calculated, and correlations in the system grow over time, leading to an overall unfavorable scaling with propagation time. In some cases, this can be mitigated by using the transfer tensor method, which makes the scaling linear with propagation time [93, 206].

In this section, an overview of the reaction coordinate mapping is presented for a reservoir or bath of harmonic oscillators interacting with a general quantum system, with Hamiltonian given by Eq. (4.1). The following derivation starts with the assumption that the spectral density is nonzero in the interval $[\omega_L, \omega_R]$. The upper limit ω_R is assumed to be finite, either because of physical constraints or because of the introduction of an artificial cutoff (with higher frequencies assumed to only contribute a renormalization of the system frequencies). The lower limit ω_L is equal to zero in many cases of practical interest. In particular, it can be assumed that the bath is at zero temperature without loss of generality[1].

An orthogonal coordinate transformation that replaces the interaction term in Eq. (4.1) with a term involving a single coordinate can be performed, so that $\vec{X} = O\vec{x}$ and $\vec{P} = O\vec{p}$, where O is an orthogonal matrix, $OO^T = O^TO = \mathbb{1}$. Then, the first basis vector, i.e., the reaction coordinate, is chosen so that it contains the full coupling between the system and the bath,

$$X_1 = \sum_k \frac{c_k \alpha_k x_k}{D_1} = \sum_k O_{1k} x_k, \tag{4.2}$$

where D_1 is a normalization constant that ensures $\sum_k O_{1k}^2 = 1$, i.e., $D_1^2 = \sum_k c_k^2 \alpha_k^2$. The transformed coordinate X_1 is unique, apart from the election

[1] A special case is given by baths at finite temperatures, which can be replaced by an effective bath at zero temperature with an extended frequency range starting at $\omega_L = -\omega_R$ [112].

of α_k. The Hamiltonian after the transformation is thus

$$\mathcal{H}_1 = H_S + D_1 A_S X_1 + \sum_{k,i,j} \frac{\omega_k}{2} O_{ik} O_{jk} \left(\frac{P_i P_j}{\alpha_k^2} + \alpha_k^2 X_i X_j \right). \tag{4.3}$$

Since this transformation is orthogonal, the orthogonality of the new coordinates X_i and P_i is ensured, i.e., $[X_i, P_j] = i\delta_{ij}$. From now on, two particular elections of α_k will be considered. These two elections correspond to the so-called "particle" and "phonon" mappings, which in the literature have been derived based on a parameterized Bogoliubov transformation [204], and are natural consequences of performing the mapping with differently scaled parameters (i.e., different choices of α_k in Eq. (4.1)).

4.2.1 Phonon mapping

The first election consists of $\alpha_k = \tilde{\alpha_k} = \sqrt{\omega_k}$, which corresponds to the phonon mapping. This picking of α_k corresponds to mass-scaled coordinates in which the kinetic term has the same form for all oscillators. Then, the transformed Hamiltonian is

$$\tilde{\mathcal{H}}_1 = H_S + \tilde{D}_1 A_S \tilde{X}_1 + \frac{1}{2} \left(\sum_i \tilde{P}_i^2 + \sum_{ij} \tilde{C}_{ij} \tilde{X}_i \tilde{X}_j \right). \tag{4.4}$$

In this scaling, the momentum operators are diagonal, but the potential energy includes linear couplings between the oscillator coordinates, given by $\tilde{C}_{ij} = \sum_k \omega_k^2 O_{ik} O_{jk}$, while the diagonal elements $\tilde{C}_{ii}$ determine the frequencies of the transformed bath modes. In particular, the reaction coordinate frequency follows from the definition of X_1 as

$$\tilde{\Omega}_1^2 = \tilde{C}_{11} = \sum_k c_k^2 \omega_k^3 / \tilde{D}_1^2 = \frac{\sum_k c_k^2 \omega_k^3}{\sum_k c_k^2 \omega_k}. \tag{4.5}$$

Apart from O_{1k}, the transformation is not specified. This allows significant liberty to choose the form of the coupling matrix $\tilde{C}_{ij}$. One possibility is

to choose the coupling matrix for $i, j > 1$ to be diagonal. The Hamiltonian then is

$$\tilde{\mathcal{H}}_1 = H_S + \tilde{D}_1 A_S \tilde{X}_1 + \tilde{X}_1 \sum_{i=2} \tilde{d}_i \tilde{X}_i + \frac{1}{2} \sum_i \left(\tilde{P}_i^2 + \tilde{\Omega}_i \tilde{X}_i^2 \right), \tag{4.6}$$

where $\Omega_i = \tilde{C}_{ii}$ and $\tilde{d}_i = \tilde{C}_{1i}$. In this Hamiltonian, both the system and all the environmental modes are coupled to $\tilde{X}_1$. The schematic picture of this representation corresponds to figure **4.1**(b). Moreover, the coupling between the coordinate $\tilde{X}_1$ and the rest of the modes defines a new spectral density $\tilde{J}_1(\omega)$, which can be related to the original spectral density $\tilde{J}_0(\omega)$.

Another possible election for the Hamiltonian is to be tridiagonal (and explicitly constructed as such by using, e.g., the Lanczos algorithm), which directly describes the bath as a chain of harmonic oscillators coupled through nearest-neighbor interactions [204]. For sufficiently well-behaved (in particular, gapless) spectral densities, at each step in the chain, the spectral density of the "residual" bath, i.e., the rest of the chain, can be obtained analytically from that of the previous bath [199, 200, 204, 207]. As the reaction coordinate mapping is independent of the system, the relation between one "residual" spectral density and the "previous" one can be found by swapping the system to a classical coordinate s and finding the equation of motion of this coordinate. Making the Fourier transform of the equation of motion, one can relate both spectral densities to the same operator so that, at the end, the relation between them is given by

$$\tilde{J}_{n+1}(\omega) = \frac{\tilde{D}_{n+1}^2 \tilde{J}_n(\omega)}{\left| \tilde{W}_n^+(\omega) \right|^2}, \tag{4.7}$$

where $\tilde{W}_n^+(\omega)$ is

$$\tilde{W}_n^+(\omega) = \lim_{\epsilon \to 0^+} \int_0^\infty \frac{\nu \tilde{J}_n(\nu)}{\nu^2 - (\omega + i\epsilon)^2} \mathrm{d}\nu. \tag{4.8}$$

For sufficiently long chains ($n \to \infty$), the spectral density in this mapping

converges to

$$\tilde{J}_\infty(\omega) = \frac{\sqrt{\left(\omega^2 - \omega_L^2\right)\left(\omega_R^2 - \omega^2\right)}}{\pi}, \tag{4.9}$$

which is independent of any properties of the original spectral density apart from its frequency support. In this limit, the mode frequency and coupling also tend to limit values

$$\tilde{\Omega}_\infty^2 = \frac{\omega_R^2 + \omega_L^2}{2}, \qquad \tilde{D}_\infty = \frac{\omega_R^2 - \omega_L^2}{4}. \tag{4.10}$$

4.2.2 Particle mapping

If the reaction coordinate mapping is instead done using $\alpha_k = 1$, which corresponds to "natural" coordinates in which x_i and p_i are unitless and appear symmetrically in the Hamiltonian, the Hamiltonian after the transformation is

$$\mathcal{H}_1 = H_S + D_1 A_S X_1 + \frac{1}{2}\sum_{i,j} C_{ij}\left(P_i P_j + X_i X_j\right), \tag{4.11}$$

with $C_{ij} = \sum_k \omega_k O_{ik} O_{jk}$. This is the so-called "particle" mapping. The diagonal elements after this transformation again determine the new mode frequencies, $\Omega_i = C_{ii}$, with the reaction coordinate frequency in this mapping given by

$$\Omega_1 = \frac{\sum_k c_k^2 \omega_k}{\sum_k c_k^2}. \tag{4.12}$$

Rewriting Eq. (4.11) in terms of ladder operators $A_k = \frac{1}{\sqrt{2}}(X_k + iP_k)$, and choosing C_{ij} to be diagonal for $i, j > 1$ leads to

$$\mathcal{H}_c = H_S + \lambda_1 A_S(A_1 + A_1^\dagger) + \sum_i \Omega_i A_i^\dagger A_i + \sum_{i=2} d_i\left(A_i A_1^\dagger + A_i^\dagger A_1\right), \tag{4.13}$$

where $d_i = C_{1i}$, $\lambda_1 = \frac{1}{\sqrt{2}} D_1$ and a constant contribution $\sum_i \frac{1}{2}\Omega_i$ has been dropped. In the same way as before, the interaction between the reaction coordinate and the rest of the bath defined a new spectral density $J_1(\omega)$.

Choosing C_{ij} to be tridiagonal leads to a chain Hamiltonian of the form

$$\mathcal{H}_c = H_S + \lambda_1 A_S(A_1 + A_1^\dagger) + \sum_i \Omega_i A_i^\dagger A_i + \sum_i \lambda_{i+1}\left(A_i A_{i+1}^\dagger + A_i^\dagger A_{i+1}\right). \tag{4.14}$$

Now, it is seen immediately that the coupling between the different chain sites conserves the number of excitations. The absence of counterrotating terms that do not conserve the excitation number is *not* due to a rotating wave or similar approximation, but is exact and directly follows from the choice of coordinate scaling.

In the particle mapping, the recursion relation for the residual spectral density can be found following the same procedure as with the phonon mapping. After n steps this relation is given by

$$J_{n+1}(\omega) = \frac{\lambda_{n+1}^2 J_n(\omega)}{\left|W_n^+(\omega)\right|}, \tag{4.15}$$

where

$$W_n^+(\omega) = \lim_{\epsilon\to 0^+}\int_0^\infty \frac{J_n(\nu)}{\nu - (\omega + i\epsilon)}\mathrm{d}\nu, \tag{4.16}$$

with the limiting spectral density for $n \to \infty$ being

$$J_\infty(\omega) = \frac{\sqrt{(\omega - \omega_L)(\omega_R - \omega)}}{2\pi}, \tag{4.17}$$

with limiting values

$$\Omega_\infty = \frac{\omega_L + \omega_R}{2}, \qquad \lambda_\infty = \frac{\omega_R - \omega_L}{4}. \tag{4.18}$$

4.2.3 System

The particular system under consideration is a two-level emitter with transition frequency ω_e and transition dipole moment μ_e placed in the central gap of a nanoantenna consisting of a bowtie coupled to a nanosphere, as shown

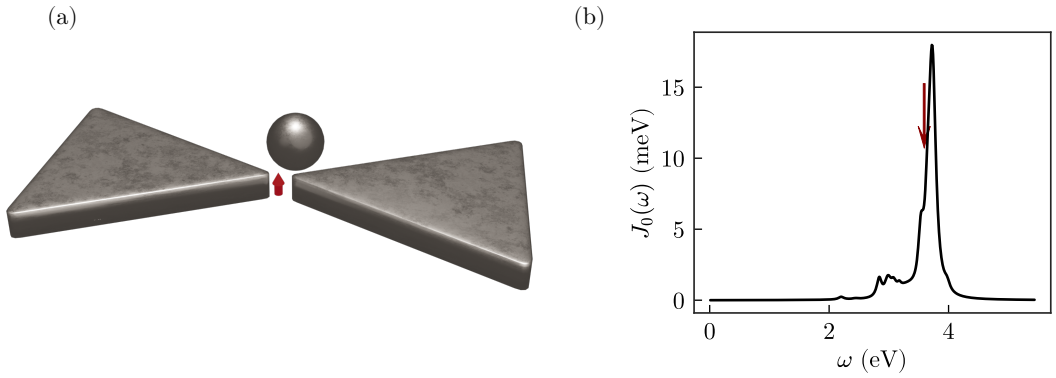

Fig. 4.2.: (a) Sketch of the physical system under consideration: A bowtie antenna and a nanosphere. In the center of the gap, a quantum emitter is placed (dark red arrow). (b) Spectral density for the emitter in the combined sphere-bowtie antenna. The emitter has a frequency chosen close to the maximum of the spectral density (indicated by the thin vertical line).

in figure **4.2**(a). For this setup, the system operators are $H_S = \omega_e \sigma^+ \sigma^-$ and $A_S = \sigma^+ + \sigma^-$, where σ^+ and σ^- are the two-level raising and lowering operators, respectively. Note that the transition dipole moment μ_e is included in the definition of the spectral density and A_S is unitless. The spectral density, given by Eq. (2.55), is shown in figure **4.2**(b) and is calculated using the SCUFF-EM package [208, 209].

The results of the frequencies and couplings at different sites of the resulting chains for the phonon and particle mappings are shown in figure **4.3**. Initially, when the number of transformations is small, i.e., at the beginning of the chain, they vary strongly, but then quickly converge to their final values and stay constant. Sufficiently far from the system, the infinitely long tail of the chain thus becomes translationally invariant. The chain mapping thus provides a description that closely resembles a spatial discretization of one-dimensional motion in a short-range "potential" that disappears at a sufficient distance to the system. This implies that any excitation that propagates along

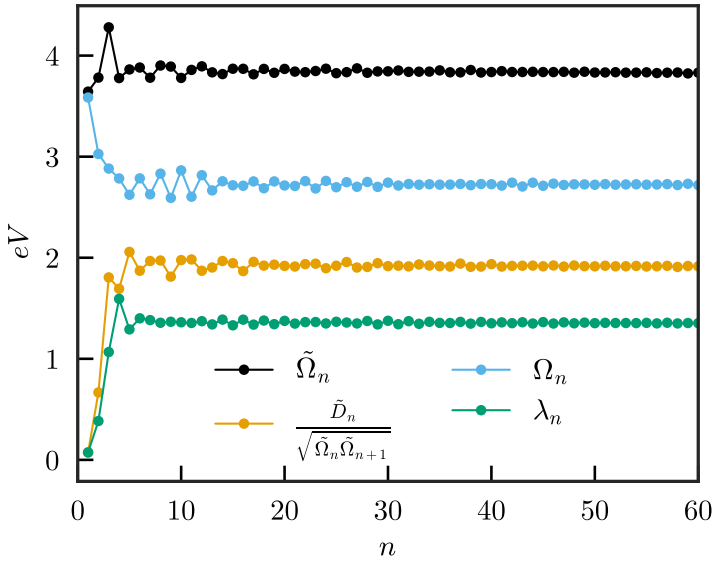

Fig. 4.3.: Chain mapping frequencies $\tilde{\Omega}_n$, Ω_n and coupling parameters $\tilde{D}_n$, λ_n for the phonon and particle mapping.

the chain will not be reflected anymore after reaching a sufficient distance and can thus not affect the system. This general structure implies that the chain mapping naturally provides a separation of any bath into

(i) a non-Markovian part close to the system, where excitations can be reflected due to the position-dependent coupling and energy at each site, and then interact again with the system, leading to memory effects,

(ii) a Markovian part far enough away from the system where excitations propagate along a featureless continuum, such that their "momentum" along the chain is conserved and they are just transported away without ever affecting the system again.

However, there is no sharp boundary between the two parts, and the transition is gradual. This evolution of the parameters as the chain length increases can also be seen in the spectral densities. Figure **4.4** shows the "residual" spectral

densities after some transformations (indicated by the number in the legend of each plot). Panel (a) corresponds to the phonon mapping and panel (b) to the particle mapping. For both transformations, it can be seen how the spectral density tends to the limiting value in a short range, although small differences persist up to longer chains, thus making slight changes in the frequencies and coupling shown in figure **4.2**(b) at intermediate longitudes.

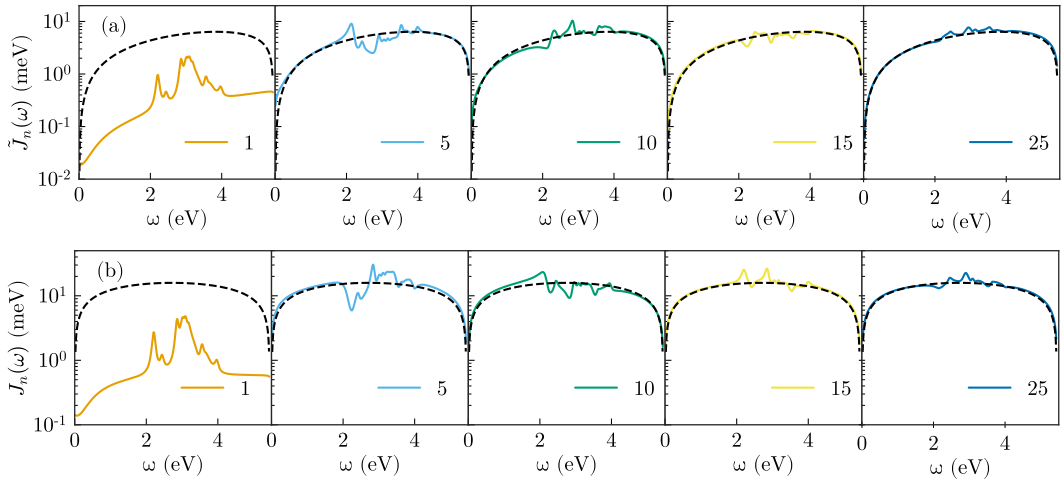

Fig. 4.4.: "Residual" spectral densities for the phonon mapping (a) and the particle mapping (b). The legend in each plot shows the position in the chain for which the spectral density is obtained, while the dotted line corresponds to the limiting spectral density.

4.3 Chain truncations

Throughout this section and in the following, results only for the particle mapping are shown, as is this mapping where the number of excitations in the

chain is a conserved quantity, which is advantageous for quantum simulations.

The previous results prove that the chain mapping is then a transformation that allows the exact description of arbitrary photonic environments. However, in practical calculations, it is not possible to explicitly treat an infinite chain, and it has to be truncated at some maximum length. When this truncation is performed by simply removing all chain sites after a given distance to the system, the wave packets propagating along the chain are reflected back and interact with the system again after some time. If time propagation simulations are performed for maximum times smaller than the ones given by the length of the chain, this direct truncation can be done and the description of the light-matter interactions are accurately done. However, this is not usually the case, and such an approach thus limits the numerical simulations to propagation times smaller than roughly twice the propagation time along the chain [90, 93, 210, 211]. This is demonstrated in figure **4.5**, which shows the Wigner-Weisskopf dynamics of a quantum emitter with frequency $\omega_e = 3.6$ eV for different chain lengths. The shortest chain shown ($N_C = 40$) is already long enough so that both Ω_n and λ_n have essentially reached their limiting values. Still, the emitter dynamics are clearly not well described for $t \gtrapprox 25$ fs due to unphysical reflections from the end. As the chain length increases, the unphysical reflections travel more distance and the maximum time for which the dynamics are well-described also increases. The results using $N_C = 300$ are exact for the whole range of times considered here (up to $T = 120$ fs), and will be taken as the reference result in the following.

The truncated chains have to become very long to be able to correctly describe the system dynamics at long times. However, the emitted wave packets should not influence the system anymore after having propagated far enough along the chain, and it thus should not actually be necessary to treat them explicitly at larger distances. Therefore, the main question in this study is

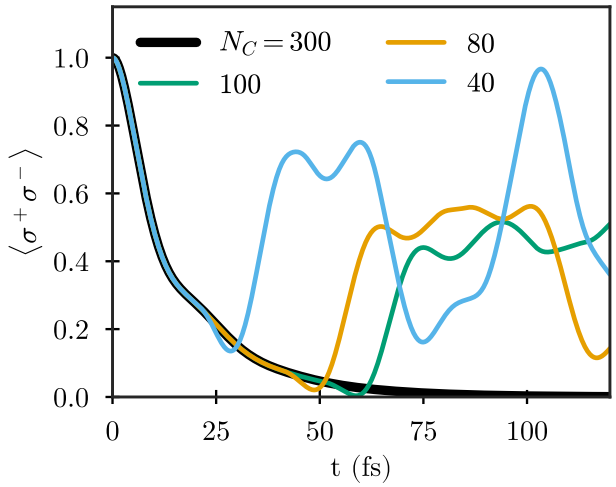

Fig. 4.5.: Excited-state population of an initially excited two-level quantum emitter with frequency $\omega_e = 3.6$ eV and dipole moment $\mu_e = 0.6$ e nm coupled to the antenna shown in figure **4.2**(a), calculated using chains truncated after different numbers of sites N_C.

whether or not a finite chain can describe the dynamics of the infinite system. Since the residual spectral density describing the rest of the chain far enough away from the system is relatively smooth, as is shown in equations (4.9) and (4.17), the most straightforward approach to attempt to reproduce the losses of the perturbation away from the chain is to simply treat that rest as a Markovian bath acting on the last chain site. This approximation replaces all chain sites with $n > N_C$ by a Lindblad term in the master equation for the density matrix ρ describing the system and chain up to site $n = N_C$:

$$\partial_t \rho = -i\,[H, \rho] + \gamma \mathcal{L}_{A_{N_C}}[\rho]\,, \tag{4.19}$$

where $\gamma = 2\pi J_{N_C}(\Omega_{N_C})$ and $\mathcal{L}_O[\rho] = O\rho O^\dagger - \frac{1}{2}\{O^\dagger O, \rho\}$.

In the particle mapping, and assuming that N_C is chosen large enough so that the limiting residual spectral density is reached, the residual spectral density is symmetric about Ω_{N_C} and there is no Lamb shift (i.e., bath-induced energy shift) on the mode frequency. The emitter dynamics using this ap-

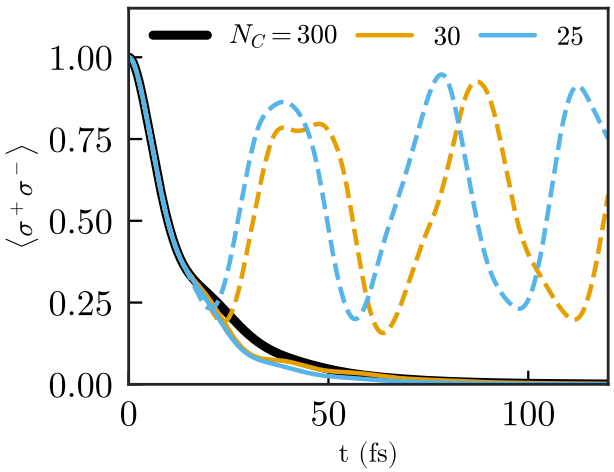

Fig. 4.6.: Population of the same emitter as in figure **4.5** for two different chain lengths: $N_C = 30$ (orange) and $N_C = 25$ (blue) compared with a long chain ($N_C = 300$), which is considered exact. Comparison between the chains without any absorbing terms (dashed lines) and chains with a single absorbing term at their end, given by $\gamma = 2\pi J_{N_C}(\Omega_{N_C})$.

proximation, shown in figure **4.6**, are much more similar to the exact results compared to the abrupt truncation for the same chain length. However, they clearly do not provide perfect agreement. As the chain length is again long enough for the limiting values of the chain to be achieved, these differences are because they still suffer from residual reflections. This outcome agrees also with the spectral shape of the residual spectral densities, given by equations (4.9) and (4.17). They are structured and not actually Markovian (which would correspond to a constant spectral density spanning an infinite frequency range). This implies that a "naive" Markovian approximation that just adds losses on the last chain site will necessarily lead to reflections.

One can thus take inspiration in the fact that the chain resembles a discretized continuum, i.e., the goal of minimizing reflections on the chain is similar to the goal of absorbing outgoing waves in numerical simulations of continuous systems. This suggests that smoothly increasing losses along the

chain, similar to the complex absorbing potentials (CAPs) used in quantum mechanics [212–214], could significantly suppress reflections along the chain. The corresponding master equation then becomes

$$\partial_t \rho = -i\,[H, \rho] + \sum_n \gamma_n \mathcal{L}_{A_n}[\rho]\,, \tag{4.20}$$

where the γ_n have to be chosen so as not to affect the dynamics close to the system, avoid reflections due to abrupt changes in the decay rate, and simultaneously absorb all outgoing wavepackets before reaching the end of the (truncated) chain.

A functional form inspired by standard CAPs is used to parametrize the decay rates,

$$\gamma_n = \Theta(x_n)(\alpha x_n + \beta x_n^2), \tag{4.21}$$

where $x_n = \frac{n-N_d}{N_C-N_d}$, $\Theta(x)$ is the Heaviside theta function, N_d determines the chain site at which losses start, and α and β are real numbers that determine the strength of the absorption. To ensure a good description of the dynamics, N_d must be chosen large enough (roughly such that the chain mode frequencies and coupling strengths have reached their asymptotic limits). In figure **4.7**(a), again the decay of the QE is considered, but now the decay rates are parametrized using the above equation, i.e., the emitter is initially excited ($\omega_e = 3.6$ eV) and different chains with smoothly increasing absorption are presented. In particular, $\alpha = 0.02$ and $\beta = 0.1$ for all chains and the combinations considered are $(N_C, N_d) = (30, 8), (25, 7), (15, 5)$.

With this choice of parameters, the emitter dynamics are well-reproduced for long enough chains, and no reflections of the population are observed. Although here the dynamics are shown within the single-excitation subspace (i.e., for the Wigner-Weisskopf problem), it is known that, as discussed in section **1.2**, if the effective spectral density of the chain with losses agrees with the full spectral density, the results will be identical regardless of the number

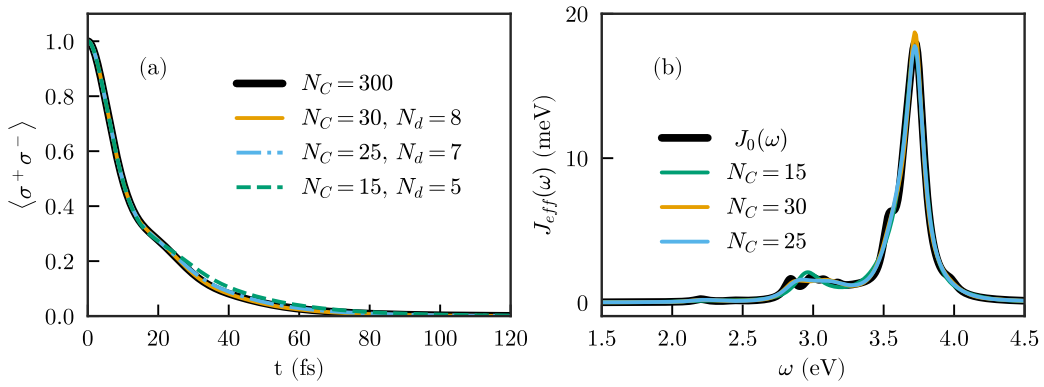

Fig. 4.7.: (a) Population for the quantum emitter for three different chain lengths: $N_C = 30$ (orange), $N_C = 25$ (blue) and $N_C = 15$ (green) compared to the "infinite" chain (black). An absorbing function has been added to the first three chains. The parameters are chosen to give a good description of the dynamics, but a wide range is valid for the first to lengths. When the chain is very short, as for $N_C = 15$, the prediction of the dynamics starts to break down. (b) Effective spectral densities when the absorbing terms are added in the Hamiltonian for the same lengths as in (a). For $N_C = 30$ and $N_C = 25$, the effective spectral density is similar to $J_0(\omega)$, although neither of them describe it in detail. For $N_C = 15$ the effective spectral density presents a shift in the frequency of the main peak of $J_0(\omega)$, affecting the dynamics.

of excitations. The effective spectral density for the lossy chains used here is shown in figure **4.7**(b), where it can be seen to indeed agree quite well with the exact spectral density of the longer chains.

However, while the approach of treating the chain index like a "spatial" coordinate and adding an absorbing potential at the end indeed works, it requires relatively long chains to produce good results, i.e., the frequencies and nearest-neighbors couplings have reached their limiting values before the decay rates become significant. For shorter chains, the requirement that the chain is approximately translation-invariant by the time the absorption sets in cannot be satisfied, and absorption necessarily leads to loss of information

about the dynamics. This is, e.g., the case for $N_C = 15$, for which both the emitter dynamics and the effective spectral density are seen to not agree as well with the exact results as for longer chains even after optimizing the parameters α and β.

4.4 Fitted chain

In the previous section, the parameters α and β were chosen "by hand". This election is possible because there is some liberty in it, i.e., small differences in the chosen parameters do not change the correct description of the dynamics for long enough chains. This fact raises the question of whether or not an optimization can be done in the choice of the parameters so that the length of the chain needed to do a complete description of the open quantum system can be decreased. In particular, this optimization is performed for a given chain length, so it is useful if the system is well-described for a shorter chain than the minimum one found when manually imposing a smooth "absorption potential". This approach is inspired by related methods to replace an arbitrary bath by a system of auxiliary oscillators with losses [101, 195], where the auxiliary modes are restricted to form a chain, i.e., they are only allowed to have nearest-neighbor interactions. Then, the emitter is only coupled to the first mode. However, instead of using the analytic chain transformation to obtain the parameters of this new chain, the chain parameters are fitted to optimally reproduce the actual bath.

As mentioned along this thesis, the quantity that fully characterizes the bath is the spectral density $J(\omega)$. Moreover, as it is related with the classical dyadic Green's function $\mathbf{G}(\mathbf{r}, \mathbf{r}', \omega)$ is an easily known quantity for arbitrary

systems. Another equivalent quantity, the correlation function $C(t)$, can be defined by doing the Fourier transform of the spectral density

$$C(t) = \theta(t) \int_{-\infty}^{\infty} J(\omega) e^{-i\omega t} \mathrm{d}\omega. \tag{4.22}$$

Here, zero temperature is assumed[2]. The correlation function $C(t-t')$ encodes the action of the bath on the system at time t due to the system dynamics at time t'. This suggests that fitting $C(t)$ up to some maximum time could be a promising strategy when only short-time dynamics are of interest, since one explicitly discards the information about long-time dynamics that is implicitly encoded in $J(\omega)$. In order to test this strategy, the fit of either the spectral density $J(\omega)$ or the correlation function $C(t)$ up to the maximum propagation time is presented.

For the model used here, the effective spectral density of the chain is given by [101]

$$J_{\mathrm{mod}}(\omega) = \frac{\lambda_1^2}{\pi} \mathrm{Im} \left\{ \frac{1}{\tilde{\mathbf{H}} - \omega} \right\}_{11}, \tag{4.23}$$

where $\tilde{\mathbf{H}}$ is a tridiagonal complex symmetric (not Hermitian) matrix, with the tridiagonal real part containing the coupling matrix of the chain, and the diagonal imaginary part encoding the losses, i.e., $\tilde{\mathbf{H}}_{i-1,i} = \tilde{\mathbf{H}}_{i,i-1} = \lambda_i$ and $\tilde{\mathbf{H}}_{i,i} = \Omega_i - \frac{i}{2}\gamma_i$. By diagonalizing $\tilde{\mathbf{H}} = V\tilde{\Omega}V^T$, where V is a complex orthogonal (not unitary) matrix containing the eigenvectors, with $V^T V = \mathbb{1}$, and $\tilde{\Omega}$ is a diagonal matrix containing the (complex) eigenvalues $\tilde{\omega}_i$, both the spectral density and the correlation function can be written as a simple sum

[2] A zero-temperature chain can represent any finite-temperature bath by adjusting the chain spectral density to reproduce the (temperature-dependent) power spectral density of the bath [112].

of independent terms,

$$J_{\mathrm{mod}}(\omega) = \frac{\lambda_1^2}{\pi} \sum_i \mathrm{Im}\left\{ \frac{V_{1i}^2}{\tilde{\omega}_i - \omega} \right\}, \tag{4.24}$$

$$C_{\mathrm{mod}}(t) = \theta(t) \frac{\lambda_1^2}{\pi} \sum_i V_{1i}^2 e^{-i\tilde{\omega}_i t}. \tag{4.25}$$

This shows that if the fit is fully converged, fitting the spectral density or the correlation function is completely equivalent. However, both quantities weigh differently different aspects of the dynamics, so their convergence behavior when fitting to one or the other quantity can be different, and using each of them may be advantageous depending on the time scale of interest.

When fitting the correlation function, a weighted error is used,

$$\mathrm{err} = \int_0^{t_{\mathrm{max}}} |C(t) - C_{\mathrm{mod}}(t)|^2 \times |C(t)| \mathrm{d}t, \tag{4.26}$$

so that it has a more significant contribution when the correlation is stronger. This definition gives better results than a "naive" fit without weight, as it improves the fit in regions where the correlation function is larger and thus more important.

In both approaches, the parameters of the truncated chain Ω_i and λ_i are the initial guesses for the fit, but they can vary freely in the fitting process. For the decay rates γ_i, the initial guess consists on small random numbers. Figure **4.8** shows the decay for the same quantum emitter for a chain of length $N_C = 15$ after using both optimizations. In both cases, the descriptions of the emitter dynamics are comparably good using a much shorter chain than with the previous approaches. While both methods offer similar results, we have found that the fit to the correlation function is more stable and less sensitive to initial parameters than the fit to the spectral density.

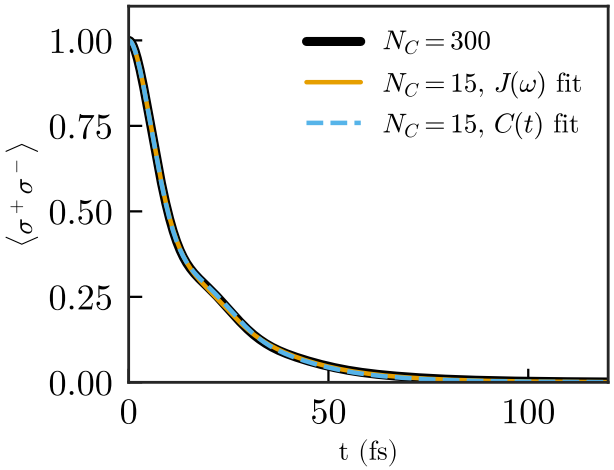

Fig. 4.8.: Population of the quantum emitter for $N_C = 15$ after the fit to the spectral density (orange) and the fit to the correlation function (blue).

4.5 Next-nearest neighbor coupled chain

In the previous section, although the chain parameters were allowed to vary freely to obtain an optimized description of the bath spectral density, the topology of the chain was maintained, i.e., only nearest-neighbor coupling, and only the first site coupled to the emitter. This restricts the possible freedom and implies that a chain with N sites has less flexibility to represent an arbitrary spectral density than a system of N modes with arbitrary couplings between each other and to the emitter, as used in [101]. The current section is devoted to prove that relaxing these conditions to allow next-nearest neighbor coupling between the chain sites and the chain and the emitter actually appears to be sufficient to represent an arbitrarily complex spectral density for a given number of sites N. To motivate this, first the model developed in Ref. [101] is summarized. A more complete derivation of this model for multiple emitters can be found in **chapter 5**.

The starting model consists of a QE coupled to an arbitrary number N of discrete modes. Each of these modes is at the same time coupled to a Markovian (i.e., spectrally flat) bath represented by a continuum of modes. Moreover, these N discrete modes are mutually interacting modes, leading to the model spectral density

$$J_{\mathrm{mod}}(\omega) = \frac{1}{\pi}\vec{g}\cdot \mathrm{Im}\left\{\frac{1}{\tilde{\mathbf{H}}-\omega}\right\}\cdot\vec{g}, \tag{4.27}$$

where $\tilde{\mathbf{H}}$ is a complex symmetric $N\times N$ matrix with real off-diagonal terms, $\tilde{\mathbf{H}}_{ij} = \omega_{ij} - i\delta_{ij}\gamma_i$, and $\vec{g} = (g_1, g_2, \ldots, g_N)$ is a real coupling vector. The expression given in Eq. (4.23) is thus simply the specialization of this expression to the case where ω_{ij} is tridiagonal and $\vec{g} = (\lambda_1, 0, \ldots, 0)$. In the general form given here, the number of fit parameters is quite large, being equal to $N(N+1)/2 + N + N$ real numbers for ω_{ij}, γ_i, and g_i, respectively. However, when $\tilde{\mathbf{H}}$ is diagonalizable, $\tilde{\mathbf{H}} = V\tilde{\Omega}V^T$, the same expression can be rewritten as

$$J_{\mathrm{mod}}(\omega) = \frac{1}{\pi}\mathrm{Im}\left\{\vec{G}\cdot\frac{1}{\tilde{\Omega}-\omega}\cdot\vec{G}\right\} = \frac{1}{\pi}\sum_i \mathrm{Im}\left\{\frac{G_i^2}{\tilde{\omega}_i-\omega}\right\}, \tag{4.28}$$

where $\vec{G} = \vec{g}V$ is the coupling vector transformed to the eigenbasis of $\tilde{\mathbf{H}}$. In this form, the effective number of distinct parameters in the system is much smaller than in the original form, and is given by the $4N-1$ real parameters necessary to describe the N complex eigenvalues $\tilde{\omega}_i$ and N complex coupling parameters G_i, with one less parameter due to the constraint that $\vec{G}\cdot\vec{G} = \vec{g}\cdot\vec{g}$ is real, i.e., $\mathrm{Im}\sum_i G_i^2 = 0$. This shows that the original form, Eq. (4.27) has many more parameters than required to characterize the spectral density. On the other hand, the tridiagonal chain form chosen in Eq. (4.23) has only $3N$ free parameters ($2N-1$ for the real symmetric tridiagonal ω_{ij}, N decay rates γ_i, one coupling λ_1), and thus necessarily induces hidden correlations in the values of G_i and $\tilde{\omega}_i$ that determine the spectral density.

It is thus tempting to directly use the diagonal form Eq. (4.28), in which the spectral density is written as a sum of simple poles (and the correlation function a sum of complex exponentials). However, in practice this turns out to be difficult, as recently discussed in some detail in [196]. First, since $\vec{G}$ is complex, this form of the spectral density cannot be directly mapped to a physical system. Second, there are physical constraints that are not easily satisfied in this form. In particular, $J_{\mathrm{mod}}(\omega)$ has to be non-negative for any ω, which is guaranteed when the loss rates γ_i are all non-negative in the original form [101], but not automatically fulfilled when fitting $\tilde{\omega}_i$ and G_i. Furthermore, even when such a set of parameters has been found, it is a highly nontrivial problem to find a complex orthogonal transformation matrix V to "undo" the diagonalization such that the resulting g_i are real and $\tilde{\mathbf{H}}$ can be mapped to a physical system, which furthermore requires that its imaginary part is positive definite. We are not aware of any constructive algorithm to achieve this, apart from the one developed for the case $N = 2$ in Ref. [196]. It is thus advantageous to perform the fitting in the original form, where the physicality can be guaranteed by constraining all γ_i to be nonnegative, and no additional work to find a physical system is necessary after the fit.

Given the above, an interesting question is whether the number of parameters in $\tilde{\mathbf{H}}$ and $\vec{g}$ can be reduced while keeping the full flexibility of the method. By maintaining the chain form, but allowing next-nearest neighbors for all the modes in the chain, including the emitter, the number of free parameters is exactly $4N-1$, equal to the number of actually independent degrees of freedom after diagonalization. The matrix $\tilde{\mathbf{H}}$ is then pentadiagonal complex symmetric, with off-diagonal entries being real, while $\vec{g} = (g_1, g_2, 0, \ldots, 0)$ has two (real) nonzero entries. This suggests that this form might be sufficient to obtain the optimal fit of any spectral density with a given number of modes N, while still maintaining the computationally advantageous property of a chain form with only short-range interactions between sites. In figure **4.9**(a), it is

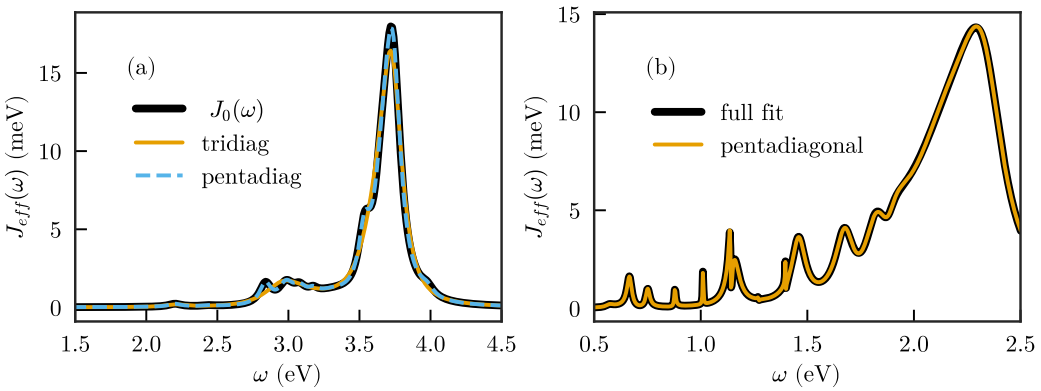

Fig. 4.9.: (a) Fit of the spectral density of **4.2**(a) when allowing next-nearest neighbor interactions in the chain, compared to a fit with only nearest neighbor interactions with the same number of modes ($N = 15$). (b) Fit of the spectral density of Ref. [101] using a chain with next-nearest neighbor interactions. Black line: Original fit using a full matrix ω_{ij}, with all modes coupled to the emitter. Yellow line: Fit of the same data using a chain with only next-nearest neighbor interactions, and the emitter only coupled to the first two sites.

shown that this form indeed permits a significantly improved description of the spectral density with the same number of modes.

While we are not aware of any formal proof that the chain with next-nearest neighbor interactions is indeed sufficient to represent any N-mode spectral density, we furthermore show the fit to the spectral density of the system treated in [101] (i.e., the spectral density for the limit of a single emitter, in particular Gap, in section **5.4**), which consists on a dual plasmonic nanoparticle antenna embedded inside a high-dielectric microsphere. The hybridization between whispering gallery modes of the microsphere and the plasmonic nanoparticle resonances leads to a complex spectral density with strong interference features [65, 66]. As seen in figure **4.9**(b), this complex spectral density is also well-represented when the fit is performed for a chain with next-nearest neighbor coupling. However, it should be mentioned here that while

the final fit does indeed reproduce the full spectral density, obtaining that fit is far from trivial. In particular, the fit with the next-nearest neighbor chain converges significantly worse and is much more sensitive to getting stuck in local minima than the fit with the full matrix. Obtaining a good fit for a complex spectral density then requires significant manual intervention (although it is possible that more advanced fitting methods than used here could mitigate this).

4.6 Conclusions

The interaction between a quantum system with an arbitrary complex environment can be described by doing a reaction coordinate transformation so that the representation of the system has the form of a chain. In particular, for nanophotonic systems, a particular transformation that preserves the number of excitations can be chosen. After this transformation, the value of the frequencies and couplings in the chain tend to a limit constant value, which indicates that the environment does not act back into the system. However, when treating finite chains, some reflections effects are encountered, as in practice the excitations never leave the system. This forces to use very long chains, but in practice it needs a computational effort that scales badly with the size of the system.

Then, in this chapter, several approaches for truncating chain mappings of open quantum systems while maintaining an accurate description of the system dynamics have been studied. The approaches are based on adding dissipation to the chain modes in a way that minimizes reflections and thus reproduces the system dynamics optimally. As a first approach inspired by

complex absorbing potentials, gradually increasing decay rates along the chain are used, which requires relatively long chains to work efficiently. After that, it has been shown that the chain length can be reduced significantly by not using the formal chain mapping and then adding losses a posteriori, but by adjusting the chain parameters in a fitting procedure to reproduce either the environment spectral density or its correlation function.

Finally, relaxing the restriction on the chain form of the transformed system and allowing next-nearest neighbor coupling (also for the system itself) has been found to be enough to describe any spectral density characterized by N_C resonances with a chain of N_C sites, i.e., the degrees of freedom given to the system are sufficient and adding more (such as longer-range coupling along the chain) is not necessary for achieving the optimal description. Chains with next-nearest neighbor coupling could thus be seen as the "sweet spot" where the chain length is minimized and computational complexity is still limited (in particular, tensor network approaches can be expected to work well due to the quasi-1D nature of the problem).

Chapter 5 | Few-mode Quantization for multiple emitters

5.1 Introduction

Strategies to describe the photonic environment when only one quantum emitter is placed within one setup have been presented in previous chapters. In the following, however, the description of multiemitter situations is attempted. In particular, this chapter presents the generalization of the method discussed in Ref. [101] for one emitter, to several ones. The previous model can treat arbitrary photonic structures, but in the formulation presented therein, it is only suitable for situations where only a single emitter is present in the system and all considered emitter dipole transitions are co-aligned. Therefore, in this chapter these restrictions are lifted and the approach is extended to a collection of emitters with arbitrary orientations of the transition dipole moments. This generalization allows to study interactions between QEs (mediated by the EM field) such

as, for example, population transfer.

The theoretical description of the photon-mediated interaction between quantum emitters and their control has generated great interest over the last years, since it is essential for quantum technology applications, such as quantum networking, quantum information and quantum computation [215–218]. Nanophotonic devices constitute promising platforms to engineer such interactions because they support subwavelength light confinement, as the large confinement achieved at this scale enables large emitter-photon coupling strengths and thus fast dynamics. At the same time, achieving strongly subwavelength confinement typically relies on the use of highly lossy constituents, such as metallic nanoparticles with plasmonic resonances [56], and furthermore requires that the quantum emitters are brought close to the material surfaces. In these conditions, the EM mode spectrum typically contains a series of broad and overlapping resonances [62]. Quantizing the electromagnetic field in such systems is highly nontrivial, as losses cannot be neglected nor treated perturbatively, such that standard approaches of quantization fail [9, 219].

One powerful approach is the macroscopic QED framework (introduced in section **2.1**). However, within this quantization scheme, the EM field is described by an extremely large continuum of bosonic modes, as they exist for any positive value of the frequency ω. While this approach has proven hugely successful for treating problems where the EM modes are treated perturbatively or integrated out in some other way, it is not directly useful for applying cavity-QED-like approaches in which the modes are treated as explicit degrees of freedom of the system. This shortcoming, combined with the increasing interest in metallic and metallodielectric subwavelength cavity QED systems, in which highly lossy resonances act as effective cavity modes, has led to the development of several approaches that allow the construction of few-mode quantized models in which the full quantized EM field is approximately de-

scribed through a (small) collection of discrete quantized modes. One approach relies on quasinormal modes, as was summarized in section **1.2**. This approach is powerful but relies on being able to select just a few quasinormal modes of the system. In the case of nanometric-sized metallic structures, a similar quantization strategy has been used, but greatly simplified through the quasi-static description of sub-wavelength-confined plasmonic fields [62, 80, 220, 221].

The approach employed in this chapter exploits the fact that, due to its linearity, a system of harmonic oscillators (such as EM modes) is fully determined by its linear response to the quantum emitter, encoded in the spectral density. This offers the possibility to construct a model system that shows the same response, but is significantly easier to solve than the original problem. One important advantage of this model lies in the fact that it can account for a peak consisting of many underlying resonances (quasinormal modes) with just one or a few model modes. Such a situation is often encountered in the so-called pseudomodes in plasmonic systems, which arise due to the collective response of high-k modes in planar systems [176] or high-order multipoles in spherical ones [220].

In order to do so, first the definition of the spectral density is generalized to the case of several light-matter interaction operators [78, 83, 222]. The spectral density $J(\omega)$, which is normally a scalar function that fully characterizes the interaction between a quantum system and a bath mediated by a single interaction operator [86, 195], then becomes an $M \times M$ matrix-valued function. Here, M is the number of distinct interaction operators that are treated ($M = 3M_e$ for M_e dipolar emitters with all three possible dipole orientations taken into account for each emitter). Then the few-mode quantization approach presented in Ref. [101] is extended to this case.

5.2 Theory

The starting point is a general model consisting of a matter part (which can represent multiple emitters) linearly coupled to a collection of bosonic modes (which will later represent the medium-assisted EM field). This model is a generalization to multiple material components presented in section **2.3**. Here and in the following $\hbar = 1$, so that the Hamiltonian is

$$H = H_m + \vec{A}^{\dagger T}\mathbf{H}\vec{A} + \left(\vec{V}^T \cdot \mathbf{M} \cdot \vec{A} + \text{H.c.}\right), \tag{5.1}$$

where H_m describes the matter (the emitters), $\vec{A} = (a_1, a_2, \ldots, a_\alpha, \ldots)^T$ collects all EM modes, and $\vec{V} = (V_1, V_2, \ldots, V_n, \ldots)^T$ collects the emitter operators describing the interaction with the bosonic modes. The main difference between this Hamiltonian and the one for the single-emitter is that the emitter operators (which in the case of the single emitter corresponds to the dipole moment μ) in the multi-emitter Hamiltonian are explicitly separated from the interaction operator, while in Eq. (2.53) $\vec{M}$ includes the emitter operator. Therefore, in the case considered below, $\vec{V}$ will contain the dipole operators (up to three per emitter if all polarizations are taken into account). The properties of the bosonic environment are thus fully encoded in the matrices $\mathbf{H}$ (size $N_a \times N_a$) and $\mathbf{M}$ (size $M \times N_a$), where N_a is the number of bosonic modes and M is the number of matter interaction operators.

The generalized spectral density associated to the bosonic environment in Eq. (5.1) is defined as

$$\boldsymbol{\mathcal{J}}(\omega) = \lim_{\epsilon \to 0} \frac{1}{\pi}\mathbf{M}\,\mathrm{Im}\left[\frac{1}{\mathbf{H} - \omega - i\epsilon}\right]\mathbf{M}^\dagger. \tag{5.2}$$

This definition is a straightforward extension of the single-emitter spectral density to the case of multiple light-matter interaction operators, obtained by

replacing a $1 \times N_a$ vector of light-matter coupling elements by the $M \times N_a$ matrix $\mathbf{M}$. This generalized spectral density has been previously obtained in the context of the Wigner-Weisskopf problem (i.e., within the single-excitation subspace) [78, 83, 222]. It is an $M \times M$ matrix-valued function of frequency and fulfils $\boldsymbol{\mathcal{J}}(\omega)^\dagger = \boldsymbol{\mathcal{J}}(\omega)$. If $\mathbf{H}$ is diagonal, $H_{\alpha\beta} = \omega_\alpha \delta_{\alpha\beta}$, analogously to the single-emitter case, the Sokhotski-Plemelj formula $\lim_{\epsilon\to 0} \frac{1}{\omega'-\omega-i\epsilon} = \mathcal{P}\frac{1}{\omega'-\omega} + i\pi\delta(\omega'-\omega)$ can be used to get

$$\boldsymbol{\mathcal{J}}_{ij}(\omega) = \sum_\alpha M_{i\alpha} M^*_{j\alpha} \delta(\omega - \omega_\alpha), \tag{5.3}$$

which is a form where the relation to conventional single-emitter spectral densities $\boldsymbol{\mathcal{J}}(\omega) = \sum_\alpha |M_\alpha|^2 \delta(\omega - \omega_\alpha)$ appears even more clearly. In its general form $\boldsymbol{\mathcal{J}}(\omega)$ also encodes the full information about the environment the emitters interact with. It is important to note here that in the limit of a single emitter, the relation between the generalized spectral density and the "conventional" one (as defined in Eq. (2.55)) is $\mu^2 \mathcal{J}(\omega) = J(\omega)$.

To connect the general Hamiltonian (5.1) to the particular physical system, which consists of a collection of emitters interacting with the EM field supported by a material structure, macroscopic QED framework is again used. The Hamiltonian in the multipolar coupling scheme (Power-Zienau-Woolley picture) and within the dipole approximation can then be written as Eq. (2.30)

$$H = \sum_\lambda \int \mathrm{d}^3 r \int_0^\infty \mathrm{d}\omega\, \omega \hat{\mathbf{f}}^\dagger_\lambda(\mathbf{r},\omega)\hat{\mathbf{f}}_\lambda(\mathbf{r},\omega) + \sum_n H_n - \sum_n \boldsymbol{\mu}_n \cdot \hat{\mathbf{E}}(\mathbf{r}_n), \tag{5.4}$$

where $\lambda = \{e, m\}$ labels the electric and magnetic contributions, $\hat{\mathbf{f}}_\lambda(\mathbf{r},\omega)$ and $\hat{\mathbf{f}}^\dagger_\lambda(\mathbf{r},\omega)$ are the bosonic annihilation and creation operators of the medium-assisted field, and H_n and $\boldsymbol{\mu}_n$ are the bare Hamiltonian and dipole operator of emitter n. The electric field operator is given by

$$\hat{\mathbf{E}}(\mathbf{r}) = \sum_\lambda \int \mathrm{d}^3 r' \int_0^\infty \mathrm{d}\omega \mathbf{G}_\lambda(\mathbf{r},\mathbf{r}',\omega) \cdot \hat{\mathbf{f}}_\lambda(\mathbf{r}',\omega) + \mathrm{H.c.}, \tag{5.5}$$

where $\mathbf{G}_\lambda(\mathbf{r}, \mathbf{r}', \omega)$ are the electric and magnetic Green's functions, which are closely related to the dyadic Green's function [74]. This Hamiltonian can be rewritten in the form of Eq. (5.1) by formally discretizing space and frequency and renaming $\hat{\mathbf{f}}_\lambda(\mathbf{r}, \omega) \to a_\alpha$, with a combined mode index $\alpha \equiv (\lambda_\alpha, \mathbf{r}_\alpha, \omega_\alpha, \mathbf{n}_\alpha)$, where $\mathbf{n}_\alpha$ labels the Cartesian directions x, y, z. This means that $H_{\alpha\beta} = \delta_{\alpha\beta}\omega_\alpha$ and $M_{i\alpha} = -\mathbf{n}_i \cdot \mathbf{G}_{\lambda_\alpha}(\mathbf{r}_i, \mathbf{r}_\alpha, \omega_\alpha) \cdot \mathbf{n}_\alpha$.

Inserting the expression for $M_{i\alpha}$ in Eq. (5.3), taking the continuum limit (i.e., replacing the sum over α with the corresponding sums and integrals), and using the Green's function integral identity,

$$\sum_\lambda \int \mathrm{d}^3\mathbf{s}\mathbf{G}_\lambda(\mathbf{r}, \mathbf{s}, \omega) \cdot \mathbf{G}_\lambda^{*T}(\mathbf{r}', \mathbf{s}, \omega) = \frac{\omega^2}{\pi\epsilon_0 c^2} \operatorname{Im} \mathbf{G}(\mathbf{r}, \mathbf{r}', \omega), \tag{5.6}$$

leads to

$$\mathcal{J}_{ij}(\omega) = \frac{\omega^2}{\pi\epsilon_0 c^2} \mathbf{n}_i \cdot \operatorname{Im} \mathbf{G}(\mathbf{r}_i, \mathbf{r}_j, \omega) \cdot \mathbf{n}_j. \tag{5.7}$$

The diagonal elements of $\boldsymbol{\mathcal{J}}(\omega)$ are equal to the "conventional" spectral density for a single transition divided by the square of the corresponding dipole moment, i.e., $\mathcal{J}_{ii}(\omega) = J_i(\omega)/\mu_i^2$. From Eq. (5.7), it can be seen that $\boldsymbol{\mathcal{J}}(\omega)$ is a real and symmetric matrix for any frequency ω, and due to the properties of the EM dyadic Green's function, it is also positive definite. This means that it can be decomposed in the form $\boldsymbol{\mathcal{J}}(\omega) = \mathbf{g}(\omega)\mathbf{g}(\omega)^\dagger$, where $\mathbf{g}(\omega)$ can be chosen real and is unique up to unitary transformations $\mathbf{g}'(\omega) = \mathbf{g}(\omega)\mathbf{U}(\omega)$. Moreover, $\mathbf{g}(\omega)$ is exactly the coupling matrix that appears in the expansion of the multi-emitter problem using emitter-centered modes in macroscopic QED [68] (a derivation of the emitter-centered modes can be found in Appendix **B**).

5.2.1 Few-mode quantization

Then, the few-mode quantization model presented in Ref. [101] can be extended in order to obtain an effective few-mode description of the multi-

emitter problem. The idea is again to find a model system that is equivalent to the actual EM environment, but has a structure that facilitates its numerical solution and interpretation of the resulting dynamics. In order to do so a discrete set of N mutually coupled discrete EM modes a_i is introduced. Each of these modes is coupled to an independent bath of "background" modes $b_{i,\Omega}$ with frequency-independent coupling determined by $\nu_i = \sqrt{\kappa_i/(2\pi)}$, and also to the emitter interaction operator V_n with coupling strength g_{ni}. The model Hamiltonian is then given by $\mathcal{H} = \mathcal{H}_S + \mathcal{H}_B$, where

$$\mathcal{H}_S = \sum_n H_n + \sum_{i,j} \omega_{ij} a_i^\dagger a_j + \sum_{n,i} V_n g_{ni} (a_i + a_i^\dagger), \tag{5.8a}$$

$$\mathcal{H}_B = \sum_i \int \left[\Omega b_{i,\Omega}^\dagger b_{i,\Omega} + \nu_i (b_{i,\Omega}^\dagger a_i + b_{i,\Omega} a_i^\dagger) \right] \mathrm{d}\Omega, \tag{5.8b}$$

Since the coupling of the discrete modes to the background baths is spectrally flat, it is Markovian. The dynamics of the system are then equivalently described [195] by the Lindblad master equation

$$\dot{\rho} = -i \left[\mathcal{H}_S, \rho \right] + \sum_i \kappa_i L_{a_i}[\rho], \tag{5.9}$$

where ρ is the system density matrix and $L_O[\rho] = O\rho O^\dagger - \frac{1}{2}\{O^\dagger O, \rho\}$ is a Lindblad dissipator.

The model Hamiltonian $\mathcal{H}$ can also be rewritten (after formal discretization of the bath continua, with N_b modes for each continuum) in the form of Eq. (5.1), where $\vec{A} = \left(a_1, \ldots, a_N, b_{1,\Omega_1}, \ldots, b_{1,\Omega_{N_b}}, b_{2,\Omega_1}, \ldots, b_{N,\Omega_{N_b}}\right)^T$, while $\mathbf{H}$ consists of the block matrix ω_{ij} in the top left, a series of diagonal blocks for each continuum, and constant off-diagonal coupling elements between all modes of a block and the discrete mode associated to it. Finally, $\mathbf{M}$ is an $M \times N(N_b+1)$ matrix whose ith row is given by $\mathbf{M}_i = (g_{i1}, \ldots, g_{iN}, 0, \ldots, 0)$.

A compact form of the generalized spectral density of the model system can be obtained from Eq. (5.2) by following the approach of Ref. [223] or by

explicit diagonalization of **H**. In the next section, the derivation following this last method is shown.

5.2.2 Compact form of the generalized spectral density

For N continua, the diagonalized Hamiltonian can be written as

$$H_F = \sum_m^N \int \mathrm{d}\omega\ \omega\ c_m^\dagger(\omega) c_m(\omega), \tag{5.10}$$

where there are N degenerate eigenmodes $c_m(\omega)$, with associated eigenstates $|\Phi_m(\omega)\rangle$, and which obey the usual bosonic commutation relation $\left[c_m(\omega), c_n^\dagger(\omega')\right] = \delta_{m,m'}\delta(\omega-\omega')$.

Then, the Fleshbach projection can be used to split the Hamiltonian in two orthogonal subspaces. One of them is defined by discrete modes given by a_i, while the other is described by a continuum of bosonic bath operators given by $b_i(\Omega)$. The projections are

$$\mathbf{A} = \sum_{j=1}^N |A_j\rangle\langle A_j|, \qquad \mathbf{B} = \sum_{j=1}^N \int \mathrm{d}\Omega |B_j(\Omega)\rangle\langle B_j(\Omega)|, \tag{5.11}$$

where **A** corresponds to the discrete mode space and **B** to the continuum bath space. As they are orthogonal, the states obey $\langle A_i|B_j(\Omega)\rangle = 0$ for any i, j. Also, they satisfy $\mathbf{A} + \mathbf{B} = \mathbb{1}$. Projecting the Hamiltonian in all the combinations, one can obtain the projected Hamiltonian in each subspace, $H_{\mathbf{AA}}$, $H_{\mathbf{BB}}$ and the coupling between the discrete and continua modes $H_{\mathbf{BA}}$. Furthermore, it is imposed that each discrete mode interacts only with a single

continuum, so that

$$\langle A_i|H|A_j\rangle = \omega_{i,j}, \tag{5.12}$$

$$\langle B_i(\Omega)|H|B_j(\Omega')\rangle = \Omega\ \delta_{i,j}\delta(\Omega-\Omega'), \tag{5.13}$$

$$\langle B_i(\Omega)|H|A_j\rangle = \frac{\kappa_i}{2\pi}\delta_{i,j}, \tag{5.14}$$

where $\omega_{i,j}$ describes the modes energies and their interactions, Ω is the eigenenergy associated to the continuum and $\sqrt{\kappa_i/2\pi}$ is the coupling between the discrete and the bath spaces. Therefore, the eigenstates can be expanded as superposition of both subspaces, so that the modes $c_m(\omega)$ can also be expanded in terms of the discrete and bath operators

$$c_m(\omega) = \sum_{j=1}^{N}\left[\alpha^*_{j,m}(\omega)a_j + \int \mathrm{d}\Omega\beta^*_{j,m}(\Omega,\omega)b_j(\Omega)\right], \tag{5.15}$$

where $\alpha_{j,m}(\omega) = \langle A_j|\Phi_m(\omega)\rangle$ and $\beta_{j,m}(\Omega,\omega) = \langle B_j(\omega)|\Phi_m(\omega)\rangle$ are expansion coefficients. This allows to write the model Hamiltonian $\mathcal{H}$.

Starting with the Schrödinger equation and using the Lippmann-Schwinger equation for each subspace and the expansions of the subspaces shown in Eq. (5.11), the coefficients can be written as

$$\alpha_{j,m}(\omega) = \sqrt{\frac{\kappa_m}{2\pi}}\langle A_j|\frac{1}{\omega-\tilde{\mathbf{H}}}|A_m\rangle = \sqrt{\frac{\kappa_m}{2\pi}}\left(\frac{1}{\omega-\tilde{\mathbf{H}}}\right)_{jm}, \tag{5.16}$$

$$\begin{aligned}\beta_{j,m}(\Omega,\omega) =& \delta_{jm}\delta(\Omega-\omega) + [\omega-\Omega-i\epsilon]^{-1}\frac{\sqrt{\kappa_m\kappa_j}}{2\pi}\langle A_j|\frac{1}{\omega-\tilde{\mathbf{H}}}|A_m\rangle = \\ & \delta_{jm}\delta(\Omega-\omega) + \lim_{\epsilon\to 0}\frac{\sqrt{\kappa_m\kappa_j}}{2\pi(\omega-\Omega+i\epsilon)}\left(\frac{1}{\omega-\tilde{\mathbf{H}}}\right)_{jm},\end{aligned} \tag{5.17}$$

where $\tilde{\mathbf{H}}$ is an $N\times N$ matrix with entries $\tilde{\mathbf{H}}_{ij} = \omega_{ij} - \frac{i}{2}\kappa_i\delta_{ij}$.

Once the expressions of the coefficients are derived, the interaction Hamiltonian between multiple emitters, that give M interactions operators, and the eigenmodes can be used to obtain the compact form of the spectral density.

This Hamiltonian is given by

$$H_I = \sum_i^M V_i \cdot \sum_m^N \int \mathrm{d}\omega \; h_{im}(\omega)(c_m(\omega) + c_m^\dagger(\omega)), \tag{5.18}$$

where $h_{im}(\omega)$ is the coupling strength between the emitter i and the mode m. The coupling between each emitter and eigenmode can also be expanded on a discrete basis, so that $h_{im}(\omega) = \sum_j g_{ij}\alpha_{jm}(\omega)$, where g_{ij} is the coupling strength between the emitter i and the discrete mode j. Now, for each frequency ω one emitter-centered (or bright) mode per emitter can be defined (see Appendix **B**). Each bright mode then corresponds to the unique linear superposition of the eigenmodes that contains the full coupling of the emitter i, $h_i^2(\omega) = \sum_m |h_{im}(\omega)|^2$. These modes can be expanded in terms of the discrete and continuous modes of the model, so that

$$\tilde{c}_i(\omega) = \frac{1}{h_i(\omega)} \sum_m h_{im}(\omega)c_m(\omega) = \sum_j \left[\tilde{\alpha}_{ij}(\omega)a_j + \int \mathrm{d}\Omega \tilde{\beta}_{ij}(\Omega,\omega)b_j(\Omega) \right]. \tag{5.19}$$

Therefore, the coupling strength is given by $h_i(\omega)$ and the spectral density for each matter operator is $\mathcal{J}_{mod,i}(\omega) = h_i(\omega)^2$. Moreover, the generalized spectral density is given by $\boldsymbol{\mathcal{J}}_{mod}(\omega) = h(\omega)\cdot h^\dagger(\omega)$. Using the expansion of the coupling in the discrete basis and equations (5.16),(5.17), the new coefficient $\tilde{\alpha}_{ij}(\omega)$ reads

$$\tilde{\alpha}_{ij}(\omega) = \frac{1}{\pi h_i(\omega)} \mathrm{Im}\left(\mathbf{g} \cdot \frac{1}{\omega - \tilde{H}} \right)_{ij}, \tag{5.20}$$

where $\mathbf{g}$ is a $M \times N$ matrix that includes the coupling between all the matter interaction operators with the discrete modes. In a similar way, the coefficients $\tilde{\beta}_{ij}(\omega,\Omega)$ are

$$\tilde{\beta}_{ij}(\omega,\Omega) = \frac{\sqrt{\kappa_j/2\pi}}{h_i(\omega)} \left[\left(\mathbf{g} \cdot \frac{1}{\omega - \tilde{\mathbf{H}}} \right)_{ij} + \frac{1}{\pi} \lim_{\epsilon\to 0} \frac{1}{\omega - \Omega - i\epsilon} \mathrm{Im}\left(\mathbf{g} \cdot \frac{1}{\omega - \tilde{\mathbf{H}}} \right)_{ij} \right]. \tag{5.21}$$

Finally, using the relation between the model generalized spectral density and the coupling $h(\omega)$, it can be written

$$\boldsymbol{\mathcal{J}}_{\mathrm{mod}}(\omega) = \frac{1}{\pi}\mathbf{g}\cdot \mathrm{Im}\left[\frac{1}{\omega - \tilde{\mathbf{H}}}\right]\cdot \mathbf{g}^{\dagger}. \tag{5.22}$$

where $\mathbf{g}$ is the real $M \times N$ matrix describing the interaction between the emitters and the discrete modes, with elements given by g_{ni}, see Eq. (5.8a). Conversely, $\tilde{\mathbf{H}}$ is a complex symmetric $N \times N$ matrix with elements given by $\tilde{\mathbf{H}}_{ij} = \omega_{ij} - \frac{i}{2}\kappa_i\delta_{ij}$. When $\tilde{\mathbf{H}}$ is diagonalizable, $\tilde{\mathbf{H}} = \mathbf{V}\tilde{\mathbf{\Omega}}\mathbf{V}^T$, where $\tilde{\mathbf{\Omega}}$ is a diagonal matrix containing the (complex) eigenvalues and $\mathbf{V}$ is a complex orthogonal (not unitary) matrix, $\mathbf{V}^T\mathbf{V} = \mathbb{1}$, this expression can be rewritten as a sum over resonances,

$$\boldsymbol{\mathcal{J}}_{\mathrm{mod}}(\omega) = \frac{1}{\pi}\,\mathrm{Im}\left[\tilde{\mathbf{g}}\frac{1}{\tilde{\mathbf{\Omega}} - \omega}\tilde{\mathbf{g}}^T\right], \tag{5.23}$$

where $\tilde{\mathbf{g}} = \mathbf{g}\mathbf{V}$. The complex eigenvalues of $\tilde{\mathbf{H}}$ are thus the poles of the spectral density and are closely related to the quasinormal modes of the classical Green's function.

As in the single-emitter case, the relatively few parameters in Eq. (5.22) can be adjusted to best reproduce the generalized spectral density given by Eq. (5.7), calculated from the dyadic EM Green's function, and thus parametrize the model Hamiltonian $\mathcal{H}$. $\boldsymbol{\mathcal{J}}(\omega)$ is a symmetric matrix, which means that this corresponds to a simultaneous fit of $M(M+1)/2$ real-valued functions. The diagonal elements of the generalized spectral density correspond to the "conventional" spectral densities and therefore they are non-negative in all the frequency range, i.e., $\boldsymbol{\mathcal{J}}_{nn}(\omega) \geq 0$ for all ω. The off-diagonal elements do not present this restriction and can have negative values, as they encode the interaction between the emitters mediated by the EM fields. The spectral density is fully determined by the position of the emitters, with no restriction on the emitter properties. In particular, this approach is not restricted to two-level

systems. However, if only one or two dipole orientations are relevant for the transitions of any emitter, the number of necessary interaction operators and thus the dimensionality of $\boldsymbol{\mathcal{J}}(\omega)$ can be reduced.

Finally, before presenting the results using this model, a brief comment on the number of parameters is presented. For the typical case $N > 2M + 1$, the number of free parameters in the diagonal form of Eq. (5.23), $2N(M + 1)$ real numbers, is (significantly) smaller than in the non-diagonal form of Eq. (5.22), which require $\frac{1}{2}N(N + 2M + 3)$ real numbers. It would thus seem that this form is more convenient for fitting than the non-diagonal form. However, this turns out not to be the case, as has been discussed in **chapter 4** for the single-emitter case: First, it is not straightforward to enforce that the fit parameters correspond to a physical system where $\boldsymbol{\mathcal{J}}_{\text{mod}}(\omega)$ is real positive semidefinite for all frequencies. Second, even when that constraint is achieved, implementation of the dynamics through a Lindblad master equation (which, as discussed above, is the final goal of this approach) requires a form in which the imaginary part of the complex symmetric $\tilde{\mathbf{H}}$ is negative semidefinite, while $\mathbf{g}$ is real. This would require an algorithm that finds a complex orthogonal matrix $\mathbf{V}$ which "undiagonalizes" the system and can be used to obtain physical $\tilde{\mathbf{H}} = \mathbf{V}\tilde{\boldsymbol{\Omega}}\mathbf{V}^T$ and $\mathbf{g} = \tilde{\mathbf{g}}\mathbf{V}^T$ for any given $\tilde{\boldsymbol{\Omega}}$ and $\tilde{\mathbf{g}}$. Therefore, in the following the non-diagonal form (5.22) is used when fitting.

5.3 Simple case: 5 emitters near a sphere

To first illustrate the few-mode quantization model, a simple example in which the number of EM modes and the number of emitters is the same is chosen, i.e., $M = N$. It consists of five quantum emitters near a metallic sphere.

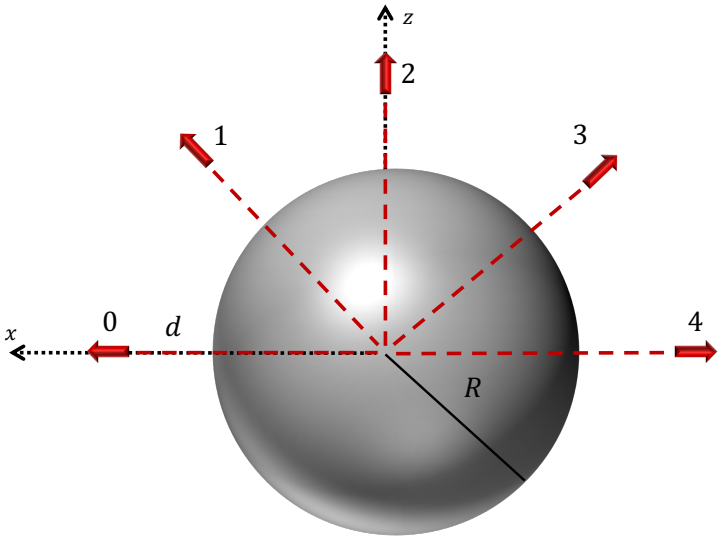

Fig. 5.1.: Five quantum emitter, numbered from 0 to 4, are placed at a distance $d = 5$ nm from a metallic sphere with radius $R = 2$ nm.

The sphere has a radius $R = 2$ nm and the emitters are placed radially at a distance $d = 5$ nm from its surface. All emitters are oriented perpendicularly to the surface of the sphere and distributed in the xz plane. They are numbered so that the first one, emitter "0", is placed at $x = -d$ and the last one, emitter "4", at $x = d$. Each emitter forms an angle $\theta = \pi/4$ with its nearest neighbor, as is shown in figure **5.1**.

Figure **5.2** shows the fit of the generalized spectral density. Since two-level quantum emitters with a single dipole transition are considered, they are included within the spectral density, $J_{ij}(\omega) = \mu_i \mu_j \mathcal{J}_{ij}(\omega)$, with values given by $\mu = 0.55$ e nm. The interaction operators are then just $V_i = \sigma_i^+ + \sigma_i^-$. Within this physical system, the number of independent functions to fit is 15. Panel (a) corresponds to the "conventional" spectral densities $J_{ii}(\omega)$, that are equal for all emitters, while $J_{i,i+1}$, $J_{i,i-1}$ corresponds to the interaction between one emitter and its nearest neighbors. The rest of the spectral densities, which correspond to the interaction between one emitter and its next-nearest neighbor and the

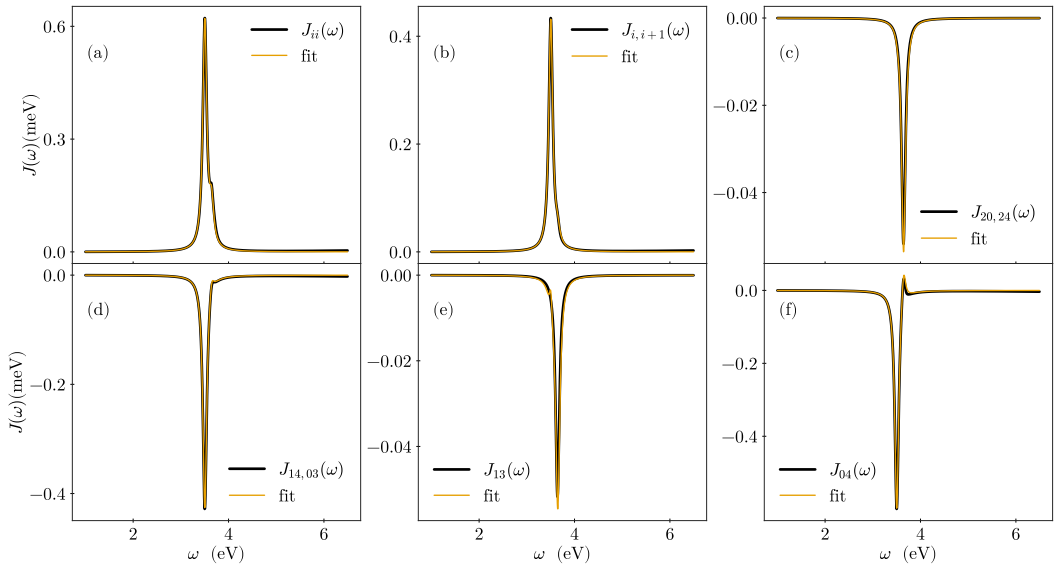

Fig. 5.2.: Fit (orange line) to the generalized spectral density for 5 emitters near a metallic sphere when 5 modes are used. The black line is the classical spectral density obtained via de Green's function.

interaction between the first and the last emitter, are shown specifying the number given explicitly to each of them. In this simple setup, using just $N = 5$ modes all spectral densities can be reproduced faithfully.

Moreover, the dynamics obtained by this model reproduces also faithfully the dynamics of the original model, i.e., the representation of the EM modes and the photon-mediated interactions between emitters are well-described using this model and therefore the few-mode multiemitter model is completely equivalent to the original one. The dynamics of all emitters are treated for the Wigner-Weisskopf spontaneous emission of one of the two-level emitters. As in this problem there is only one excitation, the Wigner-Weisskopf problem can be solved for arbitrary spectral densities. Figure **5.3** shows the excited state population of the emitters when emitter 2 is initially in its excited state and the rest of the emitters are in their ground state. This figure shows that the model is capable of reproducing the dynamics of all the emitters, and only very

small differences can be encountered for the small populations, due to slight discrepancies in the fit.

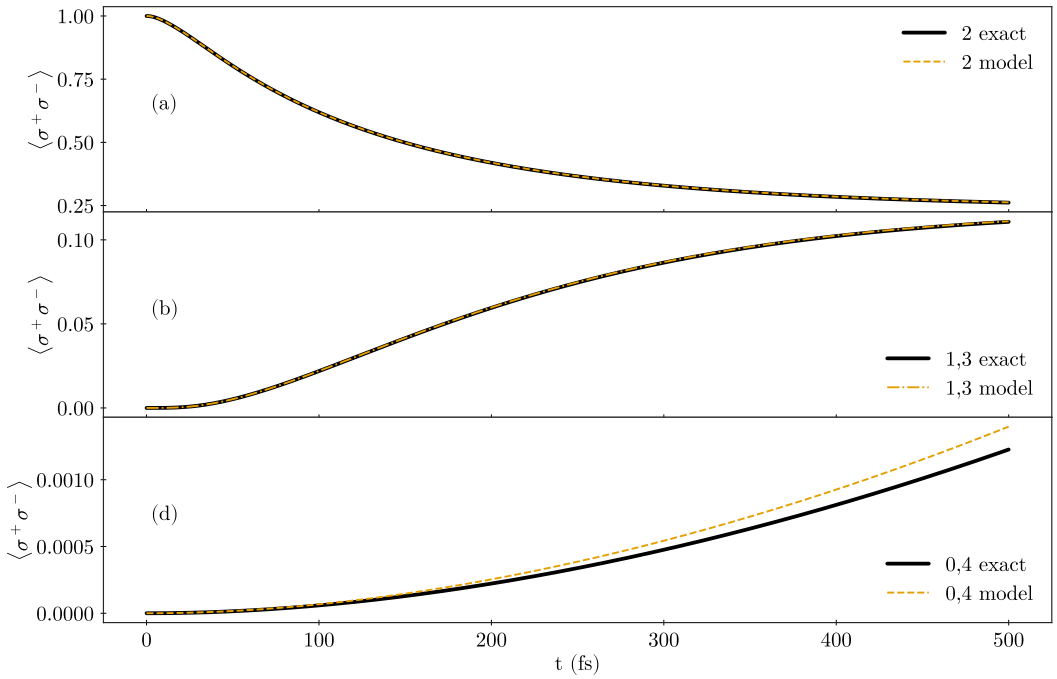

Fig. 5.3.: Population of the excited state of all the emitters when emitter 2 is initially excited and the rest are initially in their ground states. Continuous thick lines show the exact population in each case, while dashed lines show the population given by the model.

This physical system allows not only to compare the exact dynamics but also to arrive to an expression for the mode profiles of the model. This is only possible when the number of emitters and the number of discrete modes used to model the generalized spectral density is the same, as their derivation is done through the emitter-centered modes. To do so, the initial point is Eq. (B.7), which represents the electric field written in terms of the orthogonal emitter-centered modes. As these modes can be expanded in terms of the discrete and

continua modes of the model, the electric field can finally be expressed as

$$\mathbf{E}^{(+)}(\mathbf{r}) = \sum_j \left[\mathcal{E}_j^{\alpha} a_j + \int \mathrm{d}\Omega\ \mathcal{E}_j^{\beta}(\Omega) b_j(\Omega)\right] = \sum_i \int_0^{\infty} \mathrm{d}\omega\ E_i(\mathbf{r},\omega) \sum_k V_{ik}(\omega) \sum_m \left[\tilde{\alpha}_{km}(\omega) a_m + \int \mathrm{d}\Omega\ \tilde{\beta}_{km}(\Omega,\omega) b_m(\Omega)\right], \tag{5.24}$$

where $\mathcal{E}_j^{\alpha}$ and $\mathcal{E}_j^{\beta}(\Omega)$ are expansion coefficients. Applying the commutation relation between the discrete modes, the expression for the field profiles associated with both the discrete and the continua modes can be obtained. In particular,

$$\mathcal{E}_n^{\alpha} = \int_0^{\infty} \mathrm{d}\omega \sum_{jk} \boldsymbol{\epsilon}_j(\mathbf{r},\omega) S_{jk}^{-1}(\omega) \tilde{\alpha}_{kn}(\omega), \tag{5.25}$$

$$\mathcal{E}_n^{\beta}(\Omega) = \pi \mathrm{Re}\tilde{B}_n(\Omega) + \mathrm{Im}\tilde{B}_n(\Omega) \log\left(\frac{\omega_2 - \omega}{\omega - \omega_1}\right) + \int_{\omega_1}^{\omega_2} \frac{\mathrm{Im}\tilde{B}_n(\omega) - \mathrm{Im}\tilde{B}_n(\Omega)}{\omega - \Omega} \mathrm{d}\omega, \tag{5.26}$$

where $\epsilon_j(\mathbf{r},\omega)$ is given by Eq. (B.9), S is the overlap matrix of the non-orthogonal emitter-centered modes, ω_1 and ω_2 are the limits of the solution of the principal value of the integral and

$$\tilde{B}_{kn}(\omega) = \sum_{jk} S_{jk}^{-1}(\omega) \epsilon_j(\mathbf{r},\omega) \frac{\sqrt{\kappa_n/2\pi}}{\pi h_i(\omega)} \left(\mathbf{g} \cdot \frac{1}{\omega - \tilde{\mathbf{H}}}\right)_{kn}. \tag{5.27}$$

In this physical system, the number of modes profiles given by the emitter-centered modes and the ones given by the discrete modes (which are the modes that couple to the emitters) is the same. In order to compare them, as in the spontaneous emission problem the electric field is zero, i.e., $\langle a_i \rangle = 0$, the intensity can be used.

For the emitter-centered modes, the electric field in the position of the emitter is given by Eq. (B.7) and their wavefunction can be explicitly obtained,

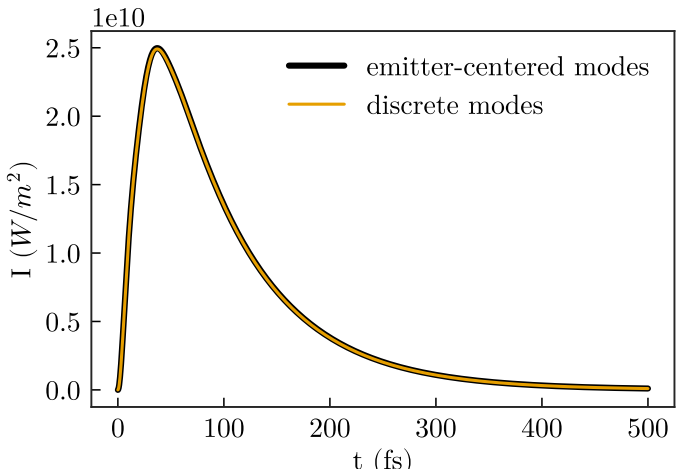

Fig. 5.4.: Intensity at the position of emitter 0 (excited at $t = 0$). The black line corresponds to Eq. (5.28) and the orange line corresponds to Eq. (5.29).

$|\psi\rangle = c_e|e\rangle + \sum_i c_i|1_i\rangle$. Therefore, the intensity is given by

$$I_{C_i} \propto \langle\psi|\mathbf{E}^{(-)}\mathbf{E}^{(+)}|\psi\rangle = \sum_{ij} E_j^* E_i c_j^* c_i = |\mathbf{E}|^2, \tag{5.28}$$

where only the expectation values $\langle\hat{C}_i\hat{C}_i\rangle$ are non-zero, while for the discrete modes the intensity is given by

$$I_{a_i} \propto \langle\mathbf{E}^{(-)}\mathbf{E}^{(+)}\rangle = \sum_{ij} \mathcal{E}_j^{*\alpha}\mathcal{E}_i^{\alpha}\langle a_j^\dagger a_i\rangle, \tag{5.29}$$

and the expectation values of all the modes must be included. At the position of one emitter, the intensity is accurately calculated using the field profiles associated with the discrete modes. It is important to note here that at different positions, the electric field is not given just by $\mathcal{E}_i^{\alpha}$, but $\mathcal{E}_i^{\beta}$ also contributes to the field. However, in contrast to the field given by the emitter-centered modes, the mode profiles for the modes of the model can be obtained for any point in space.

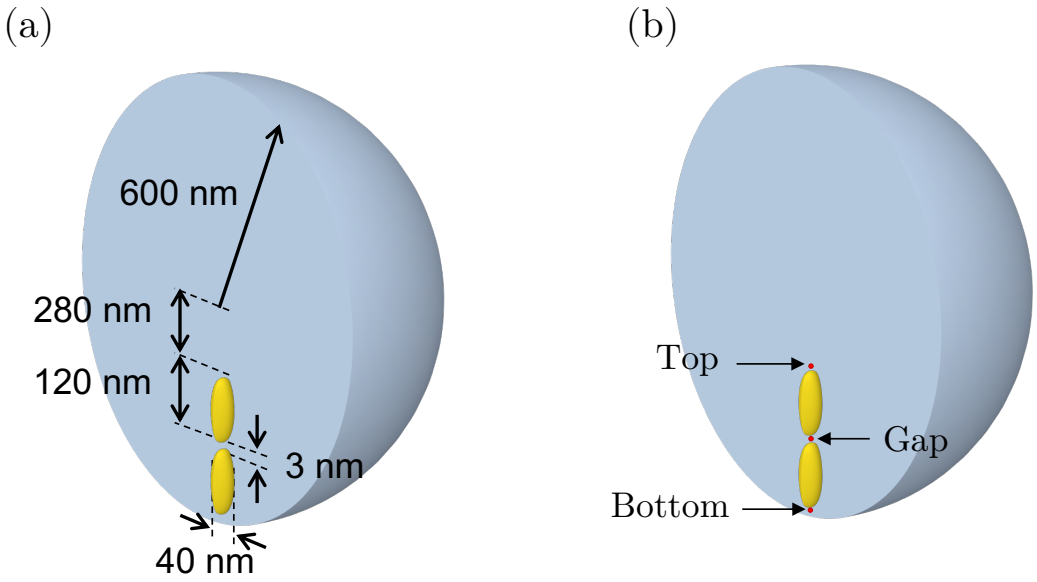

Fig. 5.5.: Sketch of the system consisting of a silver dimer nanoantenna embedded in a dielectric microsphere. (a): Physical parameters of the metallodielectric setup. (b): Positions of the three emitters.

5.4 Metallodielectric setup

In the following, a physical system that presents a more structured EM environment, in which there is a strong interference between modes, is presented because the theoretical procedure described in the previous sections has the ability to describe arbitrary photonic structures. In particular, there has been an increasing attention focused on hybrid metallodielectric setups, with the objective of combining the strong field confinement and enhanced light-matter interactions of plasmonic resonances with the long-lived nature of microcavities. Therefore, to illustrate the generalization to the multiple emitter case in a complex system, the physical setup considered is shown in Fig. **5.5**(a). It consists of two silver nanoparticles (ellipsoids with a long axis of 120 nm and a short axis of 40 nm), separated by a 3 nm gap, and embedded

in a dielectric GaP ($\epsilon_{\text{sph}} = 9$) nanosphere of 600 nm radius, with the rods substantially displaced from the center of the sphere. Therefore, the microsphere supports many long-lived Mie resonances, while the nanorods allow the formation of confined surface plasmons with subwavelength volume. Within this setup, three two-level emitters are placed in different positions, indicated by red dots in Fig. **5.5**(b). In the following, the emitter positions will be referred as:

(i) Gap (in the center between the rods),

(ii) Top (1.5 nm above the upper rod) and

(iii) Bottom (1.5 nm below the lower rod).

5.4.1 Fit to the spectral density

This arrangement permits us to show that the use of metallodielectric structures allows great control in the population transfer between emitters close to resonance to a hybrid mode, with slight changes in the emitter parameters inducing qualitatively different dynamics.

The generalized spectral density for the physical system described above is characterized by six independent functions (three diagonal and three off-diagonal). Here again, two-level quantum emitters with a single dipole transition are considered, so that they are included within the spectral density, $J_{ij}(\omega) = \mu_i \mu_j \mathcal{J}_{ij}(\omega)$, with values given by $\mu_{\text{Top}} = \mu_{\text{Bottom}} = 0.55$ e nm and $\mu_{\text{Gap}} = 0.257$ e nm. The interaction operators are again $V_i = \sigma_i^+ + \sigma_i^-$. Fig. **5.6** shows the generalized spectral density (black lines) obtained from classical simulations performed with the Maxwell equations solver implemented in COMSOL Multiphysics. The first row shows the diagonal functions (in logarith-

mic scale), i.e., $J_{ii}(\omega)$, which correspond to the "conventional" spectral densities, while the second row shows the off-diagonal functions, $J_{12}(\omega)$, $J_{13}(\omega)$, and $J_{23}(\omega)$, which encode the field-mediated interaction between the emitters. As Top and Bottom are symmetric positions with respect to the plasmonic nanoparticles, their diagonal elements and their interaction with the emitter in Gap behave quite similarly, with slight differences due to the nonsymmetric placement of the dielectric sphere.

In its most general form, there are no restrictions on the form of $\tilde{\mathbf{H}}$ apart from symmetry. However, it is possible to choose any desired structure, e.g., inspired by the physical structure of the problem, to restrict the number of free parameters. In **chapter 4** it was shown that for the single-emitter case, it is generally sufficient to use a chain form with only next-nearest neighbor coupling between the modes (i.e., $\tilde{\mathbf{H}}_{ij} = 0$ if $|i-j| > 2$), although this choice makes it more challenging to obtain converged fits. Therefore, here instead a block-diagonal form is chosen,

$$\tilde{\mathbf{H}} = \begin{pmatrix} \tilde{\mathbf{H}}_1 & \mathbf{0} & \mathbf{0} \\ \mathbf{0} & \tilde{\mathbf{H}}_2 & \mathbf{0} \\ \mathbf{0} & \mathbf{0} & \tilde{\mathbf{H}}_3 \end{pmatrix}, \tag{5.30}$$

where $\tilde{\mathbf{H}}_i$ are full $N_i \times N_i$ matrices. This form allows to significantly decrease the number of parameters while still giving a good fit for the spectral density. The physical reasoning behind this election is that there are many independent modes in the system that do not interfere significantly (e.g., the high-order "pseudomodes" coupling to each emitter [220]), and it is thus not necessary to allow arbitrary couplings between all modes. In the present case, the size of each block was chosen as $N_i = 14$, giving a total of $N = \sum_i N_i = 42$ modes.

The orange lines in Fig. **5.6** show the model spectral density obtained after fitting. Despite the complexity of the structure and the spectral densities, the fit is well-converged with a relatively small number of modes. The small

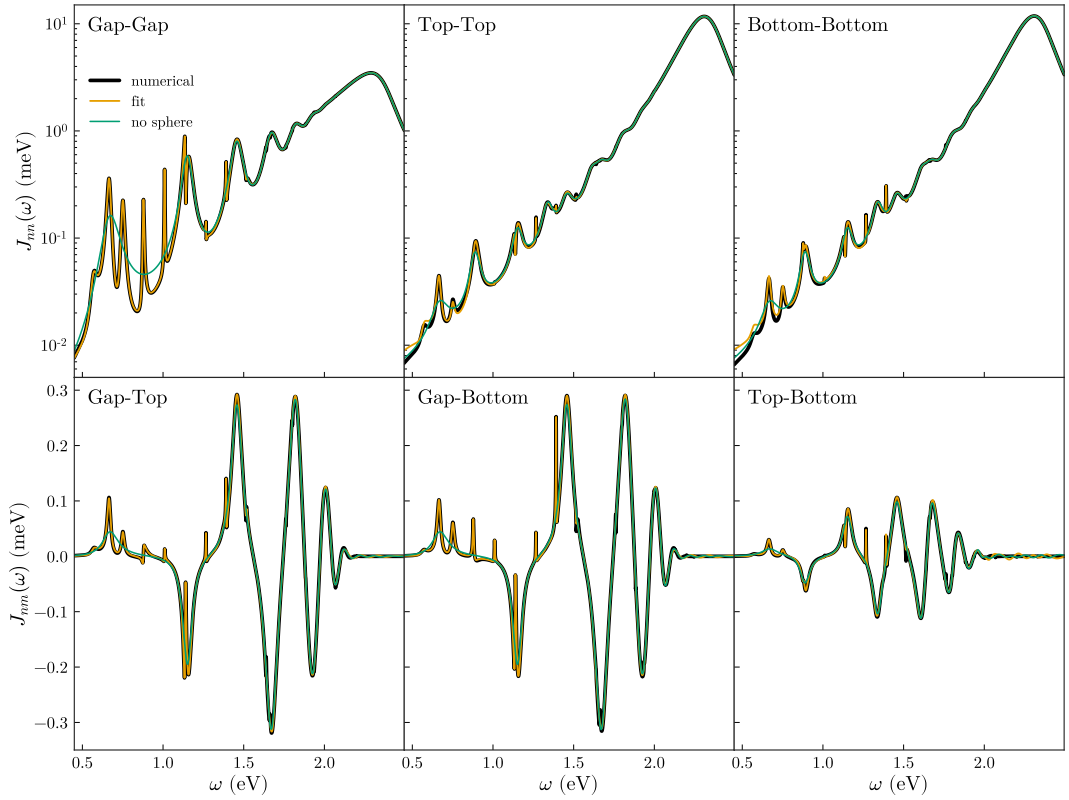

Fig. 5.6.: Generalized spectral densities for z-oriented emitters at Gap, Top and Bottom positions (thick black line), fitted model spectral density (orange line), and spectral density when the microsphere is replaced by a dielectric background (green line).

differences to the numerical spectral density visible at low frequencies for the diagonal functions and at high frequencies for the non-diagonal ones could be reduced by increasing the number of modes employed in the fit, but were found not to affect the dynamics studied in the following.

In Fig. **5.6** there is additionally shown the spectral density corresponding to the two plasmonic nanoparticles when the sphere is replaced by an infinite GaP background medium (green lines). In this case, Top and Bottom are completely equivalent positions, and their spectral densities are identical. Additionally, this change removes the Mie resonances supported by the sphere, such

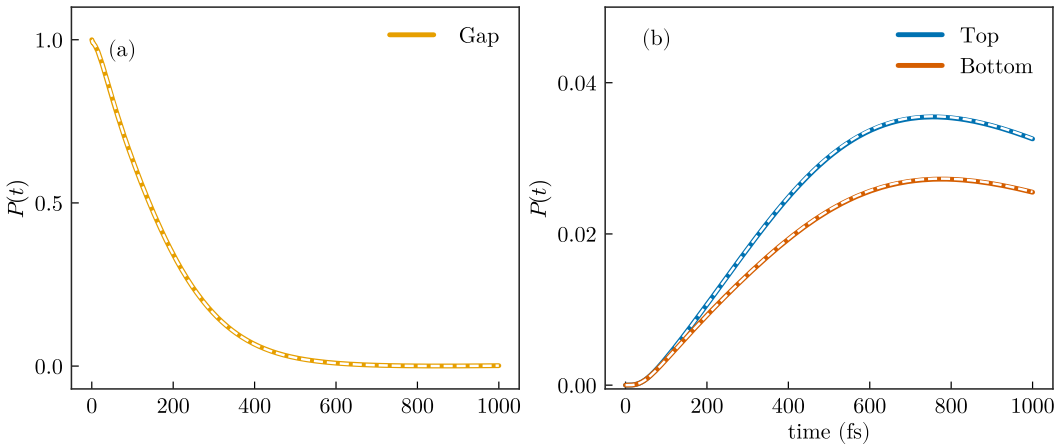

Fig. 5.7.: Dynamics of Gap (a), Top and Bottom (b) in the single-excitation subspace when the first is initially ($t = 0$) excited. The colored lines correspond to the population given by the discretization of the photon continua in frequency in the emitter-centered modes description and the dashed white lines correspond to the dynamics predicted by the few-modes approach.

that the spectral density is overall much simpler and contains fewer peaks. In particular, there are no visible interference structures, and the spectral density corresponds to a series of broad but mostly independent modes. The fitting procedure then converges much more easily and achieves even better agreement with the numerical results, with $|\boldsymbol{\mathcal{J}}_{\text{mod}}(\omega) - \boldsymbol{\mathcal{J}}(\omega)| < 0.015$ meV over the full spectral range of Fig. **5.6** using $N = 30$ modes. As the fit is visually indistinguishable from the exact spectral density, it is not shown separately in Fig. **5.6**.

To benchmark the model in this setup, first the dynamics of the three emitters are presented in comparison with the ones predicted when employing the emitter-centered modes. Figure **5.7** shows the dynamics of the Wigner-Weisskopf spontaneous emission of Gap, i.e., Gap is at time $t = 0$ excited, while Top and Bottom are initially in their ground states. Moreover, all the photonic modes at the initial time are in their ground states, i.e., the initial

state is given by $|\psi_0\rangle = \sigma^+_{\mathrm{Gap}}|0\rangle$, and the population of each emitter monitored is $P(t) = \langle\sigma_i^+\sigma_i^-\rangle$, where $i = \mathrm{Gap}, \mathrm{Top}, \mathrm{Bottom}$. The dynamics predicted by the few-mode model are indistinguishable from those predicted by the "exact" model.

5.4.2 Energy transfer dynamics

After successfully fitting the generalized spectral density, so that the model system is equivalent to the original one, and testing the dynamics described, the approach presented in section **5.2** is used to study energy transfer between emitters for three different situations:

(i) transfer of a single excitation from a coherent superposition of two emitters to a third emitter;

(ii) transfer of a single excitation from one emitter to another, mediated by the third one;

(iii) excitation transfer to a third emitter from a doubly excited state where two other emitters are initially excited.

This method is able to calculate the dynamics for these different examples at low computational cost. In particular, in the following the population transfer between the emitters is studied focusing on how the formation of hybrid modes affects it. Therefore, the emitters are chosen with frequencies close to the lowest-energy hybrid mode at ≈ 1.14 eV. Fig. **5.8**(a) shows the spectral density of the Gap emitter in that frequency range, both for the hybrid metallodielectric cavity (orange line) and for the plasmonic dimer embedded in an infinite dielectric medium (green line). For the hybrid cavity, there is significant mode hybridization and destructive interference around that fre-

quency, while for the bare dimer, only a single broad resonance peak appears. The dark-red arrows point to three different particular frequencies around the hybrid mode. Later, the emitter frequencies will be chosen to be at one of these three values.

First, situation (i) is investigated. In particular, the population transfer of interest in this scenario is the one that occurs from a coherent superposition of the Top and Bottom emitters to the Gap emitter, as schematically shown in the lower insets of Fig. **5.8**(b),(c). To be precise, the initial state is $|\psi_0\rangle = \frac{1}{\sqrt{2}}(\sigma^+_{\text{Top}} + \sigma^+_{\text{Bottom}})|0\rangle$ and the frequencies of the Top and Bottom emitters are fixed to be equal $\omega_{\text{Top}} = \omega_{\text{Bottom}} = \omega_0$. The Gap emitter frequency however vary, $\omega_{\text{Gap}} = \omega_0 + \delta\omega$. The population $P_{\text{Gap}}(t) = \langle\sigma^+_{\text{Gap}}\sigma^-_{\text{Gap}}\rangle$ as a function of time and $\delta\omega$ is shown for three distinct values of ω_0, indicated by the dark red arrows in Fig. **5.8**(a).

Panel (b) corresponds to the case of a dielectric background, for which only $\omega_0 = 1.142$ eV is considered. This is because the results for the other two frequencies are very similar due to the broad nature of the peak, as can be seen in panel (a) for the three arrows. In this setup, there is a significant excitation of the Gap emitter for a narrow range of frequencies, which however does not coincide with $\delta\omega = 0$ as could be naively expected. This is due to the fact that the EM modes induce a significant Lamb shift on the emitters, which is larger for the Top and Bottom emitters due to their higher dipole moments (even though the EM mode density at the Gap position is higher due to the interaction with both ellipsoids). Their effective frequencies are thus lowered more than that of the Gap emitter, and resonant energy transfer is only possible when the Gap emitter is detuned to a slightly lower frequency, $\delta\omega \approx -3$ meV.

In panel (c), the same situation is explored for the hybrid cavity, where the peak splits due to the interaction between the Mie resonances of the mi-

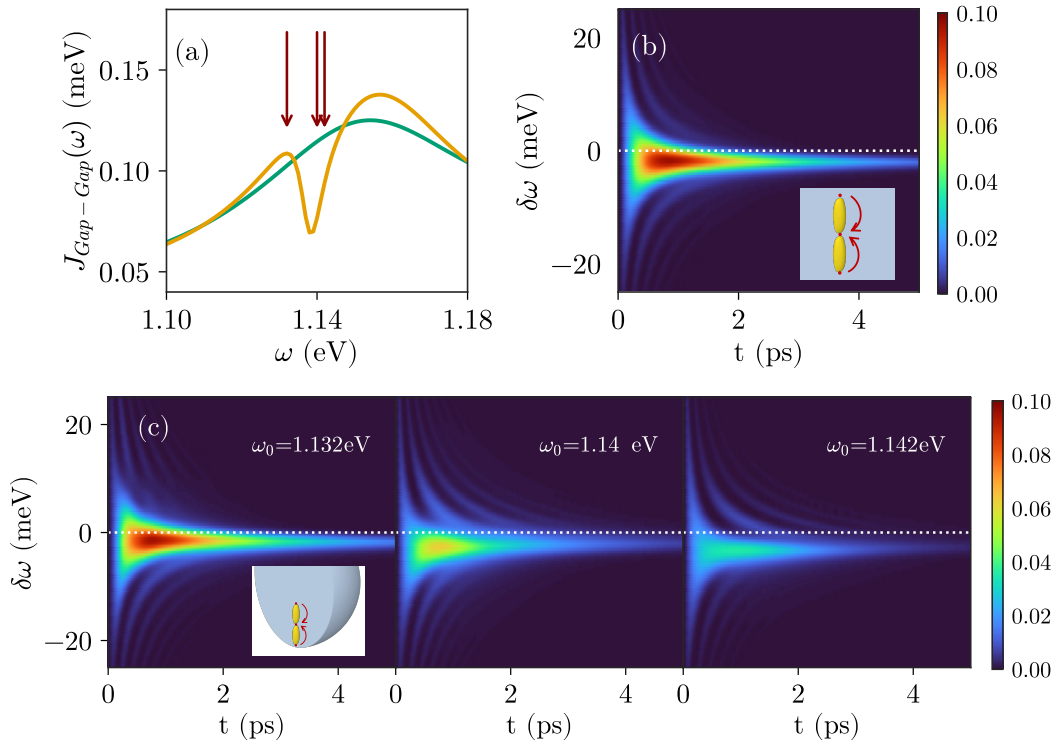

Fig. 5.8.: Subplot (a) shows the spectral density of the Gap emitter around the hybrid mode for the dielectric sphere (orange line) and the dielectric background (green line). The three dark-red arrows point to the different frequencies considered. Subplots (b) and (c) show population transfer to Gap when Top and Bottom are fixed at a frequency ω_0 and Gap is detuned from that frequency for the dielectric background. The initial state ψ_0 is a superposition of Top and Bottom excited, as shown in both sketches in subplots (b) for the dielectric background and (c) for the dielectric sphere, where three different frequencies are considered (shown in each subplot).

crosphere and the plasmonic dimer modes. Now, in the frequency range of interest, there is significantly more structure, so the energy transfer for three values of ω_0 are considered: 1.132 eV, 1.14 eV, and 1.142 eV. As shown in Fig. **5.8**(c), these small changes in frequency have a significant effect on the efficiency of energy transfer even when the detuning is optimized to compensate for the difference in Lamb shifts. In particular, the maximum population reaching the Gap emitter is decreased by a factor of more than two simply when changing ω_0 by just 10 meV. This demonstrates both the sensitivity of energy transfer at the nanoscale to the details of the EM environment and the large degree of control that hybrid metallodielectric structures offer for influencing emitter dynamics.

In the dynamics presented before, the emitters are not in the regime of strong light-matter coupling (no Rabi oscillations are visible on resonance). Nevertheless, the effects observed here could not be reproduced with traditional methods based on the weak-coupling approximation [224–227]. In that approach, the EM environment is traced out fully, with the real and imaginary parts of the Green's function giving coherent and incoherent interactions between emitters (with the diagonal parts corresponding to Lamb shifts and decay rates). However, that approach is only valid when all emitter frequencies are equal (and the emitters are two-level systems characterized by a single frequency), and furthermore does not capture the fact that the effective frequencies of the emitters are affected by the EM environment (and by the emitter-emitter coupling mediated through them). Thus, the Green's function is evaluated at the bare (unshifted) frequency. For highly structured spectral densities as in the present case, this can be a significant source of error. Moreover, the effects discussed here are not correctly represented either when only the EM modes close to resonance with the emitters are taken into account, as the Lamb shift is dominated by off-resonant contributions.

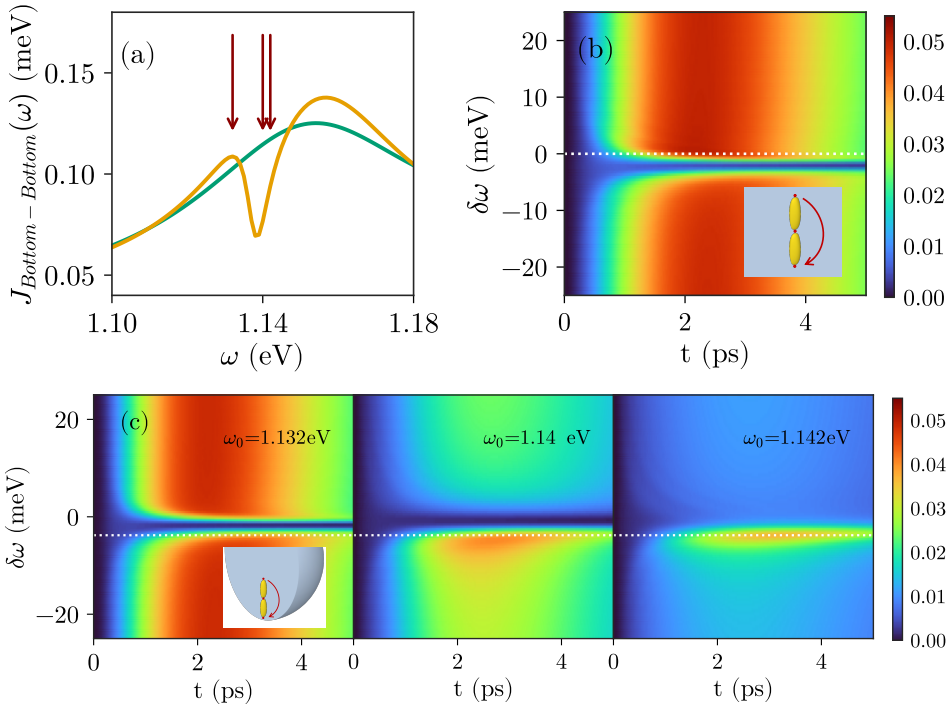

Fig. 5.9.: Subplot (a) shows the spectral density of the Bottom emitter around the hybrid mode for the dielectric sphere (orange line) and the dielectric background (green line). The three dark-red arrows again point to the different frequencies considered. Population transfer to Bottom when Top and Bottom are fixed at a frequency ω_0 and Gap is detuned from that frequency. The initial state ψ_0 corresponds to only Top excited, as shown in both sketches in subplots (a) for the dielectric background and (b) for the dielectric sphere (shown in each subplot).

Next, situation (ii) is considered. In particular, the population transfer chosen is the one from Top to Bottom, as depicted schematically in the insets of Fig. **5.9**(b),(c). The system and parameters remain the same as in the previous setup, but now the system is initialized in $|\psi_0\rangle = \sigma^+_{\text{Top}}|0\rangle$, and the population monitored is $P_{\text{Bottom}}(t) = \langle\sigma^+_{\text{Bottom}}\sigma^-_{\text{Bottom}}\rangle$.

Panel (a) shows the spectral density of the emitter Bottom again around the hybrid mode in the metallodielectric cavity (orange line), which results in a single peak for the metallic dimer (green line). Panels (b) and (c) in Fig. **5.9** again show the population of Bottom for ω_0 for different values of the detuning $\delta\omega$ for Gap emitter frequency. In particular, panel (b) corresponds to the purely plasmonic nanocavity. Population transferred to Bottom is then essentially unaffected by the presence of the Gap emitter unless that emitter is in resonance with the others (after taking into account the differing Lamb shifts). On resonance, energy transfer is significantly suppressed and the Gap emitter acts like an intermediate absorber. This simple picture is again mostly independent of ω_0, so only a single value is shown in Fig, **5.9**(b).

However, in the hybrid cavity, Fig. **5.9**(c), the picture changes drastically. In that case, the intermediate emitter can act to either enhance or suppress the population transfer depending on ω_0 and $\delta\omega$, with a clear asymmetry with regards to the sign of $\delta\omega$. For $\omega_0 = 1.14$ eV, the maximum population reaching the Bottom emitter has a clear Fano-like interference shape with a maximum followed by a steep minimum as a function of $\delta\omega$. When the frequency of the Top and Bottom emitters is further increased by just 2 meV, to $\omega_0 = 1.142$ eV, the minimum essentially disappears and the presence of the Gap emitter on resonance leads to an enhancement of energy transfer. Therefore, the hybrid modes offer the possibility to change the role of the Gap emitter from inhibiting energy transfer between two emitters to enhancing it within a narrow frequency range.

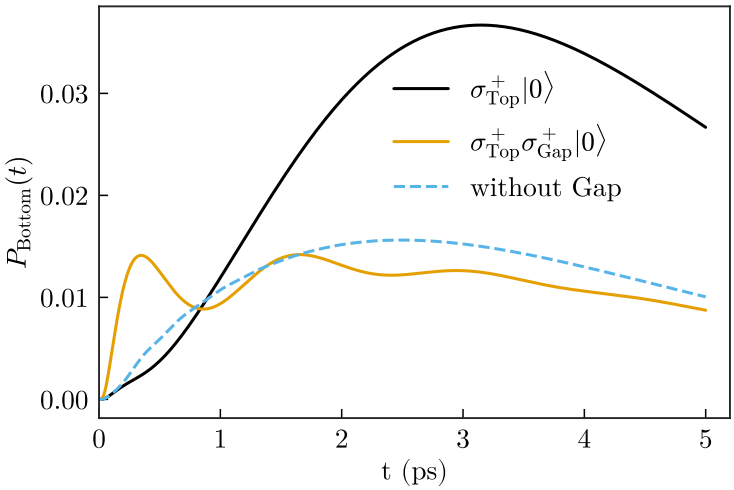

Fig. 5.10.: Population of Bottom for two-photon emission (black line) and one-photon emission (orange line) when Top and Bottom have frequencies $\omega_0 = 1.142$ eV and Gap is detuned $\delta\omega = -3.78$ meV.

Finally, situation (iii) is studied. This corresponds to the energy transfer from the Top to the Bottom emitter and how it changes when the Gap emitter is excited as well, i.e., the initial state is now $|\psi_0\rangle = \sigma^+_{\text{Top}}\sigma^+_{\text{Gap}}|0\rangle$. Now, the frequency chosen is $\omega_0 = 1.142$ eV, corresponding to the final dataset in Fig. **5.9**(c), and the frequency of the Gap emitter is chose so that in the single-excitation case studied previously the population transfer to the Bottom emitter is maximized, which corresponds to $\delta\omega = -3.18$ meV.

Fig. **5.10** shows $P_{\text{Bottom}}(t)$ for the three cases where Gap is initially in its ground state (black line, same data as Fig. **5.9**, excited state (orange line), or is not present at all (dashed blue line)). When the Gap emitter is initially excited, there is a fast initial population transfer (presumably directly from the Gap to the Bottom emitter), but the maximum population reached is significantly lower than for the previous situation where energy transfer is enhanced by the presence of the (ground-state) Gap emitter. In particular, when the Gap emitter is initially excited, the maximum population in Bottom remains smaller than for the case where no emitter is present in Gap. This

shows that the energy transfer between the Top and Bottom emitters can be controlled by exciting the emitter in the Gap, pointing toward a possible path for implementing quantum gates based on hybrid metallodielectric structures.

5.5 Conclusions

In this chapter, an extension of the few-mode field quantization approach to the case of several emitters has been introduced. First, it has been demonstrated how to define and obtain the generalized spectral density $\boldsymbol{\mathcal{J}}(\omega)$, a matrix-valued function that fully determines the properties of the EM environment interacting with the emitters. It has then been shown how to obtain a few-mode quantization of the EM field in this situation. The resulting model can be adjusted to represent arbitrary material structures by fitting the model parameters to reproduce the numerically calculated generalized spectral densities (which requires only the calculation of the dyadic Green's function of Maxwell's equations and can be done with any standard EM solver).

This approach has first been illustrated in a very simple physical problem in which five two-level emitters are placed near a metallic sphere. Within this setup, not only the emitters population can be reproduced faithfully, which demonstrates that the model system is completely equivalent to the original system, but the fit of the parameters can be done by using the same number of interacting modes as emitters, i.e., $N = M = 5$. Therefore, the mode profiles for the discrete, interacting modes can be calculated at any point in space, while it has been shown that the intensity at the position of one emitter is the same in the case of the discrete modes and the emitter-centered modes.

Following this simple model, the validity of the approach to describe arbi-

trary photonic structures has been illustrated by choosing a metallodielectric structure consisting of a metallic dimer embedded in a dielectric sphere, which produces a complex generalized spectral density. $N = 42$ modes are then required to obtain a well-converged representation of the generalized spectral density. Once the fit is obtained, the emitter dynamics can be again calculated using standard approaches of quantum optics, such as solving the Lindblad master equation. This is used to study energy transfer between three emitters in three different situations, so it has been found that hybrid metallodielectric structures can enable significant control, strongly enhancing or suppressing energy transfer for slight variations of the emitter parameters.

Chapter 6 | Conclusions

6.1 General Conclusions

THROUGHOUT the research activity summarized in this thesis, the main topic that has been addressed is the description of photonic systems in which there are a large number of degrees of freedom, with particular applications in the strong coupling regime of light-matter interactions. In practice, these degrees of freedom are a consequence of the use of a large number of emitters, which moreover can present complex internal structures, and photonic environments where a large number of (lossy) photonic modes arise. Although the focus of this thesis is on photonic setups, the majority of the conclusions presented are also valid for general open quantum systems, in which the photonic modes can be substituted by other environments which can be constituted, for example, by phonons or ensembles of other quantum particles.

Due to the complexity of the description of realistic light-matter interactions wherein both the quantum emitters and the photonic environment are included with all the degrees of freedom, the theoretical efforts here focused on a complete description of only one of the components. Therefore, the emitters

have been considered as two-level systems (which is a good approximation for some QEs, such as atoms and quantum dots), while many degrees of freedom have been considered in the photonic environments. Here, the quantum emitters embedded in a photonic structure constitute the system whose dynamics are of interest, while the environment constitutes those degrees of freedom of the whole setup whose importance lies in their effect on the system. Within any setup, the "cavity" modes that arise are not "pure" photonic modes (as they only arise in vacuum) but dressed by the material where they evolve. Therefore, another distinction must be made when theoretically describing light-matter interactions. In general, the photonic cavity modes are considered to be that part of the full system that can be well-approximated by Maxwell's equations. Moreover, these photonic structures cannot confine light perfectly, and all setups in practice present losses, which must also be well-described, especially when dealing with plasmonic systems.

The light-matter interaction between a quantum emitter and the EM field that arise in a particular setup is completely described by the spectral density. When more than one emitter is present in the system, a generalized spectral density can be defined. This matrix-valued function describes not only the interaction between each emitter and the photonic environment, but also the (photon-mediated) interaction between emitters.

Single emitter

The inclusion of many environmental degrees of freedom and their description in a quantum-mechanical way is fundamental in order to get incoherent effects, such as the spontaneous decay of a QE, which cannot be described by classical or mean-field approaches (that are widely used when classical lasers interact with a quantum system). Usually, these effects can be introduced

ad-hoc by adding external terms, but their contribution to the system must be assumed. Therefore, some attempts to extend the mean-field descriptions so that these effects are included, while maintaining a manageable computational complexity, have been made. One of them is based on the cumulant expansion method, presented in **chapter 3**, which consists of the inclusion of the description of the operator correlations up to some order. Therefore, a closed set of (numerical) equations can be solved using standard solvers. However, even for simple and known environments (in particular free space and a Fabry-Pérot cavity with a Lorentzian spectral density) the particularities of the environments and the strength of the interactions (between the QE and the cavity and the QE and the classical incident laser) modifies the order of the correlations needed to give a good description of the system, such that general statements about the validity of the mean-field expansion up to any given order are difficult to make.

Another strategy to describe light-matter interactions in photonic environments consists in transforming the latter so that the dynamics obtained in the final system are the same as the dynamics given by the original one. One common transformation is the chain mapping, in which the quantum system (a quantum emitter) interacts only with the first mode of an (infinite) string in which the bosons that describe the environment interact only with their nearest neighbors. Tensor network approaches, for example, use this mapping in order to describe complexity in both quantum emitters and photonic environments. However, in this transformation the maximum time described accurately is limited by the length of the chain, as EM field excitations (photons) "travel" along the chain and are reflected when they reach the end, and then "travel back" and interact with the emitter again, therefore giving some non-physical dynamics. This shortcoming in the chain mapping description forces us to use very long chains that increase the computational resources needed to reproduce long times. In **chapter 4**, different strategies to describe long-time

dynamics by using short chains have been explored. In particular, even in complex photonic structures, frequency and coupling parameters achieve their limiting values for relatively short chains. Therefore, the inclusion of decay at sites of the chain far enough from the system can absorb these wavepackets and suppress reflections. However, only a smooth function to describe the losses is able to reduce spurious reflections sufficiently. When optimization is performed in the spectral density or the correlation function, the chain length can be further decreased. However, the fit to neither of these quantities can be reproduced accurately in the chain form.

An accurate description of the spectral density is in fact necessary to describe light-matter interactions correctly, so that if two approaches give the same spectral density, the interactions modelled are completely equivalent to one another from the point of view of the emitter. By extending the interactions allowed along the chain to next-nearest neighbors, the number of parameters in the diagonal form of the spectral density is the same as the number of parameters of the "extended" chain for the same number of modes. Therefore, a faithful description of this quantity can be done, and the dynamics of a quantum emitter can be exactly reproduced even at long times.

Multiple emitters

Finally, by extending the previous concepts to multiple emitters (or in general multiple light-matter interaction operators) the generalized spectral density can be defined. Now, this quantity describes the light-matter interaction and the photon-mediated interaction between emitters. As in the single emitter case, if the generalized spectral density can be reproduced by using some approach, the behavior of the whole system can also be reproduced. In particular, an extended few-mode interacting approach is derived in **chap-**

ter 5. This approach consists in describing the setup with a Hamiltonian in which a small number of interacting discrete mode are coupled to the emitters, while each of these modes is also coupled to a Markovian (i.e. spectrally flat) continuum. This model can reproduce hybrid plasmonic-dielectric setups, so that complex photonic environments and in particular hybrid modes can be described. The generalized spectral density consists now of a matrix-valued function so that the fit to the whole density can be performed. In general, the number of discrete photonic modes in the model will be larger than the number of emitters, but for those setups where the generalized spectral density can be described using the same number of bosonic modes than number of emitters in the system, the mode profiles and the intensity can be obtained (in particular in the position of one emitter, the intensity of the discrete modes of the model coincides with the intensity given by the emitter-centered modes). In more general structures, once the fit is done, the population transfer between the emitters can be studied. This is done in particular for frequencies around the lowest-energy hybrid mode, and it is concluded that by changing the frequencies of the emitters slightly the population transfer can be tuned, both for a single excitation and beyond the single-excitation subspace. In the latest situation, the population transfer can be enhanced or suppressed by the inclusion of a third emitter in its ground or excited state.

6.2 Conclusiones generales

A lo largo de la actividad de investigación que se resume en este documento, el tema principal que se ha tratado es la descripción de sistemas fotónicos en los que hay un gran número de grados de libertad, en particular con aplicaciones en el régimen de acoplamiento fuerte en la interacción entre luz y materia. En la práctica, estos grados de libertad son consecuencia del uso de un gran número de emisores, que además pueden presentar una estructura interna compleja, y los entornos fotónicos donde un gran número de modos fotónicos (con pérdidas) tienen lugar. Aunque el ámbito de esta tesis son las configuraciones fotónicas, la mayoría de conclusiones que se han presentado son válidas también para sistemas cuánticos abiertos en general, donde los modos fotónicos pueden ser substituidos por otros entornos que pueden estar formados, por ejemplo, por fonones y conjuntos de otras partículas cuánticas.

Debido a la complejidad en la descripción realista de interacciones entre luz y materia, donde se incluyen todos los grados de libertad tanto de los emisores cuánticos como del entorno fotónico, los esfuerzos teóricos se han concentrado en describir de forma completa solamente uno de estos elementos. Por tanto, los emisores cuánticos se han considerado como sistemas de dos niveles (lo cual es una buena aproximación para algunos emisores, como los átomos y los puntos cuánticos), mientras que para los entornos fotónicos se han considerado muchos grados de libertad. Aquí, los emisores cuánticos forman el sistema cuya dinámica nos interesa, mientras que el entorno constituye aquellos grados de libertad de todo el sistema cuya importancia radica en su efecto sobre el sistema. En una configuración, los modos “de cavidad” que surgen no son modos fotónicos “puros” (estos únicamente surgen en el vacío) sino que están

vestidos por el material donde se desarrollan. Por tanto, es necesario hacer otra distinción cuando se describen interacciones entre luz y materia teóricamente. En general, los modos de cavidades fotónicas se consideran la parte de todo el sistema que está bien aproximada por las ecuaciones de Maxwell. Además, las estructuras fotónicas no confinan la luz de forma perfecta, y todas las configuraciones presentan pérdidas, que también deben describirse de forma correcta, especialmente cuando se está lidiando con estructuras plasmónicas.

Las interacciones entre un emisor cuántico y el campo electromagnético que tienen lugar en una configuración particular están completamente descritas por la densidad espectral. Cuando múltiples emisores se encuentran en la misma configuración, se puede definir la densidad espectral generalizada. Esta matriz de funciones no solo describe la interacción entre cada emisor y el entorno fotónico, sino también la interacción entre los distintos emisores (mediada por fotones).

Un emisor

La inclusión de muchos grados de libertad y su descripción de forma cuántica es fundamental para obtener efectos incoherentes, como el decaimiento espontáneo de un emisor cuántico, que no puede ser descrito clásicamente o con aproximaciones de campo medio (que sí se usan cuando un láser clásico interacciona con el sistema cuántico). Normalmente, estos efectos se pueden introducir añadiendo términos externos *ad-hoc*, pero su contribución en el sistema debe ser asumida. Por tanto, se han hecho algunos intentos para extender las representaciones de campo medio para incluir estos efectos manteniendo una complejidad computacional manejable. Uno de ellos se basa en el método de expansión de correlaciones, presentado en el **capítulo 3**, que consiste en la inclusión de la descripción de las correlaciones de los operadores hasta cierto

orden. Por tanto, un sistema cerrado de ecuaciones (numéricas) puede resolverse utilizando métodos estándar. Sin embargo, incluso para sistemas simples y conocidos (en particular el espacio libre y una cavidad Fabry-Pérot con una densidad espectral lorenztiana) las particularidades del entorno y la intensidad de las interacciones (entre el emisor y la cavidad y entre el emisor y el láser clásico incidente) modifica el orden de las correlaciones que se necesitan para dar una buena descripción del sistema, de forma que una conclusión general sobre la validad de la expansión de campo medio hasta un order cualquiera es difícil de hacer.

Otra estrategia para describir las interacciones entre luz y materia en entornos fotónicos consiste en transformar el último de forma que la dinámica que se obtiene en el sistema final es la misma que la del sistema original. Una transformación común para ello es la transformación de la cadena, donde el sistema cuántico (el emisor) interacciona solo con el primer modo de una cadena (infinita) donde los bosones que describen el entorno interaccionan solo con sus vecinos más cercanos. Los modelos de redes de tensores, por ejemplo, usan esta transformación para describir la complejidad tanto de los emisores como de los entornos fotónicos. Sin embargo, en esta transformación el tiempo máximo descrito de forma precisa está limitado por la longitud de la cadena, ya que después de la transformación las excitaciones del campo (fotones) "viajan" a lo largo de la cadena y se reflejan cuando llegan al final "viajando de vuelta" e interaccionando de nuevo con el emisor, dando por tanto una dinámica no física. Este inconveniente en la descripción de la transformación de la cadena obliga a usar cadenas muy largas que aumentan los recursos computacionales necesarios para reproducir tiempos largos. En el **capítulo 4** se exploran diferentes estrategias para describir la dinámica a tiempos largos con cadenas cortas. En particular, incluso para estructuras fotónicas complejas, los parámetros de frecuencia y acoplamiento alcanzan valores límite en cadenas relativamente cortas. Por tanto, la inclusión de decaimiento en sitios de la cadena lo suficien-

temente alejados del sistema hace posible absorber estos paquetes de ondas y suprimir los reflejos. Sin embargo, únicamente funciones suaves que describan estas pérdidas son capaces de reducir lo suficiente las interacciones espúreas. Cuando se optimiza la densidad espectral o la función de correlación, la longitud de la cadena puede disminuirse todavía más. Sin embargo, ninguna de estas cantidades puede reproducirse de manera precisa en la forma de cadena.

Reproducir de forma precisa la densidad espectral es de hecho necesario para describir correctamente las interacciones entre luz y materia, de forma que si dos modelos tienen la misma densidad espectral, las interacciones descritas son completamente equivalentes desde el punto de vista del emisor. Extendiendo las interacciones permitidas en la cadena a los segundos vecinos, el número de parámetros en la forma diagonal de la densidad espectral es el mismo que los de la cadena "extendida" para el mismo número de modos. Por tanto, es posible reproducir esta cantidad de forma fiel, y la dinámica de un emisor cuántico puede reproducirse de forma exacta incluso a tiempos largos.

Múltiples emisores

Finalmente, extendiendo los conceptos previos a múltiples emisores (o en general a múltiples operadores de interacción entre luz y materia) se puede definir la densidad espectral generalizada. Ahora, esta cantidad describe la interacción de los emisores con el campo electromagnético y la interacción entre emisores mediada por fotones. De forma análoga a un único emisor, si la densidad espectral generalizada puede reproducirse usando algún modelo, el comportamiento de todo el sistema puede también reproducirse. En particular, en el **capítulo 5** se deriva una extensión del modelo de pocos modos que interaccionan entre sí. Este modelo consiste en describir la configuración con un Hamiltoniano donde un número pequeño de modos discretos que interac-

cionan están acoplados a los emisores, mientras que cada uno de estos modos está acoplado a un continuo markoviano (esto es, espectralmente plano). Este modelo puede reproducir sistemas híbridos plasmónicos y dieléctricos, de forma que puede describir entornos fotónicos complejos y en partícular modos híbridos. La densidad espectral generalizada consiste ahora en una matriz de funciones de forma que se puede ajustar la densidad completa. En general, el número de modos fotónicos es mayor al número de emisores, pero para aquellos sistemas que pueden describirse usando el mismo número de modos bosónicos que de emisores embebidos en la estructura, se puede calcular el perfil de los modos y la intensidad (en particular en la posición de uno de los emisores la intensidad de los modos discretos del modelo coincide con la intensidad dada por los modos centrados en emisores). Para estructuras más generales, una vez el ajuste está hecho, puede estudiarse la transferencia de población entre los emisores. Esto se ha hecho en particular para frecuencias que están cerca del modo híbrido de menor energía, y se concluye que cambiando ligeramente las frecuencias de los emisores la transferencia de población puede sintonizarse para una única excitación y cuando se está más allá del subespacio de una única excitación. En la última de estas situaciones, la transferencia de población puede acentuarse o suprimirse con la inclusión de un tercer emisor en su estado fudamental o en su estado excitado.

Appendix A | Free space quantization

In free space, the EM field interactions are completely described by Maxwell's equations

$$\nabla \cdot \mathbf{E}(\mathbf{r}, t) = \frac{\rho(\mathbf{r}, t)}{\epsilon_0}, \tag{A.1}$$

$$\nabla \times \mathbf{E}(\mathbf{r}, t) = -\dot{\mathbf{B}}(\mathbf{r}, t), \tag{A.2}$$

$$\nabla \cdot \mathbf{B}(\mathbf{r}, t) = 0, \tag{A.3}$$

$$\nabla \times \mathbf{B}(\mathbf{r}, t) = \mu_0 \mathbf{J}(\mathbf{r}, t) + \mu_0 \epsilon_0 \dot{\mathbf{E}}(\mathbf{r}, t), \tag{A.4}$$

where $\mathbf{E}$ and $\mathbf{B}$ are the electric and magnetic field, respectively, ϵ_0 is the vacuum electric permittivity, μ_0 is the vacuum magnetic permeability, $\rho(\mathbf{r}, t)$ is the charge density, and $\mathbf{J}(\mathbf{r}, t)$ is the current density. In Maxwell's equations, the conservation of charge is implicitly contained, as charge and current densities fulfil the continuity relation $\nabla \cdot \mathbf{J}(\mathbf{r}, t) + \dot{\rho}(\mathbf{r}, t) = 0$, which states that any change in the charge density in one region produces a current flow that crosses its boundary.

The fields, which are coupled in the previous set of equations, can be writ-

ten in terms of the scalar and vector potential, $\phi(\mathbf{r},t)$ and $\mathbf{A}(\mathbf{r},t)$ respectively:

$$\mathbf{E}(\mathbf{r},t) = -\dot{\mathbf{A}}(\mathbf{r},t) - \nabla\phi, \tag{A.5}$$

$$\mathbf{B}(\mathbf{r},t) = \nabla \times \mathbf{A}(\mathbf{r},t). \tag{A.6}$$

The latter equation arises from Eq. (A.3), while the former is obtained from Eq. (A.2). Then, the other two equations can also be written in terms of the potentials,

$$\nabla^2\phi(\mathbf{r},t) + \nabla\cdot\dot{\mathbf{A}}(\mathbf{r},t) = -\frac{\rho(\mathbf{r},t)}{\epsilon_0}, \tag{A.7}$$

$$\nabla\left(\nabla\cdot\mathbf{A}(\mathbf{r},t)\right) - \nabla^2\mathbf{A}(\mathbf{r},t) + \frac{1}{c^2}\ddot{\mathbf{A}}(\mathbf{r},t) + \frac{1}{c^2}\nabla\dot{\phi}(\mathbf{r},t) = \mu_0\mathbf{J}(\mathbf{r},t), \tag{A.8}$$

where $c = 1/\sqrt{\epsilon_0\mu_0}$ is the vacuum speed of light. The definitions of the potentials given above are not unique as some transformations can change them while conserving the fields. In particular the gauge transformations $\mathbf{A}'(\mathbf{r},t) \rightarrow \mathbf{A}(\mathbf{r},t) + \nabla\Lambda(\mathbf{r},t)$ and $\phi'(\mathbf{r},t) \rightarrow \phi(\mathbf{r},t) - \dot{\Lambda}(\mathbf{r},t)$, where $\Lambda(\mathbf{r},t)$ is an arbitrary scalar function, do not alter Maxwell's equations. Therefore, it is possible to choose a gauge that simplifies the description of the fields. The Coulomb gauge, where $\nabla\cdot\mathbf{A}(\mathbf{r},t) = 0$, is typically chosen in quantum optics. Moreover, according to the Helmholtz theorem, any vector field can be written as a sum of a component with zero divergence (transverse) and a component with zero curl (longitudinal). The electric field can be written then as $\mathbf{E} = \mathbf{E}_\parallel + \mathbf{E}_\perp$[1], where $\mathbf{E}_\parallel$ corresponds to the longitudinal component and $\mathbf{E}_\perp$ to the transverse component. In the Coulomb gauge, $\mathbf{E}_\parallel = -\nabla\phi$ and $\mathbf{E}_\perp = -\dot{\mathbf{A}}$, while the magnetic field is entirely transverse, as is the vector potential. When making this decomposition to the current density, equations (A.7), (A.8) can be written as

$$-\nabla^2\mathbf{A} + \frac{1}{c^2}\ddot{\mathbf{A}} = \mu_0\mathbf{J}_\perp, \tag{A.9}$$

$$\frac{1}{c^2}\nabla\dot{\phi} = \mu_0\mathbf{J}_\parallel. \tag{A.10}$$

[1]Here and in the following, the position and time dependence $(\mathbf{r},t)$ are dropped to simplify the notation.

Therefore, in the Coulomb gauge, the equations for $\mathbf{A}$ and ϕ decouple and Maxwell's equations are separated into transverse and longitudinal sets. The former describes the EM waves and is associated with the vector potential, while the latter is associated with the scalar potential and describes the electric field that arises from the charge density.

Within free space, in the absence of charges and currents, equations (A.1) and (A.4) simplify and Eq. (A.9) is equal to $\mathbf{0}$. Moreover we can define the local classical lagrangian of the EM field

$$\mathcal{L} = \frac{\epsilon_0}{2}\int \mathrm{d}^3 r \left[{\mathbf{E}_\perp}^2 + c^2\mathbf{B}^2\right] = \frac{\epsilon_0}{2}\int \mathrm{d}^3 r \left[\left(\dot{\mathbf{A}}\right)^2 - c^2\left(\nabla\times\mathbf{A}\right)^2\right], \tag{A.11}$$

in which the right-hand side has been written in terms of the vector potential. Here, the lagrangian depends on just one variable, the vector potential. Therefore, it is taken as the generalized coordinate. Defining the canonically conjugate momentum of $\mathbf{A}$, which is, $\mathbf{\Pi} = \delta L/\delta\dot{\mathbf{A}} = \epsilon_0\dot{\mathbf{A}} = -\epsilon_0\mathbf{E}$, the Hamiltonian of the EM field can be written:

$$H = \frac{1}{2}\int \mathrm{d}t \int \mathrm{d}^3 r \left[\epsilon_0\mathbf{E}^2 + \frac{1}{\mu_0}\mathbf{B}^2\right]. \tag{A.12}$$

Moreover, Eq. (A.9) is equal to $\mathbf{0}$ and its solution can be found by separation of variables. Doing a mode decomposition, the solution to Eq. (A.9) corresponds to plane waves, while the temporal dependence is given by a harmonic oscillator. Finally, the decomposition of the vector potential can be written as

$$\mathbf{A} = \sum_\lambda \int \frac{\mathrm{d}^3 k}{(2\pi)^{3/2}}\mathbf{e}_\lambda(\mathbf{k})\left[\boldsymbol{a}_\lambda(\mathbf{k})e^{i(\mathbf{k}\cdot\mathbf{r}-\omega t)} + \text{c.c.}\right], \tag{A.13}$$

where $\lambda = \{e, m\}$ accounts for two orthogonal polarizations of the unitary vectors $\mathbf{e}_\lambda(\mathbf{k})$, whose magnitude is given by $k = \omega/c$, and $\boldsymbol{a}_\lambda(\mathbf{k})$ is a complex amplitude related to the vector potential and its canonical momentum as

$$\boldsymbol{a}_\lambda(\mathbf{k}) = \sqrt{\frac{\epsilon_0}{2\hbar\omega}}\left[\omega\mathbf{A}_\lambda(\mathbf{k}) + \frac{i}{\epsilon_0}\mathbf{\Pi}_\lambda(\mathbf{k})\right], \tag{A.14}$$

where $\mathbf{A}_\lambda(\mathbf{k})$ and $\mathbf{\Pi}_\lambda(\mathbf{k})$ are the Fourier transform of the variables.

Now, quantization can be performed by replacing the classical amplitudes $\boldsymbol{a}_\lambda(\mathbf{k})$ with operators $\hat{\boldsymbol{a}}_\lambda(\mathbf{k})$, which correspond to the ladder operators of the harmonic oscillator and fulfil the bosonic commutation relation $\left[\hat{\boldsymbol{a}}_\lambda(\mathbf{k}), \hat{\boldsymbol{a}}^\dagger_\lambda(\mathbf{k})\right] = \delta_{\lambda,\lambda'}\delta(\mathbf{k}-\mathbf{k}')$. The vector potential can be thus also replaced by an operator which, written in terms of the ladder operators, is

$$\hat{\mathbf{A}}(\mathbf{r},t) = \sum_{\lambda=1}^{2} \int \frac{\mathrm{d}^3k}{(2\pi)^{3/2}} \sqrt{\frac{\hbar}{2\epsilon_0\omega}} \mathbf{e}_\lambda \left[\hat{\boldsymbol{a}}_\lambda(\mathbf{k}) e^{i(\mathbf{k}\cdot\mathbf{r}-\omega t)} + \text{c.c.}\right]. \tag{A.15}$$

Finally, discretizing the integral in $\mathbf{k}$, the quantized Hamiltonian can be written as

$$\hat{H} = \sum_{\mathbf{k},\lambda} \hbar\omega \left(\hat{\boldsymbol{a}}^\dagger_\lambda(\mathbf{k})\hat{\boldsymbol{a}}_\lambda(\mathbf{k}) + \frac{1}{2}\right), \tag{A.16}$$

so that the field is finally represented by a set of uncoupled harmonic oscillators.

Interaction with atoms

Microscopic particles, like atoms or molecules, can act as external sources. They can be included in Maxwell's equations via the charge density, which can be written as a collection of point charges $\rho = \sum_i q_i \delta\left[\mathbf{r}-\mathbf{r}_i\right]$, and the current density, $\mathbf{J} = \sum_i q_i \partial_t \mathbf{r}_i \delta\left[\mathbf{r}-\mathbf{r}_i(t)\right]$, as shown in eqs. (A.1) to (A.4). In order to quantize the EM field again, but now taking into account the external sources, Newton's equation of motion must be added to the system of equations given by Maxwell's equations $m_i\ddot{\mathbf{r}}_i = q_i\left[\mathbf{E}(\mathbf{r}_i,t) + \dot{\mathbf{r}}_i \times \mathbf{B}(\mathbf{r}_i,t)\right]$. In the Coulomb gauge, the scalar potential ϕ obeys Poisson's equation, and its solution is the electrostatic Coulomb potential. The classical Hamiltonian is then

$$H = \frac{1}{2}\int \mathrm{d}^3r \left[\epsilon_0\mathbf{E}^2 + \frac{1}{\mu_0}\mathbf{B}^2\right] + \sum_i \frac{1}{2m_i}\left[\mathbf{p}_i - q_i\mathbf{A}(\mathbf{r}_i)\right]^2 + \sum_{i\neq j} \frac{q_i q_j}{8\pi\epsilon_0\left|\mathbf{r}_i-\mathbf{r}_j\right|}, \tag{A.17}$$

where $\mathbf{p}_i = m_i\mathbf{r}_i + q_i\mathbf{A}_i(\mathbf{r}_i)$ is the particle momentum. This Hamiltonian is referred to as the minimal-coupling Hamiltonian because it includes the microscopic description of the charged particles. The quantization of this Hamiltonian is done again replacing the c-functions with operators. Now, the quantum character of the particles is contained in their position and momentum operators, which fulfil the commutation relation $[\hat{\mathbf{r}}_i, \hat{\mathbf{p}}_j] = i\hbar\delta_{i,j}\mathbb{I}$.

Therefore, the quantum operators derived for the fields in the previous section are valid, and the quantum minimal coupling Hamiltonian is

$$H = \hat{H}_{\mathrm{EM}} + \sum_i \frac{1}{2m_i}\left[\hat{\mathbf{p}}_i - q_i\hat{\mathbf{A}}(\hat{\mathbf{r}}_i)\right]^2 + \sum_{i,j>i}\frac{q_i q_j}{4\pi\epsilon_0\left|\hat{\mathbf{r}}_i - \hat{\mathbf{r}}_j\right|}, \tag{A.18}$$

where $\hat{H}_{\mathrm{EM}}$ is the "bare" EM Hamiltonian, given by Eq. (A.16). This Hamiltonian gives the microscopic description of the interaction between the EM field and charged particles. However, in many cases a description of all the individual charges is not needed and an approach in terms of global variables is more practical.

In free space the multipolar Hamiltonian can also be obtained by applying the Power-Zienau-Woolley transformation. Again, the transformed Hamiltonian uses the global variables $\mathbf{E}$ and $\mathbf{B}$ instead of their longitudinal and perpendicular components. The Power-Zienau-Woolley transformation is $\hat{O}' = \hat{U}\hat{O}\hat{U}^\dagger$, where

$$\hat{U} = \exp\left[\frac{i}{\hbar}\int \mathrm{d}^3r \sum_i \hat{\mathbf{P}}_i(\mathbf{r})\cdot\hat{\mathbf{A}}(\mathbf{r})\right], \tag{A.19}$$

is a unitary transformation, $\hat{\mathbf{P}}_i(\mathbf{r}) = \sum_{j\in i} q_j\hat{\bar{r}}_j\int_0^1 d\sigma\delta\left(\mathbf{r} - \mathbf{r}_i - \sigma\hat{\bar{r}}_j\right)$ is the polarization operator for the emitter i and $\hat{\bar{\mathbf{r}}}_j = \hat{\mathbf{r}}_j - \hat{\mathbf{r}}_i$ is the relative position of the charge j belonging to emitter i. Expressing the Hamiltonian in terms

of the transformed variables (shown with primes) it becomes

$$\begin{aligned}\hat{H}' = &\sum_{\mathbf{k},\lambda} \hbar\omega \left(\hat{\boldsymbol{a}}_\lambda'^{\dagger}(\mathbf{k})\hat{\boldsymbol{a}}_\lambda'(\mathbf{k}) + \frac{1}{2}\right) - \sum_i \int \mathrm{d}^3\mathbf{r}\hat{\mathbf{P}}_i \cdot \hat{\mathbf{E}}'(\hat{\mathbf{r}}) \\ &+ \sum_i \left[\sum_{j\in i} \frac{\hat{\mathbf{p}}_j'^2}{2m_j} + \frac{1}{2\epsilon_0}\int \mathrm{d}^3\mathbf{r}\hat{\mathbf{P}}_i^2(\mathbf{r})\right],\end{aligned} \tag{A.20}$$

where the transformed electric field operator $\hat{\mathbf{E}}'(\mathbf{r})$ can be expressed in terms of the ladder operators through its relation with the vector potential.

Appendix B | Emitter-centered modes

As emitter-centered modes can be used to derive the model presented in **chapter 5**, this section provides an outline of their derivation and some useful expressions. A more complete review of these modes can be found in [228].

Starting with the macroscopic QED Hamiltonian given in Eq. (2.30), a linear transformation of the medium-supported EM modes $\hat{\mathbf{f}}_\lambda(\mathbf{r},\omega)$ can be done so that a minimal number of EM modes couple to each emitter. For simplicity, it is considered that the long-wavelength approximation can be made in the multipolar Hamiltonian, i.e., ir can be written as Eq. (2.30). The definition of the emitter-centered (or bright) modes is

$$\hat{B}_i(\omega) = \sum_\lambda \int \mathrm{d}^3\mathbf{r}\boldsymbol{\beta}_{i,\lambda}(\mathbf{r},\omega)\cdot\mathbf{f}(\mathbf{r},\omega), \tag{B.1}$$

where $\boldsymbol{\beta}_{i,\lambda}(\mathbf{r},\omega) = \mathbf{n}_i\cdot\mathbf{G}_\lambda(\mathbf{r}_i,\mathbf{r},\omega)/G_i(\omega)$, and $G_i(\omega)$ is a normalization factor, which takes the form

$$G_i(\omega) = \sqrt{\frac{\hbar\omega^2}{\pi\epsilon_0 c^2}\mathbf{n}_i\cdot\mathrm{Im}\mathbf{G}(\mathbf{r}_i,\mathbf{r}_i,\omega)\cdot\mathbf{n}_i}, \tag{B.2}$$

where $\mathbf{G}(\mathbf{r}_i,\mathbf{r}_i,\omega)$ is the dyadic Green's function. The expression of the normalization constant can be derived via de bosonic commutation relations for

the new operators, which is $\left[\hat{B}_i(\omega), \hat{B}_j^\dagger(\omega')\right] = S_{ij}(\omega)\delta(\omega - \omega')$, where

$$S_{ij}(\omega) = \sum_\lambda \int \mathrm{d}^3\mathbf{r}\boldsymbol{\beta}_{i,\lambda}^*(\mathbf{r},\omega)\cdot\boldsymbol{\beta}_{j,\lambda}(\mathbf{r},\omega) = \frac{\hbar\omega^2}{\pi\epsilon_0 c^2}\frac{\mathbf{n}_i\cdot\mathrm{Im}\mathbf{G}(\mathbf{r}_i,\mathbf{r}_j,\omega)\cdot\mathbf{n}_j}{G_i(\omega)G_j(\omega)} \tag{B.3}$$

is the overlap matrix. Moreover, $G_i(\omega)$ is the coupling strength between the emitter-centered modes and the emitter, as seen in Eq. (B.2). Therefore, it can be related to the spectral density, i.e., $J_i(\omega) = \left(\mu G_i(\omega)/\hbar\right)^2$.

An explicit orthogonalization of the bright modes can be made in order to rewrite the Hamiltonian in a more familiar way. The orthogonal modes are called $\hat{C}_i(\omega)$ and they are linear superpositions of the non-orthogonal modes $\hat{B}_i(\omega)$

$$\hat{C}_i(\omega) = \sum_j V_{ij}(\omega)\hat{B}_j(\omega), \tag{B.4}$$

$$\boldsymbol{\chi}_{i,\lambda}(\mathbf{r},\omega) = \sum_j V_{ij}(\omega)\boldsymbol{\beta}_{i,\lambda}(\mathbf{r},\omega), \tag{B.5}$$

where $V_{ij}(\omega)$ are the elements of the transformation matrix, chosen so that $\left[\hat{C}_i(\omega), \hat{C}_j^\dagger(\omega')\right] = \delta_{ij}\delta(\omega - \omega')$, and can be elected in different ways. As the operators $\hat{C}_i(\omega)$ are linear superpositions of $\hat{B}_i(\omega)$, they are also linear superpositions of the "original" modes $\hat{\mathbf{f}}_\lambda(\mathbf{r},\omega)$, and these last operators can be expanded in terms of the orthogonal emitter-centered modes and an infinite number of "dark" modes, which are not coupled to the emitters and therefore do not affect to the dynamics and can be dropped from the Hamiltonian, which in the end is given by

$$\hat{H} = \int_0^\infty \mathrm{d}\omega \left[\sum_i \hbar\omega\hat{C}_i^\dagger(\omega)\hat{C}_i(\omega) - \sum_{ij}\hat{\mu}_i\left(g_{ij}(\omega)\hat{C}_j(\omega) + \mathrm{H.c.}\right)\right], \tag{B.6}$$

where the coupling strength between the orthogonal bright modes and the emitters is now given by $g_{ij}(\omega) = G_{ij}(\omega)V_{ij}^{-1}(\omega)$.

Furthermore, the expression of the field modes in terms of the emitter-centered modes can also be derived. In particular

$$\mathbf{E}^{(+)}(\mathbf{r}) = \sum_i \int \mathrm{d}\omega \; \mathbf{E}_i(\mathbf{r},\omega)\hat{C}_i(\omega), \tag{B.7}$$

$$\mathbf{E}_i(\mathbf{r},\omega) = \sum_j V_{ij}(\omega)\boldsymbol{\epsilon}_j(\mathbf{r},\omega), \tag{B.8}$$

$$\boldsymbol{\epsilon}_j(\mathbf{r},\omega) = \frac{\hbar\omega^2}{\pi\epsilon_0 c^2}\frac{\mathrm{Im}\mathbf{G}(\mathbf{r},\mathbf{r}_j,\omega)\cdot\mathbf{n}_j}{G_j(\omega)}, \tag{B.9}$$

so that the field associated with each emitter-centered mode can be known.

List of Figures

Bibliography

[1]M. O. Scully and M. S. Zubairy, *Quantum optics* (Cambridge Univeristy Press, 2001).

[2]W. E. Lamb Jr and R. C. Retherford, «Fine structure of the hydrogen atom by a microwave method», Physical Review **72**, 241 (1947).

[3]H. B. Casimir, «On the attraction between two perfectly conducting plates», in Proc. kon. ned. akad. wet. Vol. 51 (1948), p. 793.

[4]F. J. Garcia-Vidal, C. Ciuti, and T. W. Ebbesen, «Manipulating matter by strong coupling to vacuum fields», Science **373**, eabd0336 (2021).

[5]J. Fregoni, F. J. Garcia-Vidal, and J. Feist, «Theoretical challenges in polaritonic chemistry», ACS Photonics **0**, null (0).

[6]H. Walther, B. T. H. Varcoe, B.-G. Englert, and T. Becker, «Cavity quantum electrodynamics», Reports on Progress in Physics **69**, 1325–1382 (2006).

[7]S. Haroche and J.-M. Raimond, *Exploring the quantum: atoms, cavities, and photons* (Oxford university press, 2006).

[8]E. M. Purcell, «Spontaneous emission probabilities at radio frequencies», Physical Review **69** (1946).

[9]C. Cohen-Tannoudji, J. Dupont-Roc, and G. Grynberg, *Photons and Atoms: Introduction to Quantum Electrodynamics*, First (Wiley, Mar. 1997).

[10]D. A. Steck, *Quantum and Atom Optics* (June 2007).

[11]I. Buluta, S. Ashhab, and F. Nori, «Natural and artificial atoms for quantum computation», Reports on Progress in Physics **74**, 104401 (2011).

[12]A. V. Kavokin, J. J. Baumberg, G. Malpuech, and F. P. Laussy, *Microcavities*, Vol. 21 (Oxford university press, 2017).

[13]H. J. Kimble, «Strong Interactions of Single Atoms and Photons in Cavity QED», Phys. Scr. **T76**, 127 (1998).

[14]P. Törmä and W. L. Barnes, «Strong Coupling between Surface Plasmon Polaritons and Emitters: A Review», Rep. Prog. Phys. **78**, 013901 (2015).

[15]D. S. Dovzhenko, S. V. Ryabchuk, Y. P. Rakovich, and I. R. Nabiev, «Light–matter interaction in the strong coupling regime: configurations, conditions, and applications», Nanoscale **10**, 3589–3605 (2018).

[16]D. N. Basov, A. Asenjo-Garcia, P. J. Schuck, X. Zhu, and A. Rubio, «Polariton Panorama», Nanophotonics **10**, 549 (2021).

[17]S. Christopoulos, G. B. H. von Högersthal, A. J. D. Grundy, P. G. Lagoudakis, A. V. Kavokin, J. J. Baumberg, G. Christmann, R. Butté, E. Feltin, J.-F. Carlin, and N. Grandjean, «Room-temperature polariton lasing in semiconductor microcavities», Phys. Rev. Lett. **98**, 126405 (2007).

[18]G. Lerario, A. Fieramosca, F. Barachati, D. Ballarini, K. S. Daskalakis, L. Dominici, M. De Giorgi, S. A. Maier, G. Gigli, S. Kéna-Cohen, and D. Sanvitto, «Room-temperature superfluidity in a polariton condensate», Nature Physics **13**, 837–841 (2017).

[19]S. Kéna-Cohen and S. R. Forrest, «Room-temperature polariton lasing in an organic single-crystal microcavity», Nature Photonics **4**, 371–375 (2010).

[20]K. Hennessy, A. Badolato, M. Winger, D. Gerace, M. Atatüre, S. Gulde, S. Fält, E. L. Hu, and A. Imamoğlu, «Quantum nature of a strongly coupled single quantum dot–cavity system», Nature **445**, 896–899 (2007).

[21]D. Sanvitto and S. Kéna-Cohen, «The road towards polaritonic devices», Nature Materials **15**, 1061–1073 (2016).

[22]X. Zhong, T. Chervy, L. Zhang, A. Thomas, J. George, C. Genet, J. A. Hutchison, and T. W. Ebbesen, «Energy transfer between spatially separated entangled molecules», Angewandte Chemie International Edition **56**, 9034–9038 (2017).

[23]J. A. Hutchison, T. Schwartz, C. Genet, E. Devaux, and T. W. Ebbesen, «Modifying chemical landscapes by coupling to vacuum fields», Angewandte Chemie International Edition **51**, 1592–1596 (2012).

[24]J. Galego, F. J. Garcia-Vidal, and J. Feist, «Cavity-induced modifications of molecular structure in the strong-coupling regime», Phys. Rev. X **5**, 041022 (2015).

[25]V. A. Yakovlev, V. G. Nazin, and G. N. Zhizhin, «The Surface Polariton Splitting Due to Thin Surface Film LO Vibrations», Optics Communications **15**, 293 (1975).

[26]I. Pockrand, A. Brillante, and D. Möbius, «Exciton–Surface Plasmon Coupling: An Experimental Investigation», J. Chem. Phys. **77**, 6289 (1982).

[27]Y. Kaluzny, P. Goy, M. Gross, J. Raimond, and S. Haroche, «Observation of Self-Induced Rabi Oscillations in Two-Level Atoms Excited Inside a Resonant Cavity: The Ringing Regime of Superradiance», Phys. Rev. Lett. **51**, 1175 (1983).

[28]M. Saffman, T. G. Walker, and K. Mølmer, «Quantum information with rydberg atoms», Rev. Mod. Phys. **82**, 2313–2363 (2010).

[29]P. Michler, *Single semiconductor quantum dots*, Vol. 28 (Springer, 2009).

[30]S. M. Reimann and M. Manninen, «Electronic structure of quantum dots», Rev. Mod. Phys. **74**, 1283–1342 (2002).

[31]S. Neeleshwar, C. L. Chen, C. B. Tsai, Y. Y. Chen, C. C. Chen, S. G. Shyu, and M. S. Seehra, «Size-dependent properties of cdse quantum dots», Phys. Rev. B **71**, 201307 (2005).

[32]F. Würthner, T. E. Kaiser, and C. R. Saha-Möller, «J-aggregates: from serendipitous discovery to supramolecular engineering of functional dye materials», Angewandte Chemie International Edition **50**, 3376–3410 (2011).

[33]P. T. Kristensen, C. V. Vlack, and S. Hughes, «Generalized effective mode volume for leaky optical cavities», Opt. Lett. **37**, 1649–1651 (2012).

[34]K. G. Cognée, W. Yan, F. L. China, D. Balestri, F. Intonti, M. Gurioli, A. F. Koenderink, and P. Lalanne, «Mapping complex mode volumes with cavity perturbation theory», Optica **6**, 269–273 (2019).

[35]C. Tserkezis, A. I. Fernández-Domínguez, P. A. D. Gonçalves, F. Todisco, J. D. Cox, K. Busch, N. Stenger, S. I. Bozhevolnyi, N. A. Mortensen, and C. Wolff, «On the applicability of quantum-optical concepts in strong-coupling nanophotonics», Reports on Progress in Physics **83**, 082401 (2020).

[36]D. R. Abujetas, J. Feist, F. J. García-Vidal, J. G. Rivas, and J. A. Sánchez-Gil, «Strong coupling between weakly guided semiconductor nanowire modes and an organic dye», Physical Review B **99**, 205409 (2019).

[37]K. J. Vahala, «Optical microcavities», nature **424**, 839–846 (2003).

[38]P Kelkar, V Kozlov, H Jeon, A. Nurmikko, C.-C. Chu, D. Grillo, J Han, C. G. Hua, and R. Gunshor, «Excitons in a ii-vi semiconductor microcavity in the strong-coupling regime», Physical Review B **52**, R5491 (1995).

[39]D. G. Lidzey, D. Bradley, M. Skolnick, T Virgili, S Walker, and D. Whittaker, «Strong exciton–photon coupling in an organic semiconductor microcavity», Nature **395**, 53–55 (1998).

[40]A. Öttl, S. Ritter, M. Köhl, and T. Esslinger, «Hybrid apparatus for bose-einstein condensation and cavity quantum electrodynamics: single atom detection in quantum degenerate gases», Review of Scientific Instruments **77**, 063118 (2006).

[41]J. M. Gérard, D. Barrier, J. Y. Marzin, R. Kuszelewicz, L. Manin, E.

Costard, V. Thierry-Mieg, and T. Rivera, «Quantum boxes as active probes for photonic microstructures: the pillar microcavity case», Applied Physics Letters **69**, 449–451 (1996).

[42]E. Peter, P. Senellart, D. Martrou, A. Lemaître, J Hours, J. Gérard, and J. Bloch, «Exciton-photon strong-coupling regime for a single quantum dot embedded in a microcavity», Physical review letters **95**, 067401 (2005).

[43]Y.-S. Park, A. K. Cook, and H. Wang, «Cavity qed with diamond nanocrystals and silica microspheres», Nano Letters **6**, PMID: 16968028, 2075–2079 (2006).

[44]V. S. Ilchenko, A. A. Savchenkov, A. B. Matsko, and L. Maleki, «Nonlinear optics and crystalline whispering gallery mode cavities», Phys. Rev. Lett. **92**, 043903 (2004).

[45]M. L. Gorodetsky, A. A. Savchenkov, and V. S. Ilchenko, «Ultimate q of optical microsphere resonators», Opt. Lett. **21**, 453–455 (1996).

[46]D. W. Vernooy, V. S. Ilchenko, H. Mabuchi, E. W. Streed, and H. J. Kimble, «High-q measurements of fused-silica microspheres in the near infrared», Opt. Lett. **23**, 247–249 (1998).

[47]A. A. Savchenkov, A. B. Matsko, V. S. Ilchenko, and L. Maleki, «Optical resonators with ten million finesse», Opt. Express **15**, 6768–6773 (2007).

[48]S. John, «Strong localization of photons in certain disordered dielectric superlattices», Physical review letters **58**, 2486 (1987).

[49]O. Painter, R. Lee, A. Scherer, A Yariv, J. O'brien, P. Dapkus, and I Kim, «Two-dimensional photonic band-gap defect mode laser», Science **284**, 1819–1821 (1999).

[50]Y. Akahane, T. Asano, B.-S. Song, and S. Noda, «High-q photonic nanocavity in a two-dimensional photonic crystal», nature **425**, 944–947 (2003).

[51]B.-S. Song, S. Noda, T. Asano, and Y. Akahane, «Ultra-high-q photonic double-heterostructure nanocavity», Nature materials **4**, 207–210 (2005).

[52]W. L. Barnes, A. Dereux, and T. W. Ebbesen, «Surface plasmon subwavelength optics», nature **424**, 824–830 (2003).

[53]A. I. Fernández-Domínguez, F. J. García-Vidal, and L. Martín-Moreno, «Unrelenting Plasmons», Nat. Photonics **11**, 8 (2017).

[54]A. I. Fernández-Domínguez, S. I. Bozhevolnyi, and N. A. Mortensen, «Plasmon-enhanced generation of nonclassical light», ACS Photonics **5**, 3447–3451 (2018).

[55]J. J. Baumberg, J. Aizpurua, M. H. Mikkelsen, and D. R. Smith, «Extreme nanophotonics from ultrathin metallic gaps», Nature Materials **18**, 668–678 (2019).

[56]J. B. Khurgin, «How to Deal with the Loss in Plasmonics and Metamaterials», Nat. Nanotechnol. **10**, 2 (2015).

[57]R. Chikkaraddy, B. De Nijs, F. Benz, S. J. Barrow, O. A. Scherman, E. Rosta, A. Demetriadou, P. Fox, O. Hess, and J. J. Baumberg, «Single-molecule strong coupling at room temperature in plasmonic nanocavities», Nature **535**, 127–130 (2016).

[58]J Bellessa, C Bonnand, J. Plenet, and J Mugnier, «Strong coupling between surface plasmons and excitons in an organic semiconductor», Physical review letters **93**, 036404 (2004).

[59]J Dintinger, S Klein, F Bustos, W. L. Barnes, and T. Ebbesen, «Strong coupling between surface plasmon-polaritons and organic molecules in subwavelength hole arrays», Physical Review B **71**, 035424 (2005).

[60]G. Zengin, M. Wersäll, S. Nilsson, T. J. Antosiewicz, M. Käll, and T. Shegai, «Realizing strong light-matter interactions between single-nanoparticle plasmons and molecular excitons at ambient conditions», Physical review

letters **114**, 157401 (2015).

[61]S. Rodriguez, J Feist, M. Verschuuren, F. G. Vidal, and J. G. Rivas, «Thermalization and cooling of plasmon-exciton polaritons: towards quantum condensation», Physical review letters **111**, 166802 (2013).

[62]R.-Q. Li, D Hernángomez-Pérez, F. García-Vidal, and A. Fernández-Domínguez, «Transformation optics approach to plasmon-exciton strong coupling in nanocavities», Physical review letters **117**, 107401 (2016).

[63]M.-K. Kim, H. Sim, S. J. Yoon, S.-H. Gong, C. W. Ahn, Y.-H. Cho, and Y.-H. Lee, «Squeezing photons into a point-like space», Nano letters **15**, 4102–4107 (2015).

[64]K. Santhosh, O. Bitton, L. Chuntonov, and G. Haran, «Vacuum rabi splitting in a plasmonic cavity at the single quantum emitter limit», Nature communications **7**, 1–5 (2016).

[65]B. Gurlek, V. Sandoghdar, and D. Martín-Cano, «Manipulation of quenching in nanoantenna–emitter systems enabled by external detuned cavities: a path to enhance strong-coupling», ACS Photonics **5**, 456–461 (2018).

[66]S. Franke, S. Hughes, M. Kamandar Dezfouli, P. T. Kristensen, K. Busch, A. Knorr, and M. Richter, «Quantization of Quasinormal Modes for Open Cavities and Plasmonic Cavity Quantum Electrodynamics», Phys. Rev. Lett. **122**, 213901 (2019).

[67]A. Bisht, J. Cuadra, M. Wersäll, A. Canales, T. J. Antosiewicz, and T. Shegai, «Collective strong light-matter coupling in hierarchical microcavity-plasmon-exciton systems», Nano letters **19**, 189–196 (2018).

[68]J. Feist, A. I. Fernández-Domínguez, and F. J. García-Vidal, «Macroscopic QED for Quantum Nanophotonics: Emitter-Centered Modes as a Minimal Basis for Multiemitter Problems», Nanophotonics **10**, 477 (2020).

[69]J. Fregoni, F. J. García-Vidal, and J. Feist, «Theoretical Challenges in

Polaritonic Chemistry».

[70]U. Fano, «Atomic Theory of Electromagnetic Interactions in Dense Materials», Phys. Rev. **103**, 1202 (1956).

[71]B. Huttner and S. M. Barnett, «Quantization of the Electromagnetic Field in Dielectrics», Phys. Rev. A **46**, 4306 (1992).

[72]S. Scheel, L. Knöll, and D.-G. Welsch, «QED Commutation Relations for Inhomogeneous Kramers-Kronig Dielectrics», Phys. Rev. A **58**, 700 (1998).

[73]L. Knöll, S. Scheel, and D.-G. Welsch, «QED in Dispersing and Absorbing Media», in *Coherence and Statistics of Photons and Atoms*, edited by J. Peřina, First (WILEY-VCH Verlag, New York, June 2001).

[74]S. Scheel and S. Y. Buhmann, «Macroscopic Quantum Electrodynamics - Concepts and Applications», Acta Phys. Slovaca **58**, 675 (2008).

[75]S. Y. Buhmann, *Dispersion Forces I: Macroscopic quantum electrodynamics and ground-state Casimir, Casimir–Polder and van der Waals forces*, Vol. 247, Springer Tracts in Modern Physics (Springer Berlin Heidelberg, Berlin, Heidelberg, 2012).

[76]S. Y. Buhmann, *Dispersion Forces II: Many-Body effects, excited atoms, finite temperature and quantum friction*, Vol. 248, Springer Tracts in Modern Physics (Springer Berlin Heidelberg, Berlin, Heidelberg, 2013).

[77]J. Galego, C. Climent, F. J. Garcia-Vidal, and J. Feist, «Cavity Casimir-Polder Forces and Their Effects in Ground-State Chemical Reactivity», Phys. Rev. X **9**, 021057 (2019).

[78]A. Cuartero-González and A. I. Fernández-Domínguez, «Light-Forbidden Transitions in Plasmon-Emitter Interactions beyond the Weak Coupling Regime», ACS Photonics **5**, 3415 (2018).

[79]T. Neuman, R. Esteban, D. Casanova, F. J. García-Vidal, and J. Aizpurua,

«Coupling of Molecular Emitters and Plasmonic Cavities beyond the Point-Dipole Approximation», Nano Lett. **18**, 2358 (2018).

[80]J. Fregoni, T. S. Haugland, S. Pipolo, T. Giovannini, H. Koch, and S. Corni, «Strong Coupling between Localized Surface Plasmons and Molecules by Coupled Cluster Theory», Nano Lett. **21**, 6664 (2021).

[81]R.-Q. Li, F. J. García-Vidal, and A. I. Fernández-Domínguez, «Plasmon-exciton coupling in symmetry-broken nanocavities», ACS Photonics **5**, 177–185 (2018).

[82]P. A. Huidobro and A. I. Fernández-Domínguez, «Transformation optics for plasmonics: from metasurfaces to excitonic strong coupling», en, Comptes Rendus. Physique **21**, 389–408 (2020).

[83]A. Cuartero-González, A. Manjavacas, and A. I. Fernández-Domínguez, «Distortion of the Local Density of States in a Plasmonic Cavity by a Quantum Emitter», New J. Phys. **23**, 073011 (2021).

[84]A. Cuartero-González and A. I. Fernández-Domínguez, «Dipolar and quadrupolar excitons coupled to a nanoparticle-on-mirror cavity», Phys. Rev. B **101**, 035403 (2020).

[85]A. Babaze, R. Esteban, A. G. Borisov, and J. Aizpurua, «Electronic Exciton–Plasmon Coupling in a Nanocavity Beyond the Electromagnetic Interaction Picture», Nano Lett. (2021) `10.1021/acs.nanolett.1c03202`.

[86]H.-P. Breuer and F. Petruccione, *The Theory of Open Quantum Systems* (Oxford University Press, 2007).

[87]M. Sánchez-Barquilla, R. E. F. Silva, and J. Feist, «Cumulant Expansion for the Treatment of Light-Matter Interactions in Arbitrary Material Structures», J. Chem. Phys. **152**, 034108 (2020).

[88]J. del Pino, F. A.Y. N. Schröder, A. W. Chin, J. Feist, and F. J. Garcia-Vidal, «Tensor Network Simulation of Polaron-Polaritons in Organic Mi-

crocavities», Phys. Rev. B **98**, 165416 (2018).

[89]J. del Pino, F. A.Y. N. Schröder, A. W. Chin, J. Feist, and F. J. Garcia-Vidal, «Tensor Network Simulation of Non-Markovian Dynamics in Organic Polaritons», Phys. Rev. Lett. **121**, 227401 (2018); «Erratum: Tensor Network Simulation of Non-Markovian Dynamics in Organic Polaritons [Phys. Rev. Lett. 121, 227401 (2018)]», ibid. **122**, 159902 (2019).

[90]J. del Pino, F. A.Y. N. Schröder, A. W. Chin, J. Feist, and F. J. Garcia-Vidal, «Tensor Network Simulation of Non-Markovian Dynamics in Organic Polaritons», Phys. Rev. Lett. **121**, 227401 (2018).

[91]J. del Pino, F. A.Y. N. Schröder, A. W. Chin, J. Feist, and F. J. Garcia-Vidal, «Erratum: Tensor Network Simulation of Non-Markovian Dynamics in Organic Polaritons [Phys. Rev. Lett. 121, 227401 (2018)]», Phys. Rev. Lett. **122**, 159902 (2019).

[92]D. Zhao, R. E. F. Silva, C. Climent, J. Feist, A. I. Fernández-Domínguez, and F. J. García-Vidal, «Impact of Vibrational Modes in the Plasmonic Purcell Effect of Organic Molecules», ACS Photonics **7**, 3369 (2020).

[93]R. Rosenbach, J. Cerrillo, S. F. Huelga, J. Cao, and M. B. Plenio, «Efficient Simulation of Non-Markovian System-Environment Interaction», New J. Phys. **18**, 23035 (2016).

[94]M. Sánchez-Barquilla and J. Feist, «Accurate Truncations of Chain Mapping Models for Open Quantum Systems», Nanomaterials **11**, 2104 (2021).

[95]C. Sauvan, J. P. Hugonin, I. S. Maksymov, and P. Lalanne, «Theory of the Spontaneous Optical Emission of Nanosize Photonic and Plasmon Resonators», Phys. Rev. Lett. **110**, 237401 (2013).

[96]P. T. Kristensen and S. Hughes, «Modes and Mode Volumes of Leaky Optical Cavities and Plasmonic Nanoresonators», ACS Photonics **1**, 2 (2014).

[97]P. Lalanne, W. Yan, K. Vynck, C. Sauvan, and J.-P. Hugonin, «Light In-

teraction with Photonic and Plasmonic Resonances», Laser Photonics Rev. **12**, 1700113 (2018).

[98]J. Ren, S. Franke, and S. Hughes, «Quasinormal Modes and Purcell Factors of Coupled Loss and Gain Resonators near an Exceptional Point».

[99]S. Franke, J. Ren, and S. Hughes, «Quantized Quasinormal Mode Theory of Coupled Lossy and Amplifying Resonators».

[100]S. Franke, S. Hughes, M. Kamandar Dezfouli, P. T. Kristensen, K. Busch, A. Knorr, and M. Richter, «Quantization of Quasinormal Modes for Open Cavities and Plasmonic Cavity Quantum Electrodynamics», Phys. Rev. Lett. **122**, 213901 (2019).

[101]I. Medina, F. J. García-Vidal, A. I. Fernández-Domínguez, and J. Feist, «Few-mode field quantization of arbitrary electromagnetic spectral densities», Physical Review Letters **126**, 093601 (2021).

[102]M. Sánchez-Barquilla, F. J. García-Vidal, A. I. Fernández-Domínguez, and J. Feist, «Few-Mode Field Quantization for Multiple Emitters», arXiv:2112.10581.

[103]B Huttner and S. Barnett, «Dispersion and loss in a hopfield dielectric», EPL (Europhysics Letters) **18**, 487 (1992).

[104]M. Wubs and L. Suttorp, «Transient qed effects in absorbing dielectrics», Physical Review A **63**, 043809 (2001).

[105]L. Suttorp and M. Wubs, «Field quantization in inhomogeneous absorptive dielectrics», Physical Review A **70**, 013816 (2004).

[106]L. Suttorp and A. Van Wonderen, «Fano diagonalization of a polariton model for an inhomogeneous absorptive dielectric», EPL (Europhysics Letters) **67**, 766 (2004).

[107]O. Di Stefano, S. Savasta, and R. Girlanda, «Microscopic calculation of noise current operators for electromagnetic field quantization in absorbing

material systems», Journal of Optics B: Quantum and Semiclassical Optics **3**, 288 (2001).

[108]S. Scheel and S. Y. Buhmann, «Macroscopic quantum electrodynamics – concepts and applications», Acta Phys. Slovaca **58**, 675 (2008).

[109]C. Cohen-Tannoudji, J. Roc, and G. Grynberg, *Photons and Atoms. Introduction to Quantum Electrodynamics.* (Wiley-Interscience, New York, 1987).

[110]V. Weisskopf and E. Wigner, «Über Die Natürliche Linienbreite in Der Strahlung Des Harmonischen Oszillators», Z. Für Phys. Hadrons Nucl. **65**, 18 (1930).

[111]L. Novotny and B. Hecht, *Principles of Nano-Optics*, Second (Cambridge University Press, Cambridge, 2012).

[112]D. Tamascelli, A. Smirne, J. Lim, S. F. Huelga, and M. B. Plenio, «Efficient Simulation of Finite-Temperature Open Quantum Systems», Phys. Rev. Lett. **123**, 090402 (2019).

[113]K. Drexhage, «Beeinflussung der fluoreszenz eins europiumchelates durch einen spiegel», Ber. Bunsenges. Phys. Chem. **70**, 1179 (1966).

[114]P. Goy, J. Raimond, M Gross, and S Haroche, «Observation of cavity-enhanced single-atom spontaneous emission», Physical review letters **50**, 1903 (1983).

[115]D. Kleppner, «Inhibited spontaneous emission», Physical review letters **47**, 233 (1981).

[116]E. Yablonovitch, «Inhibited spontaneous emission in solid-state physics and electronics», Physical review letters **58**, 2059 (1987).

[117]I. I. Rabi, «Space quantization in a gyrating magnetic field», Physical Review **51**, 652 (1937).

[118]E. T. Jaynes and F. W. Cummings, «Comparison of quantum and semiclassical radiation theories with application to the beam maser», Proceedings of the IEEE **51**, 89–109 (1963).

[119]H. Tanji-Suzuki, I. D. Leroux, M. H. Schleier-Smith, M. Cetina, A. Grier, J. Simon, and V. Vuletić, «Interaction between Atomic Ensembles and Optical Resonators: Classical Description», Adv. At. Mol. Opt. Phys. **60**, 201 (2011).

[120]G. Kewes, F. Binkowski, S. Burger, L. Zschiedrich, and O. Benson, «Heuristic modeling of strong coupling in plasmonic resonators», ACS Photonics **5**, 4089–4097 (2018).

[121]R. Sáez-Blázquez, J. Feist, F. J. García-Vidal, and A. I. Fernández-Domínguez, «Theory of energy transfer in organic nanocrystals», Advanced Optical Materials **8**, 2001447 (2020).

[122]J. J. Hopfield and D. G. Thomas, «Polariton absorption lines», Phys. Rev. Lett. **15**, 22–25 (1965).

[123]G. Morris and M. Sceats, «The 4000 å transition of crystal anthracene», Chemical Physics **3**, 164–179 (1974).

[124]Y Kaluzny, P Goy, M Gross, J. Raimond, and S Haroche, «Observation of self-induced rabi oscillations in two-level atoms excited inside a resonant cavity: the ringing regime of superradiance», Physical review letters **51**, 1175 (1983).

[125]B. M. Garraway, «The dicke model in quantum optics: dicke model revisited», Philosophical Transactions of the Royal Society A: Mathematical, Physical and Engineering Sciences **369**, 1137–1155 (2011).

[126]J. Feist, J. Galego, and F. J. Garcia-Vidal, «Polaritonic chemistry with organic molecules», ACS Photonics **5**, 205–216 (2018).

[127]R. F. Ribeiro, L. A. Martínez-Martínez, M. Du, J. Campos-Gonzalez-Angulo,

and J. Yuen-Zhou, «Polariton chemistry: controlling molecular dynamics with optical cavities», Chem. Sci. **9**, 6325–6339 (2018).

[128]M. Tavis and F. W. Cummings, «Exact solution for an n-molecule—radiation-field hamiltonian», Physical Review **170**, 379 (1968).

[129]R. H. Dicke, «Coherence in spontaneous radiation processes», Physical review **93**, 99 (1954).

[130]D. R. Abujetas, J. Feist, F. J. García-Vidal, J. Gómez Rivas, and J. A. Sánchez-Gil, «Strong Coupling between Weakly Guided Semiconductor Nanowire Modes and an Organic Dye», Phys. Rev. B **99**, 205409 (2019).

[131]D. R. Abujetas, J. Feist, F. J. García-Vidal, J. Gómez Rivas, and J. A. Sánchez-Gil, «Strong Coupling between Weakly Guided Semiconductor Nanowire Modes and an Organic Dye», Phys. Rev. B **99**, 205409 (2019).

[132]A. Canales, D. G. Baranov, T. J. Antosiewicz, and T. Shegai, «Abundance of Cavity-Free Polaritonic States in Resonant Materials and Nanostructures», J. Chem. Phys. **154**, 024701 (2021).

[133]M. Barra-Burillo, U. Muniain, S. Catalano, M. Autore, F. Casanova, L. E. Hueso, J. Aizpurua, R. Esteban, and R. Hillenbrand, «Microcavity Phonon Polaritons from the Weak to the Ultrastrong Phonon–Photon Coupling Regime», Nat Commun **12**, 6206 (2021).

[134]D Meschede, H. Walther, and G Müller, «One-atom maser», Physical review letters **54**, 551 (1985).

[135]G. Rempe, H. Walther, and N. Klein, «Observation of quantum collapse and revival in a one-atom maser», Physical review letters **58**, 353 (1987).

[136]R. Thompson, G Rempe, and H. Kimble, «Observation of normal-mode splitting for an atom in an optical cavity», Physical Review Letters **68**, 1132 (1992).

[137]C. Weisbuch, M. Nishioka, A Ishikawa, and Y Arakawa, «Observation of the coupled exciton-photon mode splitting in a semiconductor quantum microcavity», Physical Review Letters **69**, 3314 (1992).

[138]R Houdré, C Weisbuch, R. Stanley, U Oesterle, P Pellandini, and M Ilegems, «Measurement of cavity-polariton dispersion curve from angle-resolved photoluminescence experiments», Physical Review Letters **73**, 2043 (1994).

[139]J. P. Reithmaier, G Sęk, A Löffler, C Hofmann, S Kuhn, S Reitzenstein, L. Keldysh, V. Kulakovskii, T. Reinecke, and A Forchel, «Strong coupling in a single quantum dot–semiconductor microcavity system», Nature **432**, 197–200 (2004).

[140]P. A. Hobson, W. L. Barnes, D. Lidzey, G. Gehring, D. Whittaker, M. Skolnick, and S Walker, «Strong exciton–photon coupling in a low-q all-metal mirror microcavity», Applied Physics Letters **81**, 3519–3521 (2002).

[141]S. Gambino, M. Mazzeo, A. Genco, O. Di Stefano, S. Savasta, S. Patanè, D. Ballarini, F. Mangione, G. Lerario, D. Sanvitto, and G. Gigli, «Exploring light–matter interaction phenomena under ultrastrong coupling regime», ACS Photonics **1**, 1042–1048 (2014).

[142]E. Eizner, J. Brodeur, F. Barachati, A. Sridharan, and S. Kéna-Cohen, «Organic photodiodes with an extended responsivity using ultrastrong light–matter coupling», ACS Photonics **5**, 2921–2927 (2018).

[143]A. Pscherer, M. Meierhofer, D. Wang, H. Kelkar, D. Martín-Cano, T. Utikal, S. Götzinger, and V. Sandoghdar, «Single-Molecule Vacuum Rabi Splitting: Four-Wave Mixing and Optical Switching at the Single-Photon Level», Phys. Rev. Lett. **127**, 133603 (2021).

[144]J. Hopfield, «Theory of the Contribution of Excitons to the Complex Dielectric Constant of Crystals», Phys. Rev. **112**, 1555 (1958).

[145]A. A. Anappara, S. De Liberato, A. Tredicucci, C. Ciuti, G. Biasiol, L.

Sorba, and F. Beltram, «Signatures of the ultrastrong light-matter coupling regime», Physical Review B **79**, 201303 (2009).

[146]T. Niemczyk, F Deppe, H Huebl, E. Menzel, F Hocke, M. Schwarz, J. Garcia-Ripoll, D Zueco, T Hümmer, E Solano, et al., «Circuit quantum electrodynamics in the ultrastrong-coupling regime», Nature Physics **6**, 772–776 (2010).

[147]A. Frisk Kockum, A. Miranowicz, S. D. Liberato, S. Savasta, and F. Nori, «Ultrastrong Coupling between Light and Matter», Nat. Rev. Phys. **1**, 19 (2019).

[148]F. Le Roux, R. A. Taylor, and D. D. C. Bradley, «Enhanced and polarization-dependent coupling for photoaligned liquid crystalline conjugated polymer microcavities», ACS Photonics **7**, 746–758 (2020).

[149]C. W. Gardiner and P. Zoller, *Quantum Noise: A Handbook of Markovian and Non-Markovian Quantum Stochastic Methods with Applications to Quantum Optics* (Springer Berlin Heidelberg, 2004).

[150]I. de Vega and D. Alonso, «Dynamics of Non-Markovian Open Quantum Systems», Rev. Mod. Phys. **89**, 015001 (2017).

[151]J. Roden, A. Eisfeld, W. Wolff, and W. T. Strunz, «Influence of Complex Exciton-Phonon Coupling on Optical Absorption and Energy Transfer of Quantum Aggregates», Phys. Rev. Lett. **103**, 3 (2009).

[152]W. T. Strunz, L. Diósi, and N. Gisin, «Open System Dynamics with Non-Markovian Quantum Trajectories», Phys. Rev. Lett. **82**, 1801 (1999).

[153]D. Manzano, «A Short Introduction to the Lindblad Master Equation», AIP Advances **10**, 025106 (2020).

[154]H. J. Carmichael, *Statistical Methods in Quantum Optics 1* (Springer Berlin Heidelberg, Berlin, Heidelberg, 1999).

[155]G. Grynberg, A. Aspect, C. Fabre, and C. Cohen-Tannoudji, *Introduction to Quantum Optics: From the Semi-Classical Approach to Quantized Light* (Cambridge University Press, Cambridge, 2010).

[156]A. F. Kockum, A. Miranowicz, S. De Liberato, S. Savasta, and F. Nori, «Ultrastrong coupling between light and matter», Nature Reviews Physics **1**, 19–40 (2019).

[157]A. Pusch, S. Wuestner, J. M. Hamm, K. L. Tsakmakidis, and O. Hess, «Coherent amplification and noise in gain-enhanced nanoplasmonic metamaterials: a maxwell-bloch langevin approach», ACS nano **6**, 2420–2431 (2012).

[158]M. Sukharev and A. Nitzan, «Optics of exciton-plasmon nanomaterials», Journal of Physics: Condensed Matter **29**, 443003 (2017).

[159]H.-T. Chen, T. E. Li, M. Sukharev, A. Nitzan, and J. E. Subotnik, «Ehrenfest+ r dynamics. i. a mixed quantum–classical electrodynamics simulation of spontaneous emission», The Journal of chemical physics **150**, 044102 (2019).

[160]N. M. Hoffmann, C. Schäfer, A. Rubio, A. Kelly, and H. Appel, «Capturing vacuum fluctuations and photon correlations in cavity quantum electrodynamics with multitrajectory ehrenfest dynamics», Physical Review A **99**, 063819 (2019).

[161]R. F. Chang, V. Korenman, C. O. Alley, and R. W. Detenbeck, «Correlations in light from a laser at threshold», Physical Review **178**, 612 (1969).

[162]M. Fleischhauer, «Relation between the n-atom laser and the one-atom laser», Physical Review A **50**, 2773 (1994).

[163]P. Kirton and J. Keeling, «Suppressing and restoring the dicke superradiance transition by dephasing and decay», Physical review letters **118**, 123602 (2017).

[164]P. Kirton and J. Keeling, «Superradiant and lasing states in driven-dissipative dicke models», New Journal of Physics **20**, 015009 (2018).

[165]K. B. Arnardottir, A. J. Moilanen, A. Strashko, P. Törmä, and J. Keeling, «Multimode organic polariton lasing», Physical Review Letters **125**, 233603 (2020).

[166]S. Y. Buhmann and D.-G. Welsch, «Casimir-polder forces on excited atoms in the strong atom-field coupling regime», Physical Review A **77**, 012110 (2008).

[167]T. Hümmer, F. García-Vidal, L. Martín-Moreno, and D. Zueco, «Weak and strong coupling regimes in plasmonic qed», Physical Review B **87**, 115419 (2013).

[168]B. Rousseaux, D. Dzsotjan, G. C. des Francs, H.-R. Jauslin, C. Couteau, and S. Guerin, «Adiabatic passage mediated by plasmons: a route towards a decoherence-free quantum plasmonic platform», Physical Review B **93**, 045422 (2016).

[169]R. Kubo, «Generalized Cumulant Expansion Method», J. Phys. Soc. Jpn. **17**, 1100 (1962).

[170]D. Plankensteiner, C. Hotter, and H. Ritsch, «QuantumCumulants.jl: A Julia framework for generalized mean-field equations in open quantum systems», Quantum **6**, 617 (2022).

[171]J. Feist, *https://github.com/jfeist/QuantumAlgebra.jl*, Nov. 2019.

[172]J. Bezanson, A. Edelman, S. Karpinski, and V. B. Shah, «Julia: A Fresh Approach to Numerical Computing», SIAM Rev. **59**, 65 (2017).

[173]C. Rackauckas and Q. Nie, «DifferentialEquations.Jl – A Performant and Feature-Rich Ecosystem for Solving Differential Equations in Julia», J. Open Res. Softw. **5**, 15 (2017).

[174]J. Andreasen and Hui Cao, «Finite-Difference Time-Domain Formulation of Stochastic Noise in Macroscopic Atomic Systems», J. Light. Technol. **27**, 4530 (2009).

[175]H.-T. Chen, T. E. Li, M. Sukharev, A. Nitzan, and J. E. Subotnik, «Ehrenfest+R Dynamics. I. A Mixed Quantum–Classical Electrodynamics Simulation of Spontaneous Emission», J. Chem. Phys. **150**, 044102 (2019).

[176]A. González-Tudela, P. A. Huidobro, L. Martín-Moreno, C. Tejedor, and F. J. García-Vidal, «Reversible Dynamics of Single Quantum Emitters near Metal-Dielectric Interfaces», Phys. Rev. B **89**, 041402(R) (2014).

[177]K. Henschel, J. Majer, J. Schmiedmayer, and H. Ritsch, «Cavity QED with an Ultracold Ensemble on a Chip: Prospects for Strong Magnetic Coupling at Finite Temperatures», Phys. Rev. A **82**, 033810 (2010).

[178]L. Allen and J. H. Eberly, *Optical Resonance and Two-Level Atoms* (Dover, New York, 1987).

[179]J. Cuerda, F. J. García-Vidal, and J. Bravo-Abad, «Spatio-Temporal Modeling of Lasing Action in Core-Shell Metallic Nanoparticles», ACS Photonics **3**, 1952 (2016).

[180]J. Cuerda, F. Rüting, F. J. García-Vidal, and J. Bravo-Abad, «Theory of Lasing Action in Plasmonic Crystals», Phys. Rev. B **91**, 041118(R) (2015).

[181]D. M. Coles, N. Somaschi, P. Michetti, C. Clark, P. G. Lagoudakis, P. G. Savvidis, and D. G. Lidzey, «Polariton-Mediated Energy Transfer between Organic Dyes in a Strongly Coupled Optical Microcavity», Nat. Mater. **13**, 712 (2014).

[182]P. Kirton and J. Keeling, «Suppressing and Restoring the Dicke Superradiance Transition by Dephasing and Decay», Phys. Rev. Lett. **118**, 123602 (2017).

[183]Y. Tanimura and R. Kubo, «Time Evolution of a Quantum System in Con-

tact with a Nearly Gaussian-Markoffian Noise Bath», J. Phys. Soc. Jpn. **58**, 101 (1989).

[184]Y. Tanimura, «Nonperturbative Expansion Method for a Quantum System Coupled to a Harmonic-Oscillator Bath», Phys. Rev. A **41**, 6676 (1990).

[185]H. Liu, L. Zhu, S. Bai, and Q. Shi, «Reduced Quantum Dynamics with Arbitrary Bath Spectral Densities: Hierarchical Equations of Motion Based on Several Different Bath Decomposition Schemes», J. Chem. Phys. **140**, 134106 (2014).

[186]Y. Tanimura, «Numerically "Exact" Approach to Open Quantum Dynamics: The Hierarchical Equations of Motion (HEOM)», J. Chem. Phys. **153**, 020901 (2020).

[187]L. Diósi and W. T. Strunz, «The Non-Markovian Stochastic Schrödinger Equation for Open Systems», Physics Letters A **235**, 569 (1997).

[188]A. Shabani, J. Roden, and K. B. Whaley, «Continuous Measurement of a Non-Markovian Open Quantum System», Phys. Rev. Lett. **112**, 113601 (2014).

[189]D. Suess, A. Eisfeld, and W. T. Strunz, «Hierarchy of Stochastic Pure States for Open Quantum System Dynamics», Phys. Rev. Lett. **113**, 150403 (2014).

[190]G. Vidal, «Efficient Simulation of One-Dimensional Quantum Many-Body Systems», Phys. Rev. Lett. **93**, 040502 (2004).

[191]J. Prior, A. W. Chin, S. F. Huelga, and M. B. Plenio, «Efficient Simulation of Strong System-Environment Interactions», Phys. Rev. Lett. **105**, 050404 (2010).

[192]A. W. Chin, J. Prior, R. Rosenbach, F. Caycedo-Soler, S. F. Huelga, and M. B. Plenio, «The Role of Non-Equilibrium Vibrational Structures in Electronic Coherence and Recoherence in Pigment–Protein Complexes», Nat.

Phys. **9**, 113 (2013).

[193]B. M. Garraway, «Decay of an Atom Coupled Strongly to a Reservoir», Phys. Rev. A **55**, 4636 (1997).

[194]L. Mazzola, S. Maniscalco, J. Piilo, K.-A. Suominen, and B. M. Garraway, «Pseudomodes as an Effective Description of Memory: Non-Markovian Dynamics of Two-State Systems in Structured Reservoirs», Phys. Rev. A **80**, 012104 (2009).

[195]F. Mascherpa, A. Smirne, A. D. Somoza, P. Fernández-Acebal, S. Donadi, D. Tamascelli, S. F. Huelga, and M. B. Plenio, «Optimized Auxiliary Oscillators for the Simulation of General Open Quantum Systems», Phys. Rev. A **101**, 052108 (2020).

[196]G. Pleasance, B. M. Garraway, and F. Petruccione, «Generalized Theory of Pseudomodes for Exact Descriptions of Non-Markovian Quantum Processes», Phys. Rev. Research **2**, 043058 (2020).

[197]F. Hassler, J. Stubenrauch, and A. Ciani, «Equation of motion approach to black-box quantization: taming the multimode jaynes-cummings model», Physical Review B **99**, 014515 (2019).

[198]P. Strasberg, G. Schaller, N. Lambert, and T. Brandes, «Nonequilibrium Thermodynamics in the Strong Coupling and Non-Markovian Regime Based on a Reaction Coordinate Mapping», New J. Phys. **18**, 073007 (2016).

[199]J. Iles-Smith, N. Lambert, and A. Nazir, «Environmental Dynamics, Non-Gaussianity, and the Emergence of Noncanonical Equilibrium States in Open Quantum Systems», Phys. Rev. A **90**, 032114 (2014).

[200]J. Iles-Smith, A. G. Dijkstra, N. Lambert, and A. Nazir, «Energy Transfer in Structured and Unstructured Environments: Master Equations beyond the Born-Markov Approximations», J. Chem. Phys. **144**, 044110 (2016).

[201]S. Restrepo, S. Böhling, J. Cerrillo, and G. Schaller, «Electron Pumping in

the Strong Coupling and Non-Markovian Regime: A Reaction Coordinate Mapping Approach», Phys. Rev. B **100**, 035109 (2019).

[202]A. W. Chin, S. F. Huelga, and M. B. Plenio, «Chain Representations of Open Quantum Systems and Their Numerical Simulation with Time-Adaptive Density Matrix Renormalisation Group Methods», in *Semiconductors and Semimetals*, Vol. 85 (Elsevier Inc., 2011), p. 115.

[203]R. Martinazzo, B. Vacchini, K. H. Hughes, and I. Burghardt, «Communication: Universal Markovian Reduction of Brownian Particle Dynamics», J. Chem. Phys. **134**, 011101 (2011).

[204]M. P. Woods, R. Groux, A. W. Chin, S. F. Huelga, and M. B. Plenio, «Mappings of Open Quantum Systems onto Chain Representations and Markovian Embeddings», Journal of Mathematical Physics **55**, 032101 (2014).

[205]I. de Vega and M.-C. Bañuls, «Thermofield-Based Chain-Mapping Approach for Open Quantum Systems», Phys. Rev. A **92**, 052116 (2015).

[206]J. Cerrillo and J. Cao, «Non-Markovian Dynamical Maps: Numerical Processing of Open Quantum Trajectories», Phys. Rev. Lett. **112**, 110401 (2014).

[207]A. J. Leggett, «Quantum Tunneling in the Presence of an Arbitrary Linear Dissipation Mechanism», Phys. Rev. B **30**, 1208 (1984).

[208]M. T. H. Reid, *SCUFF-EM*, 2012.

[209]M. T. H. Reid and S. G. Johnson, «Efficient Computation of Power, Force, and Torque in BEM Scattering Calculations», IEEE Trans. Antennas Propag. **63**, 3588 (2015).

[210]M. P. Woods, M. Cramer, and M. B. Plenio, «Simulating Bosonic Baths with Error Bars», Phys. Rev. Lett. **115**, 130401 (2015).

[211]F. A.Y. N. Schröder, D. H. P. Turban, A. J. Musser, N. D. M. Hine, and A. W. Chin, «Tensor Network Simulation of Multi-Environmental Open

Quantum Dynamics via Machine Learning and Entanglement Renormalisation», Nat. Commun. **10**, 1062 (2019).

[212]U. V. Riss and H.-D. Meyer, «Reflection-Free Complex Absorbing Potentials», J. Phys. B At. Mol. Opt. Phys. **28**, 1475 (1995).

[213]D. E. Manolopoulos, «Derivation and Reflection Properties of a Transmission-Free Absorbing Potential», J. Chem. Phys. **117**, 9552 (2002).

[214]O. Shemer, D. Brisker, and N. Moiseyev, «Optimal Reflection-Free Complex Absorbing Potentials for Quantum Propagation of Wave Packets», Phys. Rev. A **71**, 32716 (2005).

[215]A. Reiserer and G. Rempe, «Cavity-Based Quantum Networks with Single Atoms and Optical Photons», Rev. Mod. Phys. **87**, 1379 (2015).

[216]C. T. Nguyen, D. D. Sukachev, M. K. Bhaskar, B. Machielse, D. S. Levonian, E. N. Knall, P. Stroganov, R. Riedinger, H. Park, M. Lončar, and M. D. Lukin, «Quantum Network Nodes Based on Diamond Qubits with an Efficient Nanophotonic Interface», Phys. Rev. Lett. **123**, 183602 (2019).

[217]A. González-Tudela, C.-L. Hung, D. E. Chang, J. I. Cirac, and H. J. Kimble, «Subwavelength Vacuum Lattices and Atom–Atom Interactions in Two-Dimensional Photonic Crystals», Nat. Photonics **9**, 320 (2015).

[218]J. S. Douglas, H. Habibian, C.-L. Hung, A. V. Gorshkov, H. J. Kimble, and D. E. Chang, «Quantum Many-Body Models with Cold Atoms Coupled to Photonic Crystals», Nat. Photonics **9**, 326 (2015).

[219]R. J. Glauber and M. Lewenstein, «Quantum Optics of Dielectric Media», Phys. Rev. A **43**, 467 (1991).

[220]A. Delga, J. Feist, J. Bravo-Abad, and F. J. Garcia-Vidal, «Quantum Emitters Near a Metal Nanoparticle: Strong Coupling and Quenching», Phys. Rev. Lett. **112**, 253601 (2014).

[221]A. Cuartero-González and A. I. Fernández-Domínguez, «Dipolar and Quadrupolar Excitons Coupled to a Nanoparticle-on-Mirror Cavity», Phys. Rev. B **101**, 035403 (2020).

[222]C.-J. Yang, J.-H. An, and H.-Q. Lin, «Signatures of Quantized Coupling between Quantum Emitters and Localized Surface Plasmons», Phys. Rev. Research **1**, 023027 (2019).

[223]S Glutsch, «Optical absorption of the fano model: general case of many resonances and many continua», Physical Review B **66**, 075310 (2002).

[224]H. T. Dung, L. Knöll, and D.-G. Welsch, «Resonant Dipole-Dipole Interaction in the Presence of Dispersing and Absorbing Surroundings», Phys. Rev. A **66**, 063810 (2002).

[225]A. González-Tudela, D. Martín-Cano, E. Moreno, L. Martín-Moreno, C. Tejedor, and F. J. García-Vidal, «Entanglement of Two Qubits Mediated by One-Dimensional Plasmonic Waveguides», Phys. Rev. Lett. **106**, 020501 (2011).

[226]D. Martín-Cano, A. González-Tudela, L. Martín-Moreno, F. J. García-Vidal, C. Tejedor, and E. Moreno, «Dissipation-Driven Generation of Two-Qubit Entanglement Mediated by Plasmonic Waveguides», Phys. Rev. B **84**, 235306 (2011).

[227]C. A. Downing, J. C. López Carreño, F. P. Laussy, E. del Valle, and A. I. Fernández-Domínguez, «Quasichiral Interactions between Quantum Emitters at the Nanoscale», Phys. Rev. Lett. **122**, 057401 (2019).

[228]J. Feist, A. I. Fernández-Domínguez, and F. J. García-Vidal, «Macroscopic qed for quantum nanophotonics: emitter-centered modes as a minimal basis for multiemitter problems», Nanophotonics **10**, 477–489 (2021).

Publications

1. *Cumulant expansion for the treatment of light-matter interactions in arbitrary material structures.*
   Mónica Sánchez-Barquilla, Rui E.F. Silva and Johannes Feist.
   The Journal of Chemical Physics 152 (3), 034108.

2. *Accurate truncations of chain mapping models for Open Quantum Systems.*
   Mónica Sánchez-Barquilla and Johannes Feist.
   Nanomaterials 11 (8), 2104.

3. *Few-mode field quantization for multiple emitters.*
   Mónica Sánchez-Barquilla, Antonio I. Ferández-Dominguez, Francisco J. García-Vidal and Johannes Feist.
   arXiv:2112.10581

4. *A theoretical perspective on molecular polaritonics.*
   Mónica Sánchez-Barquilla, Antonio I. Ferández-Dominguez, Johannes Feist and Francisco J. García-Vidal.
   arXiv:2201.02827